# PETROLEUM RESEARCH JOURNAL

## TECHNICAL PAPERS

### ENGINEERING

The Role of Pore Connection in Hydraulic Conductance of Sedimentary Rocks .....
*G. Szigeti* 1

### EXPLORATION

Interpretation of Gravity Data in the Murzuq Basin, SW Libya .....
*A. Sahil and C. Ebinger* 13

### CHEMISTRY

Refining of Libyan Kerosene for Use as a Solvent for Pesticide .....
*Latif H. Ali, Moftah O. Darwish and Esmail O. Elakesh* 19

Organic Matter in Petroleum Sludges a Source of Useful Materials
*Part 2:* Separation and Analysis of Petroleum Naphtha Soluble Fraction .....
*Latif H. Ali and Mohammad N. Oun* 27

Solar Detoxification of A Petroleum Wastewater in Aqueous Suspensions of Titanium Dioxide Photocatalyst .....
*Muftah Al-Ghazali and Gamil Alhakimi* 35

Determination of Chromium (III) and Chromium (VI) Using Flow Injection Coupled with Flame Atomic Absorption Spectrometry and Direct Current Plasma Technique .....
*I. S. Bushina, H. M. Kut, Seham S. Elmahmudi* 45

35S-Radiotracer Studies of Sulphur Poisoning of Platinum Supported Catalysts: 2. Hydrogenation of Ethyne .....
*Ezziddin A. Arafa* 51

The Role of Lanthanum Chloride as a Releasing Agent for Iron in its Determination by Flame Atomic Absorption Spectrophotometer in Nitrate and Sulphate Media .....
*H. M. Kut* 61

### SHORT COMMUNICATION

Lead Contamination in Soil and Vegetation Around Al Fossool Al arbaa Lead Plant in Tripoli District .....
*S. A. Jawashi & M. A. Abuhameda* 65

## VOLUME 11 - (1429) / (1999)

**Petroleum Research Centre**
**P.O. Box 6431, Tripoli**
**Great Socialist People's Libyan Arab Jamahiriya**

Petroleum Res. J. Vol. 11 (1999); P. 1-11, 6 Figs.

# The Role of Pore Connection in Hydraulic Conductance of Sedimentary Rocks

G. Szigeti*

# دور الربط المسامي في التوصيل الهيدروليكي في الصخور الرسوبية

ج. سيغاتي

في هذه الورقة تمت دراسة البنية الداخلية للصخور الرسوبية كمظومة من المسام الموصولة، حيث تم افتراض مكعب لشبكة منتظمة من المسام والقنوات الموصلة بينها بحيث تكون في حالة عشوائية من الفتح أو الإغلاق. ودرست إمكانية وجود أو عدم وجود توصيل هيدروليكي بين الوجهين المتقابلين لمكعب عينة الصخر، اعتماداً على نسبة عدد القنوات المفتوحة إلى عدد القنوات عامة.

وتم إيجاد الحل التكراري للشبكة العشوائية الموصوفة، وكذلك تشبيهه في بعدين على الحاسوب، كما وتم تشبيه نموذج مبسط منه في ثلاثة أبعاد. وقد أعطى تحليل توزيع الاحتمالات صورة كمية حية وواضحة عن دور الربط المسامي في الصخور في الحركة الهيدروليكية. وكنتيجة عامة تخص الصخور ذات البنية التكعيبية المشار إليها أعلاه يمكننا وصف دور الربط المسامي في التوصيل الهيدروليكي بالآتي: إذا كانت نسبة 6/1 من عدد القنوات مفتوحة، فإن الصخر يعتبر غير نفاذي؛ أما إذا كانت النسبة 2/1 من مجموع القنوات مفتوحة، فإن الصخر يعتبر حينذاك نفاذي.

---

**Abstract:** *The inner structure of sedimentary rocks is studied as a system of interconnected pores. A regular cubic network is considered for the pores and the channels connecting them with the latter being randomly open or closed. The problem of whether or not there is a hydraulic connection between two parallel faces of a cubic rock sample, depending upon the ratio of open edges to all the possible edges, is studied.*

*Recursive solution for the described random network problem is given. The recursive solution in two dimensions is simulated on the computer as the simplest three-dimensional case.*

*Analysis of the probability of distributions gives a vivid, quantitative picture about the role of pore connection in hydraulic movement. As a rule of thumb for rocks with the above cubic structure, this role can be described as follows: if only $^1/_6$ of the channels are open the rocks are not permeable but if $^1/_2$ of the channels are open the rocks are permeable.*

## INTRODUCTION

A porous medium only allows the displacement of fluids to the extent that its pores are interconnected. (Perrodon, 1983).

*Petroleum Research Centre, P.O. Box 6431, Tripoli, Libya

The percentage of the channels which should be open (or closed) to allow the rocks permeable or impermeable is dealt with in this study.

Let us consider a certain sedimentary rock with a texture and structure which represent the intergranular porosity in separate pores, while they are connected with thin, narrow tubes or channels. The tubes or channels can be open or closed against pore to pore hydraulic movement.

This model seems to be applicable to mature, consolidated sandstone rather than to unconsolidated sandstone of higher porosity, where the porespace does not necessarily allow its classification as pore and channel. In unconsolidated sandstone plane-like connections can represent a large part of non-solid volume. For real rocks, the question about the open or closed character of the channel is regulated by the presence and development of cementing material, or by the type and development of dispersed shale.

The determination of the numerical value of the permeability of a rock as a function, among others, of the permeability of each channel (zero for the closed one and a given constant for the open ones) has a highly complex character. Consequently, the model presented in this paper is restricted to determination of the permeable or impermeable character of the rock. In spite of this restriction, the model gives a vivid picture about the fluid movement in porous media. In this respect, the character of the results derived here can be compared with that of the porosity calculation of different regular spherical packings (Amyx, *et al.*,1960). It does not play a direct role in the solution of reservoir engineering tasks but gives a fixed scale for the interpretation of porosity data in the solution of engineering problems. This picture also helps to make a visual, qualitative estimation of permeability of a core sample on the basis of microscopic thin sections. Despite the fact that no special hydraulic properties are taken into account, one can not apply the model for the questions of electrical conductivity, because shale (and cementing materials), in general, are not perfect insulators.

Percolation theory deals with the conductivity and permeability of random networks. The achieved results are summarised by monographs (Dullian, 1992; Stauffer and Aharony, 1992). The main method of the percolation theory, since the earliest result (Broadbent, 1954), is the Monte Carlo simulation of the random network. Consequently the nodes of the network should be relatively high, in the range of $10^3$-$10^4$ nodes (Seliakov and Kadet, 1996).

The present work deals with random network as well, however as it will be explained latter on, there is one essential assumption, namely, only one way connections are considered in the direction of the fluid flow. This new assumption gives the basis for the application of recursive solution, which, as it is proven in this paper, dramatically reduces the number of necessary nodes for getting the stabilised solution. This feature of the solution gives a good chance for the application of the recursive method for further tasks. In general, the results derived here are similar to that of the percolation theory, e.g. the percolation thresholds for the square and cubic arrangements are close to that of Korvin, 1992. The aim of the present work is the introduction of the recursive method, rather than the detailed comparison of the two, similar but not identical, tasks.

## SETTING UP THE HYDRAULIC CONNECTION MODEL AND QUANTIFICATION OF THE PROBLEM

Suppose the following construction is of a logical rather than an experimental character consisting of spheres of uniform diameter of one length unit with centres in the integer grid points $(i_x,i_y,i_z)$, where $1 \le i_x \le n_x+1$; $1 \le i_y \le n_y+1$; $1 \le i_z \le n_z+1$. Exerting pressure, as a compaction model of the rock, on each of the side walls of the packing can change the spheres shape into cubes with rounded edges while vertexes have the shape of common dice. The centres are described with the same $(i_x, i_y, i_z)$ grid points but with a reduced length. Shifting the coordinate system of the packed model by the vector ($^1/_2$, $^1/_2$, $^1/_2$) and considering $(i_x, i_y, i_z)$ only for $1 \le i_x \le n_x$; $1 \le i_y \le$ ny; $1 \le i_z \le n_z$, gives the pore volume in the form of $n_x\, n_y\, n_z$ separate pores. Each inner pore volume is connected to six others by narrow channels. It is also assumed, as a model of further consolidation of the rock, that any of the unit

length edges can be randomly blocked against hydraulic movement by cementation or by dispersed shale fraction. Assuming high hydraulic pressure on the $i_z = 1$ plane and low pressure on $i_z = n_z$ plane the question of whether fluid movement is possible between the two parallel faces is posed (Fig. 1).

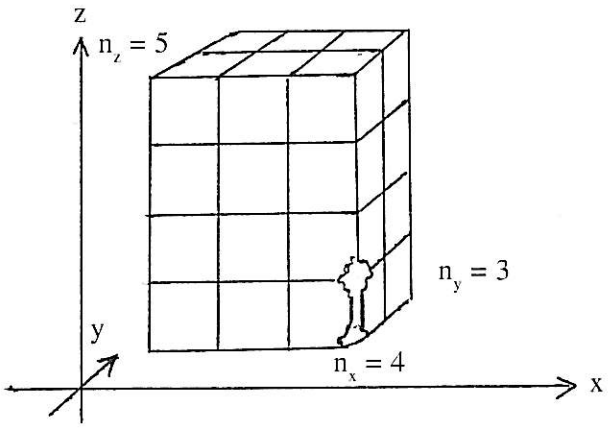



Fig. 1. Cubic arrangement for modelling the grains, the pores and the pore connections.

The network of Fig. 1 has $n_x\, n_y\, n_z$ pore centre points and the number of edges are denoted as $N_{edges}^{block}(n_x, n_y, n_z)$. If we group edges in that of x, y and z direction, then their numbers are arrived at in the form:

$$N_{edges}^{block}(n_x, n_y, n_z) = n_y\, n_z\, (n_x - 1) + n_x\, n_z\, (n_y - 1) + n_x\, n_y\, (n_z - 1) = 3\, n_x\, n_y\, n_z - n_x\, n_y - n_x\, n_z - n_y\, n_z \qquad (1)$$

The derivation requires the number of edges on plane surface as well, as an example, on the $i_z=1$ plane. Introducing the $N_{edges}^{rect}(n_x,n_y)$ notation for the number of edges for the rectangle, similar to eq.(1) but in two dimensions, gives:

$$N_{edges}^{rect}(n_x,n_y) = n_y\, (n_x - 1) + n_x\, (n_y - 1) = 2\, n_x\, n_y - n_x - n_y \qquad (2)$$

The question about the presence or absence of connection between the parallel faces depends on the ratio of the sizes (dimensions). To be conductive a thin layer ($n_z << n_x$ and $n_z << n_y$) requires only a few open connections, while an elongated object ($n_z >> n_x$ and $n_z >> n_y$) requires a higher number of open channels.

Thus, a cubic rock sample is examined. The fluid enters into the pores, given by $i_z = 1$, should reach the face given by $i_z = n_z$. The cube corresponds to the situation where the n-width pore openings require the same number of edges for the fluid molecules to travel in order to reach the opposite face. So, the size of our hydraulic cube for z direction conductance is defined as

$$n_x = n_y = n \quad \text{and} \quad n_z = n + 1 \qquad (3)$$

The hydraulic pressure should only have a z direction on the $i_z = 1$ and $i_z = n_z$ faces, thereby deleting from the system the x and y edges direction from these two parallel planes. For the sake of conciseness, the object remaining after deleting the superfluous edges is referred to as *hydraulic network of n- story* (Fig. 2).

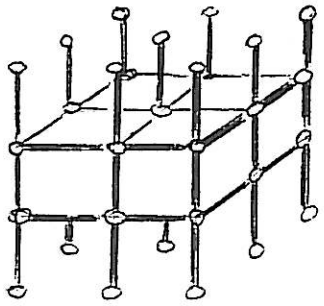


Fig. 2. Hydraulic network of 3-story.(3D, n=3).

The number of edges, denoted by $N_{edges}^{hyd}(n, n, n+1)$, of the hydraulic network can be easily obtained. By virtue of the construction,

$$N_{edges}^{hyd}(n_x, n_y, n_z) = N_{edges}^{block}(n_x, n_y, n_z) - 2\, N_{edges}^{rect}(n_x, n_y) \qquad (4)$$

Substituting eq.(3) into eq.(4) and applying eq.(1) and eq.(2) gives:

$$N_{edges}^{hyd}(n, n, n+1) = 3\, n^3 - 4\, n^2 + 2\, n \qquad (5)$$

Exact mathematical form of the problem is the following. Having a hydraulic network of n-story and a fixed i integer number $1 \le i \le N_{edges}^{hyd}(n, n, n+1)$ all the different hydraulic networks are studied, where the exact i number of channels are open. The question derived from this is:

$C\,(N_{edges}^{hyd}(n, n, n+1), i)$

[where C(n,k) = n! / ((n-k)!k!)] number of models, how many allow fluid movement from the $i_z = 1$ plane to the $i_z = n+1$ plane. In all the z-direction edges, fluid movement only in z-direction is assumed (minus z-direction movement is not allowed). This assumption simplifies the task and is adequate from petroleum engineering point of view.

As an example, the 3-story hydraulic network of Fig. 2 is taken. According to eq. (5) we have 51 edges. When i = 3 (3 randomly selected open edges) the number of different models become C(51,3) = 20825. Reaching the upper plane from the lower one with just three open edges is possible only if all the three edges are vertical and are on the same string ($i_x$ = constant and $i_y$ = constant for the end points of the open edges). This can be done in 9 different ways. Thus, the probability of the event of having a hydraulic connection between the two faces (the ratio of the favourable models to the number of models) is 9/C(51,3) = 0.00043 which is very small. It is noted that even for n=3 for models with a higher number of open edges i > 3, it becomes very difficult to determine the number of conductive models.

## RECURSIVE SOLUTION AND COMPUTER ALGORITHM OF THE PROBLEM

The solution of the problem for all open edges i from 1 to $N_{edges}^{hyd}(n,n,n+1)$ is needed. The number of models, for n = 3, is $2^{51}$ ($\approx 10^{15}$), while by eq. (5) for n = 4, it is $2^{136}$ ($\approx 10^{40}$). It is fairly possible to build up an algorithm which determines each model (open edge system) whether or not hydraulic connection is established. However, the number of models is enormously high and increasing rapidly with growing n. Consequently, such a direct algorithm is not applicable, starting from some small n, regardless of the capacity of the applied computer system.

Here, examining the hydraulic connection story by story, a recursive solution is given. For a fixed n-story hydraulic network, the dependency of the number of models, which connect any of the points $n_z = 1$ to a given point system of $n_z$ =j, upon the number of open edges up to the level $n_z = j$, is studied.

Before setting forth the solution in detail, some general notes should be mentioned.

(a) Any recursion brings useful results only if it can be solved. The main formula of the present paper is complex enough to make it difficult to obtain a solution by hand calculations, but it allows computer solution even for large n values.

(b) The recursive solution, described here, with changes in the main formula, is valid for the general three-dimensional case ($n_y > 1$). However, its description and its computer solution become more difficult than the two-dimensional case $n_y = 1$. The analysis of the three-dimensional general hydraulic network will be given on the basis of the results obtained for the two-dimensional $n_y = 1$ case.

Thus, returning to the recursive solution, the case $n_y = 1$ is supposed, with $n_x = n$ and $n_z = n+1$; where n is a fixed, unchanged integer. For this case, the two-dimensional network, which corresponds to the hydraulic network of n-story can be seen on Fig. 3 for the case n = 4. This object will be referred to as *hydraulic ladder of n-story*, and the number of edges of this object is denoted by $N_{edges}^{lad}(n, n+1)$. Applying the same reasoning as was done for eq. (4),and, also using eq. (2) gives:

$$N_{edges}^{lad}(n, n+1) = N_{edges}^{rect}(n, n+1) - 2(n - 1) = n^2 + (n - 1)^2 \qquad (6)$$

Fixing n, alongside the hydraulic ladder of n-story its parts are also defined as follows. Those $(i_x, i_z)$ points and edges for which, in case of points, $i_z \le i+1$ and edges, at least for one end point $i_z < i+1$ will be referred to as *$i^{th}$ story of n-story hydraulic ladder*. This object and at the same time the number of its edges will be denoted as $N_n(i)$. For i = 1, the 1st story consists of n-vertical edges, and for i = 2 it consists of the previous vertical edges plus (n - 1) horizontal edges plus n new vertical edges, etc.. In this way

$$N_n(i + 1) - N_n(i) = n + (n - 1) = 2n - 1 \qquad (7)$$

The last, $n^{th}$ story gives back the whole hydraulic ladder of n-story, i.e.

$$N_n(n) = N_{edges}^{lad}(n, n+1) \quad (8)$$

Fig. 3 demonstrates the 2nd story of the hydraulic ladder of 4-story as well.

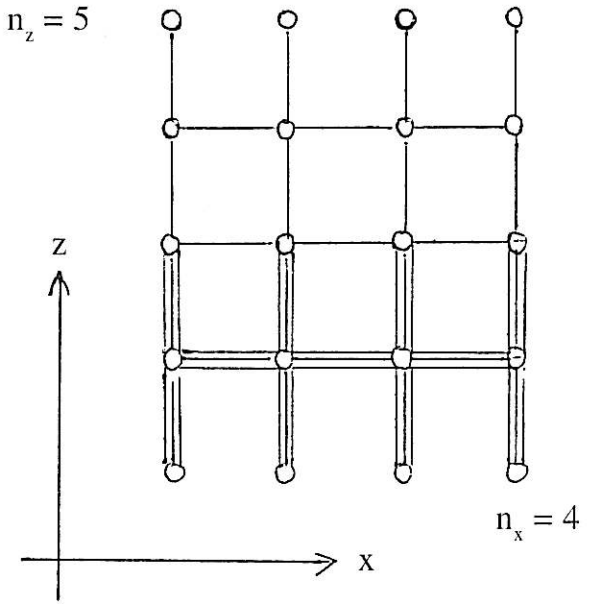



Fig. 3. Hydraulic ladder of 4-story and its 2nd story.(2D, n=4).

Those $(i_x, i_z)$ end points of the $i^{th}$ story of n-story hydraulic ladder for which $i_z = i$ and which are hydraulically connected to the base line $(i_z = 1)$ by a given system of open edges are defined as *wet points* (as to the naming to this definition, dry rock sample is considered, which becomes gradually wet as a result of fluid movement through the open connections).

A system of wet points, given by different systems of open edges, can produce any order of zeros and units (0 corresponds to dry and 1 corresponds to wet points). In connection to this fact, $\{Bs(n, j)\}_{j=0}^{2^n-1}$ denotes the set of those binary sequences, which consist exactly n number of 0 -s and 1 -s in the way, that the sequence gives the number j in binary number system [e.g. Bs(5,2) = (0,0,0,1,0)]. Because of the need to refer to the number of units (e.g. number of wet points) in the binary sequence Bs(n,j) it is denoted by |j| (continuing the previous example, |2| = 1). As negative numbers are not used in this paper, there is no danger to read this notation as the absolute value of a number.

For the sake of conciseness, the definition of each integer used in this paper will be fixed. n denotes the size of hydraulic ladder of n-story as before, with a fixed value. m is the $m^{th}$ story of this ladder, $1 \le m \le n$. i is the number of open edges of the ladder up to the $m^{th}$ story, $0 \le i \le Nn(m)$. j and k stand for the binary sequences of wet points of $(m-1)^{th}$ and $m^{th}$ stories, respectively, $0 \le j \le 2^n-1$ or $0 \le |j| \le n$ and the same holds for k. *l* is the binary sequence which describes the horizontal open edges of the $i_x = m$ row of edges, which are the only horizontal edges, part of the $m^{th}$ ladder but not part of the $(m-1)^{th}$ ladder. 1 stands for the open edges and 0 for the closed ones. Having n-1 horizontal edges, evidently, $0 \le l \le 2^{n-1}-1$ or $0 \le |l| \le n-1$. Fig. 4 illustrates the notations we introduced. Dark points and bold circles represent the wet points of $(m-1)^{th}$ ladder and $m^{th}$ ladder respectively. Single continuous line represents the horizontal open edges of $m^{th}$ ladder (their number is |*l*|), while double lines give these vertical edges of the $m^{th}$ ladder, which are running upwards to wet points.

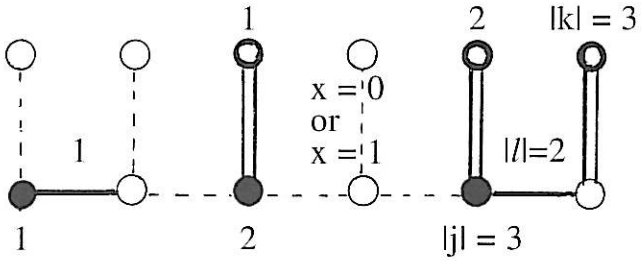



Fig. 4. Notation system for points and edges in different relations to each other.

The question, having the $m^{th}$ story of the hydraulic ladder of n-story and selecting exactly i number of open edges from the $m^{th}$ ladder, can be done in

$$C(Nn(m), i) \quad (9)$$

different ways, how many times the end wet stage of the $m^{th}$ ladder is the Bs(n,k) binary sequence. This number is denoted by

$$|N_{Bs(n,k)}(N_n(m), i) \quad (10)$$

The relation between the Bs(n,j) wet point system of the $(m-1)^{th}$ ladder and the Bs(n,k) wet point system of the $m^{th}$ ladder is needed for the recursive solution. New wet points can be generated only by vertical edges, consequently all the |k| vertical edges given by Bs(n,k) are open. Because of having only z-direction fluid movement, they establish hydraulic connection only in the case when the $|l|$ new horizontal edges connect all the |k| points of the $(m-1)^{th}$ ladder, which lays directly under the Bs(n,k) end points, to the |j| end wet points of the $(m-1)^{th}$ ladder. This can be realized by quite different Bs(n-1, $l$). At any given Bs(n-1, $l$) there can be a certain number of end points of the $(m-1)^{th}$ ladder which remains dry even after connecting the new $|l|$ horizontal open edges. One can open vertical edges to the top of any of these points without changing the wet end point system of the $m^{th}$ ladder. Suppose x vertical edges of this type is placed. This classification of the role of edges is described by the following formula:

$$IN_{Bs(n,k)}(N_n(m), i) = \sum_{j=0}^{2^n-1} \sum_{l=0}^{2^{n-1}-1} \{H_{Bs(n,k)}(Bs(n, j), Bs(n-1, l)) \sum_{x=0}^{Voids(k, j, l)} C(Voids(k, j, l), x) \cdot IN_{Bs(n, j)}(N_n(m-1), i-|k|-|l|-x)\} \quad (11)$$

Here, H is a logical function, which can assume only 0 or 1 values, and describes the hydraulic relation. H is the only one in the case when the Bs(n,j) wet point system of the $(m-1)^{th}$ ladder and the Bs(n-1, $l$) horizontal open edge system make all the |k| points, which are directly under the |k| points of the Bs(n,k) system; wet. H is zero otherwise.

Voids(k,j, $l$) are the functions which tell the maximum possible number of x-points, at a given Bs(n,j), Bs(n-1, $l$) selection, with the Bs(n,k) end point system. If the i-|k|-|$l$|-x argument of IN is less than zero (which is fairly possible even at H = 1), then IN = 0 should be taken into the right hand side of formula (11) (controversial edge system can not give model realising the Bs(n,k) end stage).

Formula (11) finds any open edge system which produces the Bs(n,k) end wet point system. Indeed, this open edge system is a definite Bs(n,j), Bs(n-1, $l$) binary sequence. For these two binary sequences H=1, and for the x-value belonging to the open edge system $C \geq 1$ [for the special case x = 0, regardless of the value of Voids(k,j, $l$), C(Voids(k,j, $l$), 0) = 1] consequently, the given edge system is taken into consideration in the sum of eq. (11).

Any two edge system, which positively increases the right hand side of formula (11), is given by different edge systems. Indeed, if they belong to different j value, then the two systems of edges differ already in the $(m-1)^{th}$ ladder, if they belong to different $l$ then they differ in the new horizontal edge system. If j and $l$ are the same then they are counted in the sum, i.e. H=1, only in the case if the end stage is Bs(n,k). In this case the two edge system differs at the selection of vertical void edges. This means either x is different for the two systems or the selection from the possible number of horizontal edges (Voids(k,j, $l$)) is different. This way, the validity of formula (11) is proven.

The recursion character of formula (11) is reflected by the fact that its right hand side consists of the number of models IN only for the $(m-1)^{th}$ story, but for different number of open edges, while the left hand side gives the number of models for the $m^{th}$ story.

To start the recursion, some initial values for the number of models IN establishing the Bs(n,k) end wet point system are needed. Because for the first row ($n_x = 1$) all the points are wet, for the first story (the $n_x \leq 2$ points) Bs(n,k) is regulated exceptionally by the presence or absence of vertical edges, i.e.

$$IN_{Bs(n,k)}(N_n(1), i) = \begin{cases} 1 & \text{if } i = |k| \\ 0 & \text{otherwise} \end{cases} \quad 12$$

Having the initial value from eq. (12) for m=1 and the recursive step given by eq. (11), the number of models IN, which is described at (10), can be calculated, up to the $n^{th}$ story.

This recursive algorithm requires solving by computer the applied logical function H and

integer function Voids. Both depend on the new end stage of wet points Bs(n,k), the old one Bs(n,j) and the system of selected horizontal edges Bs(n-1, *l*). There is no major difficulty in these steps. Moreover, their value is not a function of m and therefore there is no need to calculate them only at the first step of the recursion.

The solution of the recursive formula (11) requires a sequence of tables, having $2^n$ rows for all the different Bs(n,k) values and a changing number of columns. For m = 1, the number of columns is n+1 (we have 0, 1,.. n number of open edges for the first story). For m=2, according to eq. (7), this number increases by 2n-1, the number of possible new open edges, up to m = n, when we have $N_n(n) + 1$ columns. To fill up the next table we only need the previous one.

| | m=1 | ... | m=n |
|---|---|---|---|
| k lkl Bs(n,k) | $0 \le i \le N_n(m)$ | | |
| | $lN_{Bs(n,k)}(N_n(m),i)$ | | |
| | $C(N_n(m),i)$ | $2^{N_n(m)}$ | |

Fig. 5. The structure of Table 1, notations are given by the nomenclature.

The structure of this sequence of tables, with the introduced mathematical notations, is shown in Fig. 5. The three header columns describe the resulting binary sequence of wet points, while for m = 1, m = 2, ... m = n the sub-tables of the sequence of tables are obtained one by one. In each sub-table, the values show the number of different models given by different open edge systems, which give the given Bs(n,k) end wet stage with exactly i number of open edges. The sum of each column is $C(N_n(m), i)$, because $0 \le k \le 2n - 1$ describes all the possible end wet stages. These numbers give the last row, while their total is evidently the sum of all the possible different models of edge systems, i.e. $2^{N(m)}$. This number is given as the last number of the last row for each sub-table.

Table 1 reflects the results of the whole process of calculations for n = 3. In the table, Bs(n,k) and the $m^{th}$ story of 3-story hydraulic ladder is given in graphical form. The sub-table belonging to m=1 is given by initial values of eq. (12). The consecutive ones are the result of application of the main recursive formula (11). The last row, which is the sum of the values in the corresponding column, is the $C(N_n(m), i)$ coefficients, and is used to confirm that the program solution of formula (11) is correct. Direct checking of the smaller values, observing some symmetricity in the table and the rigorous inner check of program code are convincing as to the validity of our calculations.

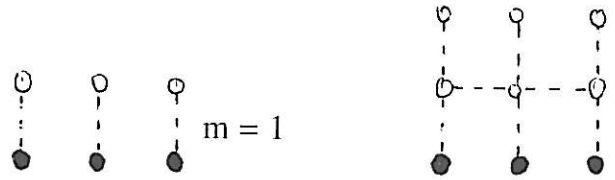
An example of reading data from the table is as follows. The numerical value 209 in the first row of the third sub-table means that selecting 8 open edges out of the 13 potential edges, which can be done C(13,8) = 1287 different ways, 209 models do not establish hydraulic connection between the faces.

Tables belonging to higher n values can be created similarly. Before reaching the limit of the necessary amount of memory or processing time, the following difficulty is met. The highest integer which can be represented on four bytes is about $2^{32}$, while the maximum number of models falling into the same category can be higher than $2^{32}$, which means the answer can not be received in exact integer terms. From this n value less accurate real numbers can be applied for getting the classification of models. Working with four bytes integers, the necessity of real numbers comes up at n =5. For n=4 e.g. selecting 13 open edges out of the $4^2 + 3^2 = 25$, which can be done C(25,13) = 5 200 300 by different ways, the number of impermeable models is 2 211 406.

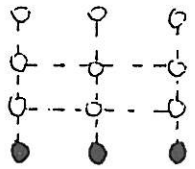
## Analysis of the Results

Table 1 gives the probability of having all the end points dry (k = 0) as a function of the probability, that a randomly selected edge is open. First probability is given by the ratio of favourable models to all possible models, i.e. by the ratio of the first row to the last row in the last, m = n, sub-table of Table 1. The second probability is given by eq. (6), by the $i/[n^2+(n-1)^2]$ ratio. The functional relationship between the dependent variable probability of the rock being impermeable and the independent probability of the edge being open is given on (Fig. 6) for n = 2, 3 and 4 values. The probability distributions for different n values are

**Table 1. Sequences of tables belonging to the 1st, 2nd and 3rd story of hydraulic ladder of 3-story (2D, n=3), describing the distribution of models.**




| k | \|k\| | Bs(n,k) | 0 | 1 | 2 | 3 | | 0 | 1 | 2 | 3 | 4 | 5 | 6 | 7 | 8 | |
|---|---|---|---|---|---|---|---|---|---|---|---|---|---|---|---|---|---|
| 0 | 0 | | 1 | 0 | 0 | 0 | | 1 | 8 | 25 | 34 | 14 | 2 | 0 | 0 | 0 | |
| 1 | 1 | | 0 | 1 | 0 | 0 | | 0 | 0 | 1 | 7 | 16 | 7 | 1 | 0 | 0 | |
| 2 | 1 | | 0 | 1 | 0 | 0 | | 0 | 0 | 1 | 8 | 17 | 7 | 1 | 0 | 0 | |
| 4 | 1 | | 0 | 1 | 0 | 0 | | 0 | 0 | 1 | 7 | 16 | 7 | 1 | 0 | 0 | |
| 3 | 2 | | 0 | 0 | 1 | 0 | | 0 | 0 | 0 | 0 | 3 | 12 | 6 | 1 | 0 | |
| 5 | 2 | | 0 | 0 | 1 | 0 | | 0 | 0 | 0 | 0 | 1 | 9 | 5 | 1 | 0 | |
| 6 | 2 | | 0 | 0 | 1 | 0 | | 0 | 0 | 0 | 0 | 3 | 12 | 6 | 1 | 0 | |
| 7 | 3 | | 0 | 0 | 0 | 1 | | 0 | 0 | 0 | 0 | 0 | 0 | 8 | 5 | 1 | |
| | | | 1 | 3 | 3 | 1 | 8 | 1 | 8 | 28 | 56 | 70 | 56 | 28 | 8 | 1 | 256 |




| k | \|k\| | Bs(n,k) | 0 | 1 | 2 | 3 | 4 | 5 | 6 | 7 | 8 | 9 | 10 | 11 | 12 | 13 | |
|---|---|---|---|---|---|---|---|---|---|---|---|---|---|---|---|---|---|
| 0 | 0 | | 1 | 13 | 78 | 283 | 677 | 1078 | 1089 | 629 | 209 | 38 | 3 | 0 | 0 | 0 | |
| 1 | 1 | | 0 | 0 | 0 | 1 | 12 | 64 | 183 | 277 | 184 | 64 | 12 | 1 | 0 | 0 | |
| 2 | 1 | | 0 | 0 | 0 | 1 | 14 | 77 | 211 | 298 | 188 | 64 | 12 | 1 | 0 | 0 | |
| 4 | 1 | | 0 | 0 | 0 | 1 | 12 | 64 | 183 | 277 | 184 | 64 | 12 | 1 | 0 | 0 | |
| 3 | 2 | | 0 | 0 | 0 | 0 | 0 | 2 | 23 | 96 | 186 | 138 | 53 | 11 | 1 | 0 | |
| 5 | 2 | | 0 | 0 | 0 | 0 | 0 | 0 | 4 | 40 | 120 | 103 | 44 | 10 | 1 | 0 | |
| 6 | 2 | | 0 | 0 | 0 | 0 | 0 | 2 | 23 | 96 | 186 | 138 | 53 | 11 | 1 | 0 | |
| 7 | 3 | | 0 | 0 | 0 | 0 | 0 | 0 | 0 | 3 | 30 | 106 | 97 | 43 | 10 | 1 | |
| | | | 1 | 13 | 78 | 286 | 715 | 1287 | 1716 | 1716 | 1287 | 715 | 286 | 78 | 13 | 1 | 8192 |

similar. The only two non-trivial probabilities belonging to n = 2, fall very close to the distribution curve belonging to n = 4. This indicates that there is no need to increase n further to estimate higher n probability distributions. The curve tells that if P(edge is open) = 6/25 = .24 then the conditional probability P(rock is impermeable) = .993. If half of the edges are open, then the number of permeable and impermeable models are equal for the examined two-dimensional rock model.

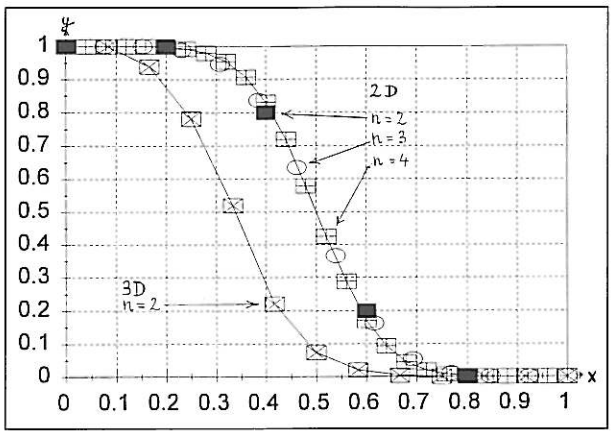



Fig. 6. Probability distribution curves for the hydraulic network in two and three dimensions with different number of story. x axis shows the probability that the edge is open, while y axis gives the probability that the rock is impermeable.

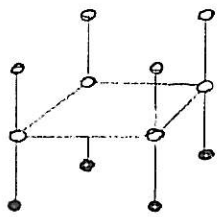
The high stability of the probability distributions of Fig. 6. obtained for the hydraulic ladder of n-story is convincing and that the required distribution from low n values can be obtained. Applying this experience to the 3-dimensional problem of the hydraulic network of n-story, instead of solving by a computer the recursive formula analogue to that of given by formula (11), direct computer program for the 2-story hydraulic network was made. There is no major difficulty in the development of this program, but it does not allow generalisation for any higher n. Indeed, the direct program ran 0.16 seconds on a Pentium processor for n = 2. For n = 3, according to the estimation made using eq. (5), the computer time would be $2*8/3*2^{51-12}$ times longer, which is more than $10^4$ years.

Results of this 3-dimensional analysis are given in Table 2. According to formula (5), with n = 2, the model has 12 edges. The 16 possible end stages of wet points are indicated in Table 2 by small drawings, without repetition of the symmetrical ones. The very last row of Table 2 gives the required probabilities. The probability distribution belonging to the 3-dimensional hydraulic network is also represented (Fig. 6). Comparing the 3-dimensional distribution with the two-dimensional one, indicates that while for the 2-dimensional case, when half of the edges are open, there is an equal chance for the rock being permeable or impermeable. In the 3-dimensional case one third of the edges open makes these probabilities equal. If only 1/6 part of the edges are open, i.e. P(edge is open) = .166, then P(rock is impermeable) = .939 which means a confidence level of .939 one can declare the rock is

**Table 2. Distribution of models for the hydraulic network of 2-story (3D, n=2).**

m = 2

| k | \|k\| | Bs(n²,k) | 0 | 1 | 2 | 3 | 4 | 5 | 6 | 7 | 8 | 9 | 10 | 11 | 12 | |
|---|---|---|---|---|---|---|---|---|---|---|---|---|---|---|---|---|
| 0 | 0 | | 1 | 12 | 62 | 172 | 257 | 176 | 68 | 16 | 2 | 0 | 0 | 0 | 0 | |
| 1 | 1 | | 0 | 0 | 1 | 12 | 56 | 119 | 87 | 34 | 8 | 1 | 0 | 0 | 0 | |
| 2 | 1 | | 0 | 0 | 1 | 12 | 56 | 119 | 87 | 34 | 8 | 1 | 0 | 0 | 0 | |
| 4 | 1 | | 0 | 0 | 1 | 12 | 56 | 119 | 87 | 34 | 8 | 1 | 0 | 0 | 0 | |
| 8 | 1 | | 0 | 0 | 1 | 12 | 56 | 119 | 87 | 34 | 8 | 1 | 0 | 0 | 0 | |
| 5 | 2 | | 0 | 0 | 0 | 0 | 1 | 18 | 72 | 64 | 30 | 8 | 1 | 0 | 0 | |
| 3 | 2 | | 0 | 0 | 0 | 0 | 3 | 26 | 83 | 70 | 31 | 8 | 1 | 0 | 0 | |
| 6 | 2 | | 0 | 0 | 0 | 0 | 3 | 26 | 83 | 70 | 31 | 8 | 1 | 0 | 0 | |
| 9 | 2 | | 0 | 0 | 0 | 0 | 3 | 26 | 83 | 70 | 31 | 8 | 1 | 0 | 0 | |
| 12 | 2 | | 0 | 0 | 0 | 0 | 3 | 26 | 83 | 70 | 31 | 8 | 1 | 0 | 0 | |
| 10 | 2 | | 0 | 0 | 0 | 0 | 1 | 18 | 72 | 64 | 30 | 8 | 1 | 0 | 0 | |
| 7 | 3 | | 0 | 0 | 0 | 0 | 0 | 0 | 8 | 58 | 58 | 29 | 8 | 1 | 0 | |
| 11 | 3 | | 0 | 0 | 0 | 0 | 0 | 0 | 8 | 58 | 58 | 29 | 8 | 1 | 0 | |
| 13 | 3 | | 0 | 0 | 0 | 0 | 0 | 0 | 8 | 58 | 58 | 29 | 8 | 1 | 0 | |
| 14 | 3 | | 0 | 0 | 0 | 0 | 0 | 0 | 8 | 58 | 58 | 29 | 8 | 1 | 0 | |
| 15 | 4 | | 0 | 0 | 0 | 0 | 0 | 0 | 0 | 0 | 45 | 52 | 28 | 8 | 1 | |
| | | | 1 | 12 | 66 | 220 | 495 | 792 | 924 | 792 | 495 | 220 | 66 | 12 | 1 | 4096 |
| | | | 1 | 1 | .939 | .782 | .519 | .222 | .074 | .020 | .004 | 0 | 0 | 0 | 0 | |



n = 2

impermeable. On the other hand, just with the half of edges open, i.e. P(edge is open) = .5, it can be declared that the rock is permeable with the confidence level 1-.074 = .926. If the ratio of open edges is between 1/6 and 1/2 then judgement can not be made about the permeability character of the rock without having a more detailed knowledge of the inner structure of the cementation or shaliness of the sedimentary rocks.

## CONCLUSIONS

1- Complex questions related to the permeability of sedimentary rocks require adequate mathematical models on the basis of the theory of probability.

2- Probabilistic model with a relatively low number of random edges can give a correct answer.

3- Assuming cubic-like arrangement for the pore and pore connection system with randomly selected open edges (connections), and taking a cubic sample from such kind of theoretical rock, analysis of the probability distribution revealed that if only 1/6 of the channels are open the rock is impermeable but if 1/2 of the channels are open the rock is permeable.

## NOMENCLATURE

$n_x$, $n_y$, $n_z$ number of pores in cubic structure in x, y, z directions, respectively

$i_x$, $i_y$, $i_z$ running indices for the pores, integer numbers, e.g. for the x direction, $1 \le i_x \le n_x$

$N_{edges}^{block}(n_x, n_y, n_z)$ number of edges (channels) for the 3D block

$N_{edges}^{rect}(n_x, n_y)$ number of edges (channels) for the 2D block (rectangle)

n number of pores in the x and y directions (3D case), or in the x direction (2D case)

$N_{edges}^{hyd}(n, n, n+1)$ number of edges for the hydraulic network of n-story (3D case)

$N_{edges}^{lad}(n, n+1)$ number of edges for the hydraulic ladder of n-story (2D case)

C(n,k) number of combinations, selecting k objects out of n objects, regardless of the order of selection; C(n,k) = n! / ((n-k)!k!)

Bs(n,j) The binary sequence of 0-s and 1-s, which gives the $0 \le j \le 2^n - 1$ number in binary number system and which is filled up to n digits from the left by padding zeros if it is necessary. E.g. Bs(5,2) = (0,0,0,1,0).

|j| The number of units (1-s), necessary for describing number j in Bs(n,j). Note that |j| is not a function of n. Continuing the previous item of nomenclature, |2| = 1.

m is the $m^{th}$ story of hydraulic ladder of n-story.

i number of open edges in the $m^{th}$ story of hydraulic ladder of n story, $0 \le i \le N_n(m)$.

j, k describe the system of wet points of the $(m-1)^{th}$ and $m^{th}$ story, respectively, with the aim of Bs(n,j), Bs(n,k) binary sequences, $0 \le j \le 2^n-1$ or, what is the same, $0 \le |j| \le n$.

*l* describes those horizontal open edges, which are part of the $m^{th}$, but not part of the $(m-1)^{th}$ story of hydraulic ladder of n-story, with the aid of binary sequence Bs(n-1,*l*), $0 \le l \le 2^n - 1$ or $0 \le |l| \le n-1$.

x number of those open vertical edges, which are part of the $m^{th}$, but not part of the $(m-1)^{th}$ story of hydraulic ladder of n-story, and, which do not contain wet point as an end point.

$|N_{Bs(n,k)}(N_n(m), i)$ the number of those different open edge systems (network models), which create (give) the Bs(n,k) wet point system for the $m^{th}$ story of hydraulic ladder of n story, and which contain exactly i open edges.

$H_{Bs(n,k)}$ (Bs(n,j), Bs(n-1,*l*)) Logical function, assuming only values 0 or 1. H assume 1, if the Bs(n-1,*l*) horizontal open edge system connects the Bs(n,j) wet points to all the points, which are directly under (in -z direction) the Bs(n,k) wet points. H is 0 otherwise.

Voids(k,j,*l*) is the maximum value for x.

## REFERENCES


[1] Amyx J.W., Bass D.M., Whiting R.L., 1960. *Petroleum Reservoir Engineering*, McGraw-Hill Book Company.

[2] Broadbent S.R., 1954. Discussion on Symposium on Monte Carlo Methods. *J.Roy. Statistic. Soc. B.* 68 p.

[3] Dullien F.A.L., 1992. *Porous Media. Fluid Transport and Pore Structure.*, (2nd ed.), Academic Press, New York.

[4] Korvin G., 1992. A percolation model for the permeability of kaolinite-bearing sandstones. *Geophysical Transactions* **37**, 2-3, 177-209, Budapest.

[5] Perrodon A., 1983. *Dynamics of Oil and Gas Accumulations*, ELF Aquitaine, page 93.

[6] Seliakov V.I. and Kadet V.V., 1996. *Percolation Models for Transport in Porous Media*. Kluwert Academic Press, Dordrecht- Boston- London.

[7] Stauffer D. and Aharony A., 1992. *Introduction to Percolation Theory*, Taylor and Francis, London.

Petroleum Res. J. Vol. 11 (1999); P. 13-17, 4 Figs.

# Interpretation of Gravity Data in the Murzuq Basin, SW Libya

A. Sahil* and C. Ebinger**

# تفسير معلومات الجاذبية في حوض مرزق بجنوب غرب ليبيا

أحمد صاهيل و سندي أبنجير

الخريطة البوجيرية المستنبطة من معلومات الجاذبية المتوفرة عن حوض مرزق تبين وجود بروز في اتجاه الشمال الشمال الغربي – الشمال والشمال الشرقي. الجهة الشمالية الشرقية والشمالية من حواف حوض مرزق لها درجة ميلان شديدة، أما في منتصف الحوض فإن قيمة الشاذة السالبة التي مداها 50 مليجال مرتبطة أساساً بالجزء الأكثر عمقاً بالحوض. توضح معلومات الجاذبية أن الصخور القاعيّة ضحلة في الجزء الشمالي والشمالي الغربي من الحوض حيث لوحظ أن هناك إزدياد للقيم نحو الشمال، أما الحافة الغربية للحوض فقد لوحظ أن لها ميلان شديد وقد يعزى هذا الميلان إلى كثافة المعلومات المغطى. تم تطبيق طريقة المشتقة الأفقية على المعلومات البوجيرية للجاذبية لتحديد التراكيب الجيولوجية وتبين الخريطة المستنبطة من المشتقة الأفقية وجود قيم عالية لدرجة الميلان في الاتجاه الشمال الشرقي – الجنوب الغربي والتي بدروها تحدد حواف الحوض في الجهة الشرقية أما الاتجاه الشرقي – الشمال الشرقي والغربي – الجنوب الغربي في الجهة الشمالية من الحوض فله علاقة بالصدوع السطحية والتحت سطحية الموجودة بالمنطقة.

**Abstract:** *A Bouguer gravity map of Murzuq Basin, produced from the compilation of available data, shows prominent NNW and NNE trends. The northeastern and northern flanks of the Murzuq Basin are marked by steep gradients. In the central part, a negative anomaly of amplitude ca. 50 mGal is associated with the deepest part of the basin. The gravity data suggest the basement is shallower in the north and northwest since the values increase northwards. The western flank is marked by a steep gradient that may be related to data coverage. Horizontal derivative method was applied to the Bouguer gravity data to delineate subsurface structures. The total horizontal derivative map shows high gradient values with NE-SW trends which mark the boundary of the basin in the east. The ENE-WSW anomaly trends in the north may be related to fault structures on the surface and subsurface.*

## INTRODUCTION

The Murzuq Basin covers an area of about 250,000 km$^2$. Even though exploration activity in Libya started more than 40 years ago, little is known about this basin because all the activity was concentrated in the Sirt and Ghadamis basins which are the main petroleum producing basins of Libya.

This study involves the analysis of gravity data from the Murzuq Basin and surrounding area. The gravity data were collected from different sources,

*Petroleum Research Centre, P.O. Box 6431, Tripoli, Libya
**University of Leeds, Department of Earth Sciences, LS2 9JT, UK

i.e. Africa Gravity Project (AGP), Petroleum Research Centre (PRC), and Geodetic Survey Department of Libya (SDL). In total 17269 gravity values were assembled of which 1706 were taken from SDL, 5133 from PRC, and 10430 from AGP (Fairhead *et al.*, 1988).

The main purpose of this study is to compile all available gravity data in order to: a) better understand the tectonic evolution of the Murzuq Basin and b) to define more accurately and in more detail the border/regional interpretations of this area.

## GEOLOGICAL SETTING

Several authors have studied the tectonic history of the Murzuq Basin (Fig. 1). Unpublished works mainly concerned the geology of the Palaeozoic outcrops of the western and eastern flanks of the basin (Amoseas, 1958, Echikh and Suleiman,1984). Studies conducted by the Industry Research Centre were within the geological survey of Libya (Banerjee,1980).

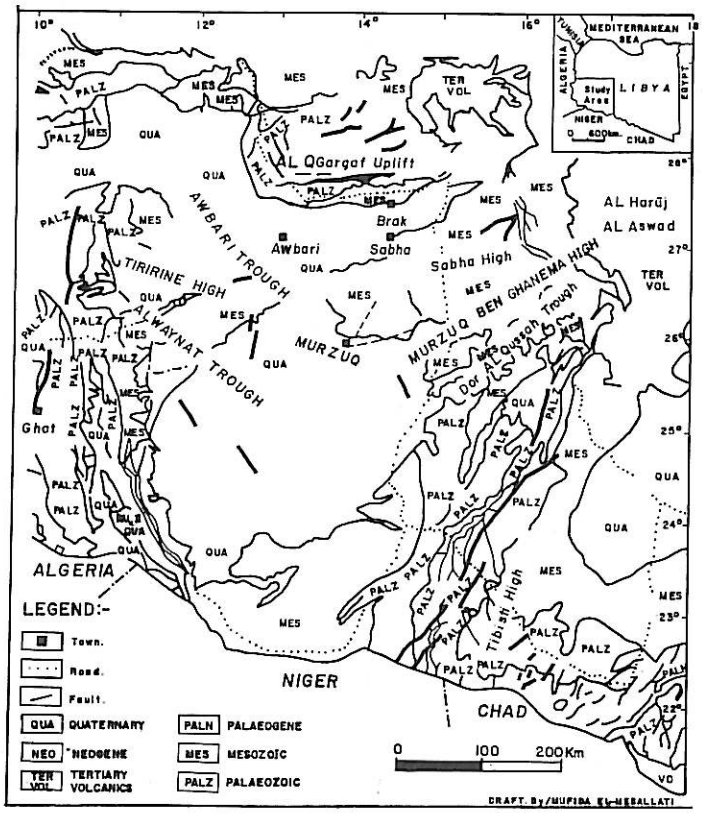



Fig. 1. Geologic sketch map of the Murzuq Basin.

The Murzuq Basin was subjected to three major periods of structural development (Klitzsch, 1969). The first stage started in Precambrian time with folding and consolidation. The second stage began in Cambrian time with the formation of northwest to north-northwest striking horsts which later, in Silurian and Devonian time, became the core of uplifts separated by troughs (Adamson *et al.*, 1998). The structural relief of early Palaeozoic time was the result of a northeast- southwest tension (Echikh and Sola,1998). The third stage was initiated during late Mesozoic time by the formation of the northeast trending uplifts and troughs (Glover, *et al.*, 1998). During Jurassic time or within the Jurassic-Cretaceous transgression, block faulting occurred along the edge of some uplifts.

Triangular shaped depression of the Murzuq Basin is bounded on the west and south by the Precambrian Hoggar and Tibisti massifs. On the north it is bounded by the Qargaf uplift, which separates it from the Ghadamis Basin and on the east by the Tibisti-Al Haruj uplift.

## GRAVITY DATA

The first compilation of the Bouguer gravity maps of Libya was prepared by Essed (1978), using data obtained from Shell Libya Oil Company, Libyan-American Oil Company, and Mobil Oil Company.

Thirty percent of the Murzuq Basin is covered by gravity surveys whose data are generally available only as simple Bouguer gravity anomaly maps. These maps have been prepared by petroleum companies alone in the 1950's, in their search for hydrocarbon accumulations. Most of the surveys were tied to the Potsdam base station at Tripoli airport, which has a value of 979538.80 mGals. The reduction of the gravity data to simple Bouguer anomaly maps for most of the surveys was carried out using the International Gravity Formula 1930 (IGF-30) and a reduction density of mostly 2200 kg/m$^3$. The Petroleum Research Centre digitized Bouguer anomaly maps to produce a gravity map of Libya. In 1985 the Geodetic Survey Department of Libya created a gravity network tied to the International Gravity Standardisation Network 1971 (IGSN 71). In

1988, the University of Leeds Industrial Services produced a gravity map of all Africa (AGP). All these values (Fig. 2) were recalculated using the Moritz (1984) gravity formula and 2670 kg/m$^3$ density to produce a Bouguer gravity map of the Murzuq Basin.

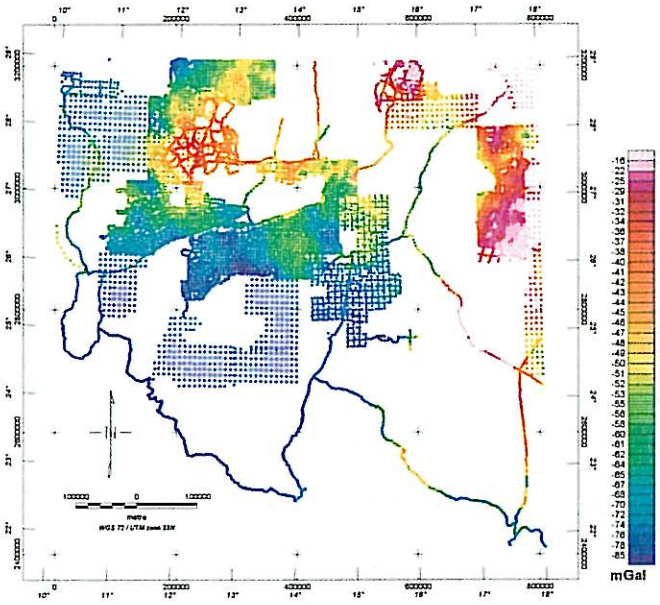



Fig. 2. Showing gravity station distribution in the Murzuq Basin.

## Adjustment to a Common Datum and Reduction Densities

All gravity data from SDL and PRC have been tied to the Geodetic Reference System 1980 (GRS 80), using the formula below (Moritz, 1984):

$$g_{th} = 9.780327(1+0.0053024 \sin\theta - 0.0000058 \sin 2\theta) \text{ m s}^{-2}$$

where $g_{th}$ is the theoretical gravity in m s$^{-2}$ (1 mGal $=10^{-5}$m s$^{-2}$) and $\theta$ is the latitude (in degrees) of the gravity station. The Bouguer gravity values were computed using a reduction density of 2670 kg/m$^3$. Most of gravity data have been converted from the gravity formula 1967 to the gravity formula 1980, using the formula below (Moritz, 1984):

$$g_{80}-g_{67} = (0.8316+0.0782\sin^2\theta - 0.0007 \sin^4\theta) \text{ mGal}$$

where $\theta$ is the latitude (in degrees) of the gravity station and $g_{80}$ gravity formula in 1980 and $g_{67}$ gravity formula in 1967.

## Projection, Gridding and Contouring

The software used for data manipulation and presentation in this study was the Geosoft PC program. This includes projection, gridding, contouring and plotting. The data were available with latitude and longitude locations. For mapping purposes, the UTM zone33° N Projection was chosen because the longitude range straddled more than one UTM zone. The actual gridder used was Geosoft's RANGRID, which begins with a coarse grid interval and successively refines it, using a minimum curvature criterion. It shows detail where it is existed without making pointlessly large grid files with strange "scars" along traverse lines. The chosen grid interval of 5 km honoured most detail in the point data without introducing gridding artefacts.

## Bouguer Gravity Map

The Bouguer gravity anomaly map of Murzuq Basin and surrounding areas (Fig. 3) shows that the gravity values are generally between -18 and -110 mGal. It shows two main positive trends of relative negative values. The first, is the northern part of the area with ENE trending gravity anomaly traversed by N-S trends. The second positive anomaly zone is in the eastern part of the study area where a generally NNE trend is superimposed

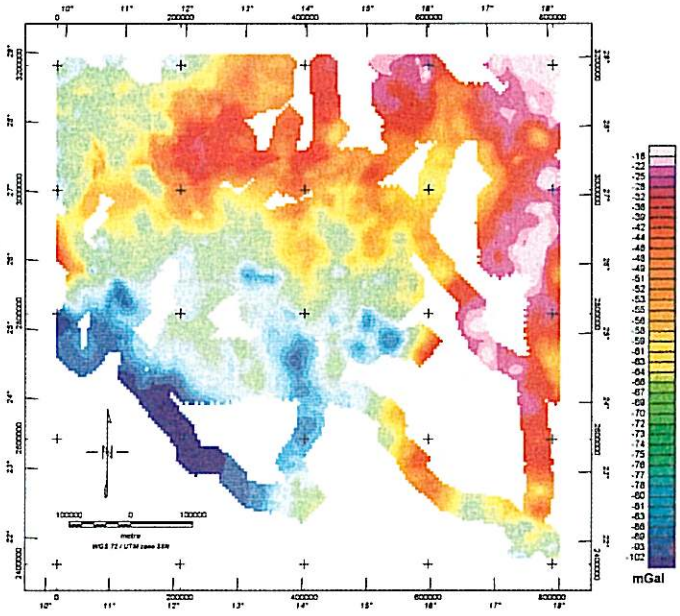



Fig. 3. Bouguer gravity map of the Murzuq Basin.

by smaller N-S oriented anomalies. These positive anomaly zones have strong gradients in the direction of Murzuq Basin, usually between the values -59 to -32 mGal. A negative anomaly covers the central and western part of the area, usually with gentle gradients between the values -66 to -102 mGal. Two extensions of this negative zone extend northward in the western part of study area with NE-SW orientations indicates the presence of another basin north of the Murzuq Basin.

## FILTERING TECHNIQUES

In order to delineate lithological boundaries and faults, a horizontal gradient technique was employed in the study area.

### Horizontal Derivative

The horizontal gradient method has been used for many years to locate density or susceptibility boundaries from gravity data (Cordell, 1979) or magnetic (as pseudogravity) data (Cordell and Grauch, 1982). These authors discussed a technique to estimate the location of abrupt lateral changes in magnetization or mass density of upper crust rocks. The method is normally applied to gridded data rather than profiles. Maximum magnitudes of horizontal gravity gradient normally occur above geological boundaries such as faults or steeply dipping lithological boundaries. However, in the Murzuq Basin, lithological boundaries within the sedimentary strata are subhorizontal, therefore, horizontal gradient anomalies are related to basin structures. Areas of steep lateral gradients have higher scalar amplitude values of horizontal gravity gradient (Blakely and Simpson, 1986).

The horizontal gravity gradient (Fig. 4) map shows that the northern and eastern parts of the basin are traversed by strong horizontal gradient anomalies. The central part of the basin can be divided into two parts (Fig. 4, area A1, A2): the eastern part (area A1) shows many short anomalies of NNE-SSW orientation; and the southwestern part (area A2) is relatively quiet.

A strong E-NE trending anomaly (Fig. 4, area B) cuts across the northern Murzuq Basin and seems to be the only continuous strong trend of

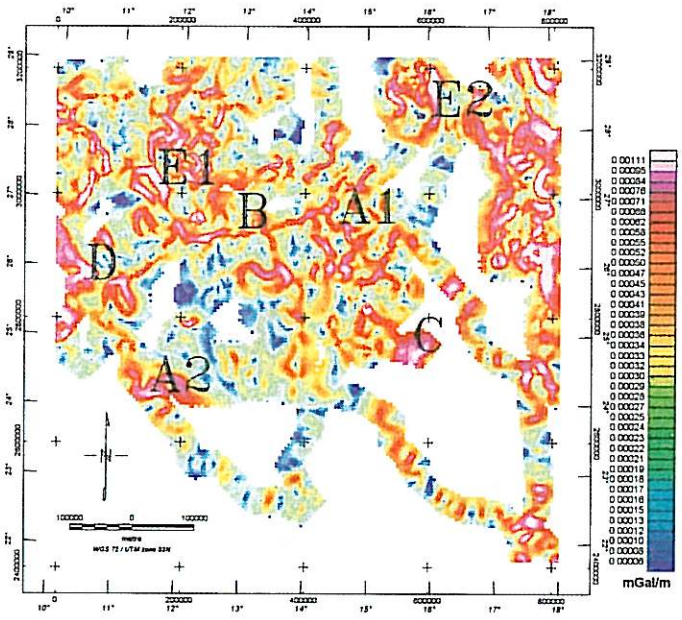



Fig. 4. Total horizontal derivative of gravity from the Murzuq Basin.

that direction. NE-SW (area C) -and NW-SE- (area D) trending anomalies are observed in the map area. North-south trends seem to be predominant in the northern part (areas E1, E2).

## CONCLUSIONS

Two main conclusions may be added to the scientific knowledge concerning the geology of the Murzuq Basin and surrounding area as produced from the results of the present research study. The boundary of the Murzuq Basin is better defined than before.

(1) The interpretation of the limited Bouguer gravity data with geological information from the Murzuq Basin has confirmed some geological concepts and brought to light new ideas in previous related geological information. However, the gravity data, in general, shows northeast-southwest trends in the eastern part of the area (Fig. 3) that are occasionally bounded by steep gradients which could indicate faulting. The high anomalies (-18 to -30 mGal) in the northeastern part of the study area are associated with shallow basement. In the northern part of the area, Bouguer anomalies range from -45 to -55 mGal, and are N-S oriented blocks extending across the Qargaf

uplift that may represent horst and graben structures. Negative anomalies ranging from -75 to -90 mGal values of north-northwest-south-southeast trend generally corresponding to the basin margin (Fig. 3). In the central and southern part of the study area, gravity values less than -85 mGal are associated with significant thickness of sedimentary cover (Fig. 3).

(2) Horizontal gradient results have been overlaid with geological information of the Murzuq Basin showing high gradient values trending NE-SW. NW-SE trends mark the boundary of the basin in the eastern and western part of study area (Fig. 4). New faults are ENE-WSW anomaly trends in the north part of the Murzuq Basin. In the northwest part of the study area, N-S oriented anomalies are probably fault blocks traversing the Qargaf uplift.

## ACKNOWLEDGEMENTS

The author (A.S.) wishes to express his gratitude to the management of the Petroleum Research Centre for supporting this research and providing the assistance in collecting the necessary gravity data. Thanks are also extended to Dr. Ebinger for her supervision during the period of MPhil research and to Prof. Fairhead for providing the gravity data.

## REFERENCES

Adamson, K., Glover T., Fitches B., Whittington R., Craig J. and Rushworth D., 1998. Controls in sequence development of Devonian units of the Murzuq intracratinic Basin southwest Libya. In: *The Geological Conference on Exploration in Murzuq Basin.* p.7(abstr.)

Amoseas, 1958. *Interpretation Report of an Airborne Geophysical Survey of the Fezzan-Libya* by Hunting Geophysics Ltd. Unpubl. report.

Banerjee, S., 1980. Stratigraphic lexicon of Libya. *Ind.Res.Cent. Bull.*, **13,** 300p.

Blakely, R. J., and Simpson, R. W., 1986, Locating edges of source bodies for magnetic or gravity anomalies: *Geophysics*, **51,** 1489-1498.

Cordell, L., 1979. Gravimetric expression of graben faulting in Santa Fe country and the Espanola Basin, New Mexico: Guidebook, 30th Field conf., Santa Fe Country, *N.Mex-Geol. Soc.*, 59-64.

Cordell, L., and Grauch, V.J.S., 1982. Mapping basement magnetization zones from aeromagnetic data in the San Juan basin, *New Mexico* (abstr.): *Abstr.Program, SEG, 1982 Annu. Meet.*, 246-247.

Echikh, K. and Sola, M., 1998. Geology and hydrocarbon occurrences in the Murzuq Basin southwest Libya. In: *The Geological Conference on Exploration in Murzuq Basin.* p.2(abstr.)

Echikh, K. and Suleiman, S., 1984. Geological study and petroleum evaluation of Murzuq Basin. *Unpublished Report. National Oil Corporation, Libya*,1984.

Essed, A., 1978. A Reconnaissance Bouguer Gravity Anomaly Map of Libya. *Unpubl. M.Sc., thesis Purdue University, USA.*

Fairhead, J. D., Watts, A. B., Chevalier, P., El-Haddadeh, B., Green, C. M., Stuart, G.W., Whaler, K. A., and Windle, I., 1988. African gravity project technical report, *University of Leeds Industrial Service Ltd, UK.*

Glover, T., Adamson, K., Fitches, B., Whittington, R., and Craig, J., 1998. Intraplate deformation in the Murzuq intracratonic Basin. S.W. Libya. In: *The Geological Conference on Exploration in Murzuq Basin. p.18*(abstr.)

Klitzsch, E., 1969. The structural development of parts of North Africa since Cambrian time ; in Gray,C.,ed., *Symposium on the Geology of Libya*: Faculty of Science, University of Libya, 253-262.

Moritz, H., 1984. Geodetic reference system 1980, *Bull., Geode'sique*, **58,** 388-393.

Petroleum Res. J. Vol. 11 (1999); P. 19-25, 1 Fig.

# Refining of Libyan Kerosene for Use as a Solvent for Pesticide

Latif H. Ali*, Moftah O. Darwish* and Esmail O. Elakesh*

# تنقية الكيروسين الليبي لغرض إستعماله مذيباً في خلطة مبيدات الحشرات

لطيف حميد علي ومفتاح عمر الدرويش وإسماعيل عمر العكش

تعد عمليات خفض محتوى الكربون العطري وإزالة الرائحة الغير مقبولة من المشتقات النفطية ذات أهمية بالغة نظراً لطبيعة إستعمالاتها، حيث تستخدم من بين إستعمالاتها بنسبة 30% في خلطة المواد القاتلة للحشرات إضافة إلى استعمالاتها العادية الأخرى في التدفئة والطبخ... إلخ.

لقد تحقق في هذه الدراسة تقليصاً فعالاً لمحتوى الكربون العطري وإزالة تامة للرائحة من كيروسين خام السرير باستعمال مواد مازة صلبة مثل الكربون المنشط وتحسنت نتائج عمليات التنقية أكثر بمرافقة الكربون المنشط مع مواد مازة صلبة أخرى مثل هلام السليكا والألومينا.

تم خفض محتوى الكربون العطري إلى 1% بمعاملة نسبة وزنية بمقدار 1:1 من كيروسين خام السرير إلى مزيج المواد المازة والتي احتوت على 14% كربون منشط و43% سليكا و43% ألومينا ضمن هذا المزيج.

توضح هذه النتائج تفوق عملية إزالة المواد العطرية بالمواد المازة الصلبة مقارنة بإزالتها بالاستخلاص بالمذيبات الإنتقائية مثل مادة مثيل البيراليدينون (NMP) على إن الاستخلاص بهذا المذيب مكّننا من فصل وتعريف عدة مركبات أحادية وثُنائية الحلقة الأروماتية في مشتق الكيروسين من خام السرير وقد تم تعريف هذه المركبات بواسطة التحليل بتقنية كروموتوغرافيا الغاز وبمطابقة نتائج هذا التحليل مع نتائج قياس مركبات أروماتية معروفة.

---

**Abstract:** *Reducing aromatic carbon content and removal of obnoxious odour are operations of prime importance for the purpose of domestic use of petroleum derived materials such as kerosene. This derivative is widely used as a solvent for pesticides and usually represents about 30% of the total formulation.*

*Effective reduction of aromatic carbon content and removal of bad odour from Sarir kerosene was achieved by using solid adsorbents, mainly activated carbon (AC). Attainment of improved results was possible by synergism between AC, silica and alumina adsorbents. Thus, removal of bad odour and reduction of aromatic carbon content to 1% was possible by a 1:1, volume to weight ratio of kerosene to combined adsorbents weights; activated carbon (14%), silica (43%)and alumina (43%).*

*The use of solid adsorbents for dearomatization was superior to solvent extraction by N-methyl pyrrolidinone (NMP). Meanwhile, extraction by NMP enabled the identification of several mono- and di-ring aromatic compounds in Sarir kerosene by capillary gas chromatography. The*

*Petroleum Research Centre, P.O. Box 6431, Tripoli, Libya

*identification was ascertained by matching with authentic aromatic compounds.*

## INTRODUCTION

Kerosenes represent a class of the most widely used solvents for pesticides. Libya imports several hundred tons per year of expensive, special grade kerosene for the manufacturing of pesticides. Petroleum naphtha in the kerosene range from most libyan crude oils, which are known to be paraffinic in nature and contain low sulfur percentages, are expected to be suitable solvents for pesticides after some mild treatment.

The presence of sulfur in kerosene, and especially in the form of mercaptans, is detrimental to its use as a pesticide solvent because of unacceptable bad odour. Another important aspect is the aromatic carbon content which should be reduced to a minimum permissible limit because of potential health hazards [1]. It is well established that mono - and di- ring systems comprise the aromatic carbon content, which ranges between 10 to 20 % in most kerosenes [2]. It is thus expected that the main obstacles encountered in the use of Llibyan kerosenes as solvents for pesticides are the following:

1. Proper choice of the kerosene source.
2. Reducing aromatic contents to permissible limits.
3. Removal of bad odour.

The specifications of the imported kerosene [3] and relevant characteristics of some Libyan kerosenes [4] and methods of their determinations are given in Table 1.

Perhaps it is imperative to give a few words on the standard methods of aromatic carbon content determination in petroleum fractions. The ASTM-D 1319-77 (IP:156/70) measures volume percent of aromatic carbon content after development and elution according to specified standard steps. This means that aliphatic carbon in olefinic, alkylenic and naphthenic substituents on the aromatic rings are included in the aromatic carbon content. Added to this, and as stated in this particular standard method, all sulfur, nitrogen and oxygen compounds are also included in the aromatic carbon content. This is so, since these compounds have similar adsorption affinities on silica gel when they are desorbed by isopropyl alcohol. Another shortcoming of the method is that the fluorescent dye indicator (Petrol Red AB4) is quite sensitive and should be stored in the dark under nitrogen atmosphere. Even with such precautions, batches stored over six months should be considered suspect. One final important point concerning this method, is that the determination of the PONA (Paraffin, Olefin, Naphthene and Aromatic) layer boundaries is subject to human error since these boundaries are assessed and observed by the analyser's naked eye.

A modification of the ASTM method was registered in 1989 [ASTM-D1319-89;IP156/84]. This modification put further limitations on the applicability of the method. The method will not be precise for aromatic carbon concentration of less than 5%. Since in our work we intend to achieve aromatic carbon concentrations much lower than 5%, thus this standard method is of no use to us. We successfully developed a new spectroscopic method which measures the actual aromatic carbon content with no interference from substituted, olefinic, alkylenic, or naphthenic carbons on the aromatic rings [5]. Also, interference from heteroatoms (S,O,N) is excluded. The new method gives the following relationship for the determination of the percentage of the real aromatic carbon content (CA).

$$\% \text{ CA} = 1.053 \sum_{250}^{290} A + 0.0196$$

CA = Carbon in mono-and di-aromatic ring systems.

$\sum_{250}^{290} A$ = Summation of the Absorbance values of the total aromatic envelope measured at:

$\lambda$ = 250, 260, 270, 280 and 290 nanometers.

Specialty grade kerosenes can be produced by a special hydro-treating operation (chemical refining) at the refinery. However, and to the best of our knowledge, such a refining line is non-existent at the Libyan refineries. In the present paper, the results of an alternative physical refining scheme are cited.

**Table 1. Specifications of imported kerosene and relevant values of some Libyan kerosenes**

| Specification | Imported kerosene (Typical value) | Libyan kerosenes | | | | Determination method |
|---|---|---|---|---|---|---|
| | | Sarir | Brega | Sedra | Hamada | |
| Density $g.cm^{-3}$ at 15°C | 0.793 | 0.793 | 0.800 | 0.809 | 0.798 | ASTM D1298 |
| Total sulfur % | 0.0002 | 0.03 | 0.06 | 0.14 | 0.03 | ASTM D1266 |
| Mercaptic sulfur, ppm | - | 3 | 3 | 89 | 3 | ASTM D3227 |
| Flash point °C | 53 | 66 | 65 | 66 | 65 | IP 170 |
| Aromatics, wt % | 1.5 | 9.0 | 13.6 | 14.6 | 10.2 | ASTM D1319 |
| Distillation: | | | | | | ASTM D86 |
| IBP°C | 155 | 192 | 188 | 188 | 188 | |
| 50 % vol. °C | 203 | 202 | 202 | 202 | 202 | |
| 95 % vol. °C | - | 220 | 221 | 221 | 236 | |
| FBP °C | 253 | 233 | 227 | 225 | 236 | |

Experiments were designed to arrive at solutions for the reduction of the aromatic carbon content to acceptable limits and the removal of bad odour from Sarir kerosene since it possesses the most proper characteristics as inferred from Table 1. Emphasis was on operations that achieve both goals simultaneously. Thus, attention was focused on refining by solid adsorbents. Further justification for this choice will be given later in the discussion section.

## EXPERIMENTAL

### Refining of Crude Sarir Kerosene (CSK) by Commercial Activated Carbon

10 g of granulated activated carbon (AC) was packed in a 30 x 1.6 cm glass column and 100 ml of crude Sarir kerosene was eluted through the AC bed. Rate of elution was 3 ml per minute and room temperature was 23°C. 10 ml fractions were collected in clean test tubes and aromatic carbon content was determined at certain kerosene: AC, vol. to wt. ratios.

### Refining of CSK by Petroleum Research Centre (PRC) - Prepared Activated Carbon

5 g of PRC-AC was packed in the same glass column as above, and 50 ml of crude Sarir kerosene was eluted through it at a flow rate of 3 ml. $min^{-1}$, at room temp. (25°C). Fractions (5 ml each) were collected and aromatic carbon content was determined.

### Refining of CSK by Commercial -AC with Mechanical Mixing at Elevated Temperatures

(a) 15 ml of crude Sarir kerosene was mixed with 5 g of comm.-AC in a 100 ml conical flask. The mixture was agitated for 15 min. in a thermostated box agitator at 60°C. Kerosene was filtered and aromatic carbon content was determined.

(b) In a similar experiment as in (a) above, agitation was carried out at 90°C, followed by filtration and aromatic carbon content determination.

**Refining of CSK by Activated Silica - Alumina Adsorbents**

5 g silica (thermally activated 1h at 110°C) + 5 g alumina (thermally activated 1h at 200°C, were packed in the same 30 x 1.6 cm glass column. Crude Sarir kerosene (100 ml) was eluted through the chromatographic bed at an uncontrolled rate of 0.5 ml. $min^{-1}$ at room temperature of 25°C. Ten fractions (10 ml each) were collected and aromatic carbon content was determined.

**Refining of CSK by Combined Silica - Alumina - AC Bed**

Thermally activated Comm. AC, was stationed at the lower part of a 50 x 1.6 cm glass column. Two millimeter glass wool cover was positioned on top of the AC layer followed by activated $SiO_2$ (15 g) and $Al_2O_3$ (15 g). Crude Sarir kerosene (100 ml) was eluted through the combined bed and the first five 10 ml fractions were examined for their aromatic carbon content.

**Refining of CSK by N-Methyl Pyrrolidinone (NMP)**

A series of solvent extraction experiments were carried out by mixing certain volumes of kerosene (K) and NMP as given below:

(a) 40 ml K + 20 ml NMP
(b) 20 ml K + 20 ml NMP
(c) 20 ml K + 40 ml NM
(d) 20 ml K + 80 ml NMP

The mixtures were shaken 30 minutes at 60°C in a thermostated agitating box. The solutions were cooled, kerosene layer was separated and aromatic carbon content was determined.

**Spectroscopic Determination of Aromatic Carbon Content (CA) in Kerosene (K)**

One milliliter (accurately measured) of the Kerosene sample was dissolved in 500 ml of iso-propyl alchohol (IPA) in a volumetric flask, and the ultra-violet (UV) spectrum of the solution was obtained; against IPA in the reference cell; in the range 400-200 nanometer. The absorbance values at 250, 260, 270, 280 and 290 nm were used to calculate the percentage of carbon in aromatic rings according to an already published mathematical relationship [6].

**Determination of Some Aromatic Compounds in Sarir Kerosene by Gas Chromatography**

20 ml of crude Sarir kerosene sample were extracted with 60 ml of NMP at room temperature (25°C). NMP extract was directly injected in a capillary GC column operating under the following conditions:

GC column: CP-Sil 5 CB; 50 m X 0.32 mm, df = 0.12 μm
Conditions: inj. temp. 300°C, detect temp. 300°C, rate/rise 5°C/min.
Instrument: Packard GC Mod. 439.

Peak assignment was obtained by running authentic aromatic, mono-and di-ring, compounds under identical conditions.

**Removal of Bad Odour from Crude Sarir Kerosene**

Complete removal of obnoxious odour affected by stirring 25 ml of crude Sarir kerosene with 1g of activated carbon, followed by filtration of the odourless kerosene. The operation was carried out at room temperature.

## RESULTS

The results of refining of crude Sarir kerosene by elution on a chromatographic bed of commercial activated carbon (comm. AC) and PRC prepared activated carbon (PRC-AC) [6] are given in Table 2. This table also gives the results of refining the same kerosene by mechanical mixing with Comm. AC. Aromatic carbon content (CA) was determined by the newly developed spectroscopic method [5].

The results of refining of crude Sarir kerosene with thermally activated silica (Si), alumina (Al)

**Table 2. Refining Sarir kerosene by activated carbon**

| Type of operation | Volume eluted or treated (ml) | K/AC (vol.: wt) | Operation temperature (°C) | % Carbon in aromatic rings (CA) |
|---|---|---|---|---|
| (a) Chromatographic | Crude Sarir K | | - | 3.82 |
| bed of Comm. AC. | 5 | - | Room T.(25°C) | 0.60 |
| | 10 | 0.50:1 | | 0.70 |
| | 20 | 1:1 | | 1.75 |
| | 30 | 2:1 | | 1.66 |
| | 40 | 3:1 | | 1.80 |
| | 50 | 4:1 | | 1.96 |
| | 60 | 5:1 | | 2:10 |
| | 80 | 6:1 | | 2.33 |
| | 100 | 8:1 | | 3.21 |
| | | 10:1 | | |
| (b) Chromatographic | | | | |
| bed of PRC-AC | | | Room T.(25°C) | 0.82 |
| | 5 | | | 1.07 |
| | 10 | 1:1 | | 1.15 |
| | 15 | 2:1 | | 3.77 |
| | 25 | 3:1 | | |
| | | 5:1 | | |
| (C) Mechanical | 15 | 3:1 | 60°C | 1.63 |
| mixing with Comm. | 15 | 3:1 | 90°C | 1.63 |
| AC | | | | |

and activated carbon (AC) conducted by elution chromatography on mixed adsorbents beds at room temperature, are given in Table 3.

Table 4 presents the results of refining of crude Sarir kerosene by solvent extraction with N-methylpyrrolidinone (NMP) at 60°C.

The results of the determination of some aromatic compounds,

**Table 3. Refining of crude Sarir kerosene by elution through mixed adsorbents beds.**

| Chromatographic system | Volume eluted (ml) | K/Si+Al (vol.:wt.) | K/Si+Al+AC (vol.:wt.) | K/AC (vol.:wt.) | % Carbon in aromatic rings (CA) |
|---|---|---|---|---|---|
| (a) Silica (5 g) | | | | | |
| +Alumina (5 g) | 10 | 1 : 1 | | | 0.48 |
| | 20 | 2 : 1 | | | 2.67 |
| | 30 | 3 : 1 | | | 2.81 |
| | 50 | 5 : 1 | | | 2.53 |
| | 80 | 8 : 1 | | | 2.41 |
| (b) Silica (15 g) | | | | | |
| + Alumina (15 g) | | | | | |
| +AC (5 g) | 10 | 1 : 3 | 0.29 : 1 | 2 : 1 | 0.18 |
| | 20 | 2 : 3 | 0.57 : 1 | 4 : 1 | 0.29 |
| | 30 | 1 : 1 | 0.86 : 1 | 6 : 1 | 0.76 |
| | 50 | 4 : 3 | 1.14 : 1 | 8 : 1 | 1.06 |
| | 80 | 5 : 1 | 1.43 : 1 | 10 : 1 | 1.38 |

**Table 4. Refining crude Sarir kerosene by NMP at 60°C**

| Kerosene volume (ml) | NMP volume (ml) | K/NMP (vol.:vol.) | % Carbon in aromatic rings |
|---|---|---|---|
| 40 | 20 | 2 : 1 | 1.33 |
| 20 | 20 | 1 : 1 | 0.80 |
| 20 | 40 | 1 : 2 | 0.50 |

actually present in the kerosene cut of Sarir crude oil, are given in Table 5.

**Table 5. Some aromatic compounds identified in NMP extract from Sarir kerosene.**

| Retention time (min) | Carbon number zone | Aromatic compound | % Concentration |
|---|---|---|---|
| 7.448 | i*-$C_8$ | Benzene | 0.0082 |
| 8.513 | i-$C_9$ | Toluene | 0.0653 |
| 11.030 | i-$C_{10}$ | Ethylbenzene | 0.0931 |
| 11.631 | i-$C_{10}$ | (p+m) Xylene | 0.1778 |
| 11.937 | i-$C_{10}$ | o-Xylene | 0.1240 |
| 13.080 | i-$C_{10}$ | Cumene | 0.1242 |
| 13.978 | i-$C_{11}$ | n-propyl benzene | 0.1757 |
| 14.508 | i-$C_{11}$ | Mesitylene | 0.2692 |
| 21.467 | i-$C_{13}$ | Naphthalene | 0.3907 |
| 25.388 | i-$C_{14}$ | 1-Methyl naphthalene | 0.3710 |

(*) i- = (iso-) = all forms of carbon except paraffinic straight chain (normal).

## DISCUSSION

The results of refining crude Sarir kerosene by Comm. AC and PRC-AC, performed by elution chromatography, and measured by the new spectroscopic method are given in Table 2. The commercially activated carbon was provided by the Arabian Company for the Production of Beverages in Tripoli. It was a granulated type of particle with a diameter around 1-2 millimeters. This carbon was thermally activated in a tubular furnace at 800°C under a stream of nitrogen gas, for 30 minutes prior to use, and in a manner similar to that used in the preparation of activated carbon [6].

The results of examining the efficiency of refining by activated carbon by mechanical mixing at mildly elevated temperature of 60°C and 90°C are also given in Table 2. The concentration of CA is lowered to 1.63 % for the K/AC ratio of 3 : 1 which is almost identical with that obtained by elution chromatography. This indicates that neither agitation nor temperature improved the efficiency when a fixed 3:1 K/AC ratio was examined. Other solid, multi-adsorbent systems (a) a 50%+50% di-combination system of alumina + silica and (b) a 43% +43% +14% tri-combination system of alumina + silica + activated carbon were examined for the reduction of aromatic carbon content .The results are given in Table 3. Very high efficiency was observed for only the 1:1 ratio of K/Si +Al di-combination system. Beyond that, efficiency was lowered drastically. On the other hand, a pronounced improvement in the AC activity in terms of increasing K/AC ratio and decreasing %CA content was obtained by the combined action of Si + Al + AC. It seems that Si + Al treatment removes compounds that adversely affect AC activity by blocking pores which are normally active in removing mono- and di-ring compounds present in the kerosene fraction.

Figure 1 is constructed from data in Tables 2 and 3, and it displays a comparison between the three refining systems. The superiority of the three adsorbents combined action is clearly indicated. This suggests a practical procedure in which a known weight of crude kerosene is stirred with nearly equivalent weight of silica-alumina (50%-

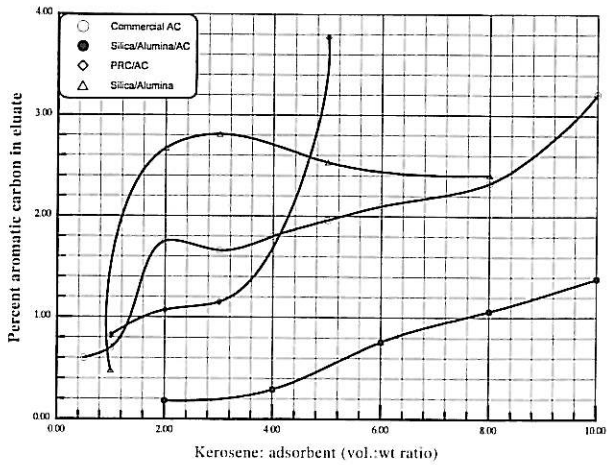



Fig. 1. Efficiency of pure and mixed adsorbents in removing aromatic compounds from kerosene.

50%). The solution is let to settle and the decantate is eluted through AC bed of a weight equivalent to one eighth (1/8) that of the kerosene original weight. The operation, carried out at room temperature, may yield a refined kerosene containing about 1 % carbon in aromatic rings (CA).

It is of significance at this stage to look into the possibility and efficiency of reducing % CA by solvent extraction methods [7].One of the used solvents to extract aromatics from petroleum fractions is N-methyl pyrrolidinone (NMP). We conducted a series of experiments using this solvent and the results are given in Table 4. It is evident that reducing % CA to less than 1% requires a 1:1 volume ratio of K/NMP. This is in a way comparable to the AC results alone (Table 2), but much less efficient compared to the combined Si + Al + AC results (Table 3).

The price and availability of adsorbents or solvents, their ease of regeneration and their ease of application coupled with their efficiency in reducing aromatic carbon content, are prime factors directing the choice of an industrial process. In this particular study, results show that adsorbents are clearly preferable to solvents in reducing aromatic carbon content.

To supplement the last conclusion, in regards with the availability of adsorbents, we refer again to the series of experiments which were carried out on the efficiency of activated carbon prepared at our Petroleum Research Centre (PRC-AC) [6]. The results are re-presented in Table 2. Further to this, a comparison of the activity of PRC-AC with that of the commercial-AC and $SiO_2 + Al_2O_3$ is indicated in Figure-1. It is obvious that PRC-AC is superior to both Comm-AC and $SiO_2 + Al_2O_3$ when applied alone and when K/adsorbent ratio is $\leq 3:1$.

Finally, in order to present a proof on the prevalence of mono-and di-aromatic systems in the kerosene under investigation (Sarir kerosene), separation of some of these aromatic compounds by capillary column-GC from the NMP extract was obtained. The assignment of peaks was ascertained by matching with authentic aromatic compounds. The results are given in Table 5.

## CONCLUSIONS

Major conclusions from this work are the following:

1 Reducing aromatic carbon content is more effective with solid adsorbents than with solvent extraction using NMP. The adsorption operation also effectively removes the obnoxious bad odour.

2 Solid adsorbent technology is expected to be preferred in comparison with solvent extraction on the basis of ease of operation and control, lower economical requirements, and lower general and place of work environmental impacts.

3 Most important solid adsorbent in this field is activated carbon, which may be prepared locally. We have already presented successful results in this respect [6].

## ACKNOWLEDGEMENT

The authors wish to express thanks to the management of the Petroleum Research Centre for supporting this work and granting permission to publish it.

## REFERENCES

[1] Esber I. Shaheen, 1964. *Environmental Pollution: Awarenes and Control* Engineering Tech. Incorp. Mahomet, Illinois.

[2] Speight. J.G. ,1981. *The Chemistry and Technology of Petroleum.* Marcell Dekker Inc., New York.

[3] Data borrowed from the General Establishment for Soaps and Detergents at Tripoli, GSPLAJ.

[4] Data borrowed from the Industrial Processing Department at the Petroleum Research Centre, P. O. Box 6431, Tripoli, GSPLAJ.

[5] Ali, L.H. and Al-Darwish, M.O. 1998. Spectroscopic determination of carbon in aromatic rings in petroleum kerosenes. *Petroleum Science and Technology* 16, 9 & 10. Marcel Dekker, Inc. New York.

[6] Ali, L.H., and Shibly, A.B. 1998. Preparation of activated carbon from carbonaceous wastes. *Petroleum Res. J.*, **9**, Tripoli.

[7] Ali, L.H. and Al-Dobouni, I.A. 1986, *Petroleum: Origin, Composition and Technology,* University of Mosul Press. No. 959 (1986) The National Liberary, Baghdad, Iraq.

Petroleum Res. J. Vol. 11 (1999); P. 27-33, 2 Figs.

# Organic Matter in Petroleum Sludges a Source of Useful Materials

## *Part 2:*

## Separation and Analysis of Petroleum Naphtha Soluble Fraction

Latif H. Ali* and Mohammad N. Oun*

# المادة العضوية في المخلفات النفطية مصدر لمواد مفيدة

## الجزء الثاني:

## فصل وتحليل الجزء القابل للذوبان في النفثا البترولية

لطيف حميد علي و محمد نجيب عون

تتمحور الدراسة حول فصل وتجزئة المادة العضوية في مخلفات (كدارة) خامي السدرة والحمادة باستعمال نفثا بترولية. يمتلك خاما السدرة والحمادة الصفات الفيزيائية والكيميائية المبينة أدناه على التوالي:

الكثافة بمقياس معهد البترول الأمريكي (API) = 37 و 39

المحتوى الكبريتي (S%) = 0.08 و 0.39

المحتوى النتروجيني (N%) = 0.06 و 0.17

محتوى المواد غير الذائبة في الهبتان الطبيعي ($\%n\ C_7$ Insol) = 0.30 و 0.73

تم استعمال الأنواع التالية من النفثا البترولية في عملية الفصل:

نفثا خفيفة مجال درجة غليانها بين 20–50° م

نفثا ثقيلة مجال درجة غليانها بين 80–160° م

نفثا مصدرية نقية هي الهبتان الطبيعي درجة غليانها 101° م لغرض المقارنة.

أجريت عملية الفصل معملياً باستعمال نسبة مذيب إلى ترسبات بمقدار 1:25 وتم رج المزيج لمدة محدودة بواسطة الأمواج فوق الصوتية وحققت العملية فصل المادة المالتينية (الجزء المذاب في النفثا) حيث تم عزل المادة الأسفلتينية المتخلفة (الجزء غير المذاب في النفثا) بواسطة تقنية الطرد المركزي وتستخلص الحالتين أخيراً بواسطة تقطير النفثا. شملت الدراسة تحليل نسب العناصر الرئيسية CHN وكذلك محتوى العناصر الثقيلة في جزء المالتين وبيّنت النتائج عند إستعمال النفثا الثقيلة في عملية الفصل أن 65% من مكونات المادة العضوية في كدارة خام الحمادة هي مادة مالتينية بينما ترتفع هذه النسب إلى 79% في مخلفات خام السدرة. عند محاولة فصل المادة العضوية الثقيلة من الجزء الأسفلتي بواسطة استخلاصها بالمذيب رباعي هيدروفيوران (THF) شوهدت مؤشرات قوية تدل على تفاعل المذيب مع المادة الإسفلتية في الكدارة وأدى هذا التفاعل إلى زيادة غير مألوفة في ناتج الفصل بلغت أضعاف ما كان متوقعاً وهذه الظاهرة لم تحدث عند استعمال مذيب أروماتي هيدروكربوني مثل التلوين في عملية الفصل. من المتوقع أن يكون لهذه الظاهرة مردودات تطبيقية وتتطلب دراسة خاصة بها.

*Petroleum Research Centre, P.O. Box 6431, Tripoli, Libya

**Abstract:** *The organic matter in sludges from two Libyan crude oils [Sedra, API = 37, S = 0.39%, N = 0.17%, n -C7 insolubles = 0.73%; and Hamada, API = 39, S= 0.08%, N = 0.06%, n - C7 insolubles = 0.3%] were sub-fractionated with light naphtha (LN, boiling range 20 - 50°C) and heavy naphtha (HN, boiling range 80 - 160°C). A reference fractionation with n-heptane (HEPT = boiling point 101°C) was also conducted for comparison purposes. Solvent to sludge ratio was 25 : 1 and agitation was performed supersonically. The separation of undissolved asphaltics was achieved by centrifugation.*

*Results are presented on fractionation of organic matter, elemental analysis of maltenes and determination of ash and heavy metal contents in the fractions.*

*Average values of 65% and 79% of total sludge weight was separated as a maltene fraction from Hamada and Sedra sludges respectively, using heavy petroleum naphtha as a solvent.*

*Extraction of organics from the asphaltic portion with tetrahydrofuran resulted in a several folds increase in the expected yield of organics, indicating reaction with the solvent. No such reaction took place when the extraction was performed using toluene.*

## INTRODUCTION

Sludge material depositing in storage tanks over the years represents net loss of valuable resources. It also reduces the storage capacity of the storage installations and has to be removed periodically. If sludge material is not processed into useful feeds or products, it will impart a heavy burden on oil industry and on the environment. Composition of sludges from storage tanks of various crude oils has been reported [1,2,3,4]. Solvent fractionation of sludges from waxy crude oils also was investigated [5]. The motives and aims of this study were reported in Part 1 [6b]. Fractionation of toluene soluble organics, extracted from sludge deposits in Part 1, was conducted using alkane solvents: n-pentane and n-heptane. Analysis of sludge in terms of water and inorganic contents and distribution of heavy metals in the sub-fractions were also assessed in that part of the study.

In the present work a more applied motivated approach was investigated to effect the fractionation of sludge matter into major fractions, namely: Maltenes and Asphaltics, using locally produced petroleum naphtha. The diagram (Fig. 1) illustrates the fractionation scheme used in our investigation. The results of this study were partly presented in a conference in Egypt [7].

## EXPERIMENTAL

### *Materials and Instruments:*

- Light naphtha was obtained from Az Zawiyah refinery, and was expected to possess a boiling range of 30 - 80°C; however the boiling point never exceeded 45°C, when the solvent was recovered after use.
- Heavy naphtha was obtained from Az Zawiyah refinery, and possessed a boiling range of 80 to 160°C.
- Normal heptane (n-C7), boiling point 101°C was obtained from Aldrich Chemical Company.
- Centrifuge used was: Seta - Iec, Oil test centrifuge.
- Supersonic vibrator used was: Karl Kolb, Telsonic D - 6072
- C, H, N analyzer used was: Carlo Erba Strumentazione MOD 1106.
- Sulfur was determined by HORIBA SLFA - 1100 method.
- Heavy metals were determined by atomic absorption spectroscopy using a spectrophotometer model VARIAM A.A. 1475.

### *Experimental Procedures*:

#### 1. *Separation of maltenes from sludge:*

Toluene (20 ml) was added to 20 g, accurately weighed sludge in a 1000 ml conical flask. The mixture was warmed to 60°C with shaking. The naphtha solvent (500 ml); LN, HN or n-HEPT, was added (in three separate determinations) and the

whole mixture was supersonically shaken for 2 h in a water bath at 60°C. After this, the mixture was centrifuged 15 minutes at 2000 rpm in a suitable centrifuge. The upper layer containing the dissolved maltenes was decanted into a distilling flask, followed by distillation of solvent and determination of maltenes yield.

The insoluble asphaltic portion was transferred by a spatula from the centrifuge tubes to a labeled sample jar.

**2. *Separation of organics from asphaltics by tetrahydrofuran and by toluene:***

A sample of about 2 g of mixed Hamada and Sedra asphaltics (accurately weighed to three decimals) was extracted with 100 ml of THF (or Toluene) in a soxhlet system. The extraction was continued until complete discoloration of the extracts, (2 h in case of THF and 4 h in case of Toluene). The solvents were then removed by distillation, followed by drying for 2 h at 105°C. The weight of extracted organics was determined and their percentage was calculated.

Inorganics in the thimble were determined by drying and weighing the thimble.

**Table 1. Analysis of Hamada and Sedra crude oils performed by SGS.**

| Property | Crude oil and value | | Method of analysis |
|---|---|---|---|
| | Hamada | Sedra | |
| Density, 15.5°C, (g.ml$^{-1}$) | 0.8296 | 0.8395 | IP 365/D 4052 |
| API gravity, 15.5°C | 38.98 | 37.00 | Calculated |
| Total sulfur, (wt.%) | 0.08 | 0.39 | IP 336/D 4294 |
| Total nitrogen, (wt.%) | 0.06 | 0.17 | IP 379 Mod./D 462g Mod |
| Asphaltenes, (wt.%) | 0.25 | 0.53 | IP 143 |
| n-Heptane insolubles, (Wt.%) | 0.30 | 0.73 | D 893 |
| Ash content, (wt%) | <0.01 | <0.01 | IP 143 |
| Vanadium,(ppm) | 1.6 | 2 | IP 377 Mod |
| Nickel,(ppm) | 1.1 | 7 | IP 377/Mod |

**Table 2. Separation of maltenes from Hamada and Sedra sludges with petroleum naphtha and n-heptane.**

| Name of sludge and No. of determinations | Percent soluble maltenes | | |
|---|---|---|---|
| | Light naphtha | Heavy naphtha | n-heptane |
| Hamada | | | |
| 1 | 60.20 | 61.62 | 68.77 |
| 2 | 58.56 | 72.56 | 70.05 |
| 3 | 49.26 | 62.21 | 73.22 |
| Average (S.D.) | 56.01 (± 5.90) | 65.46 (± 6.45) | 70.68 (± 2.23) |
| Sedra | | | |
| 1 | 51.95 | 72.40 | 72.76 |
| 2 | 49.85 | 84.33 | 75.74 |
| 3 | 55.00 | 80.64 | 78.17 |
| Average (S.D.) | 52.23 (± 2.59) | 79.12 (± 6.07) | 75.56 (± 2.70) |

## RESULTS

In the beginning, some of the analysis results of Hamada and Sedra crude oils that are of relevance to our work are listed in Table 1. The analysis was conducted by the English consultant company SGS [8].

The results of separating the maltenes from the two sludges using light and heavy petroleum naphtha are given in Table 2.

The ultimate analysis (C, H, N, S & O) of maltenes separated by the three solvents LN, HN and HEPT from Hamada and Sedra sludges are given in Table 3.

**Table 3. Elemental analysis of maltenes separated by LN, HN and HEPT from Hamada and Sedra sludges.**

| Source of maltenes | % C | % H | % N | % S | % O[1] | H/C ratio |
|---|---|---|---|---|---|---|
| HM[2] LN | 74.22 | 11.33 | 1.05 | 1.172 | 12.23 | 1.83 |
| HM HN | 79.88 | 12.46 | 0.85 | 0.988 | 5.82 | 1.87 |
| HM HEPT | 81.27 | 12.58 | 1.08 | 1.066 | 4.00 | 1.86 |
| SM[3] LH | 80.55 | 12.43 | 0.88 | 1.170 | 4.97 | 1.86 |
| SM. HN | 81.27 | 12.02 | 0.85 | 0.845 | 5.02 | 1.78 |
| SM HEPT[4] | 79.28 | 12.32 | 0.99 | 1.052 | 6.36 | 1.86 |

1- Calculated by difference.
2- HM = Hamada maltenes.
3- SM = Sedra maltenesSM.
4- HEPT = Sedra maltenes soluble in n-heptane.

Detailed analyses of ash and heavy metals content in maltenes separated by the three solvents from Hamada and Sedra sludges are given in Table 4.

**Table 4. Ash and heavy metals content in maltenes separated from Hamada and Sedra sludges.**

| Maltenes sample | % Ash | Trace heavy metals, (ppm) | | | | | | |
|---|---|---|---|---|---|---|---|---|
| | | V | Ni | Zn | Mn | Pb | Cu | Fe |
| HM. LN | 0.0/ | 0.9 | 0.6 | 4.0 | 0.5 | 30.5 | n.d(*) | 10.5 |
| HM. HN | 0.88 | 3.0 | 2.1 | 14.4 | 2.3 | 182.3 | n.d. | 101.8 |
| HM. HEPT | 0.56 | 1.8 | 1.0 | 7.0 | 1.0 | 82.3 | n.d. | 52.6 |
| SM. LN | 0.01 | 0.5 | 0.4 | 0.8 | 0.2 | 11.2 | 0.5 | 1.6 |
| SM. HN | 0.31 | 1.2 | 3.4 | 13.5 | 8.2 | 3.1 | 4.8 | 99.7 |
| SM. HEPT | 0.18 | 1.2 | 2.3 | 9.4 | 4.4 | 3.2 | 3.4 | 74.4 |

(*) n.d = not determined.

The results on the separation of organics from the mixed Hamada and Sedra asphaltics by terahydrofuran are given in Table 5.

**Table 5. Separation of organics from mixed asphaltics by THF and toluene.**

| Type of mixed asphaltics | % Organics | % Inorganics | Remarks |
|---|---|---|---|
| [H+S]. As. LN (*) | 452[1]<br>313[2]<br>256[3] | 2.19<br>–<br>0.80 | (1), (2), (3), Increase in yield registered by three different operators |
| [H+S]. As. HN | 369<br>99.3[4] | 2.39<br>1.80 | (4) Separation by toluene |
| [H+S]. As. HEPT | 279 | 1.38 | |

(*) [H+S]. As. LN = Mixed Hamada and Sedra asphaltics separated by light naphtha.

## DISCUSSION

### Maltenes Yield:

Factors affecting the yield of maltenes extraction from the sludges under investigation are:

1- The chemical composition of the parent crude oils, mainly in terms of sulfur, nitrogen, asphaltenes and heavy metals contents.

2- The physical characteristics of the parent crude oils, mainly density expressed as API gravity value.

3- The boiling range of naphtha used in extracting the maltenes from the sludge.

4- The degree of homogeneity of the sludge components (i.e. bitumen, fines and water).

5- Time of exposure of the sludge to the atmospheric conditions (i.e. age of sludge). Aged sludge is expected to be more oxidized, containing more fines, asphaltenes and water and thus less maltenes.

Inspection of the data in Table 1 affords information on the physical and chemical characteristics of the parent crude oils. The interaction between factors 3 through 5 mentioned above, taking into accounts the basic characteristics in factors 1 and 2, gave the results shown in Table 2 on the yields of extracted maltenes. These results might be further explained as follows:

In line with the API gravity and chemical composition of Hamada and Sedra parent crudes, the average yield of light naphtha extracted Hamada maltenes was higher than that of Sedra [cf. HM.LN = 56.01% Vs SM.LN = 52.23%].On the other hand, when heavy naphtha is concerned, the trend is altered with a much more pronounced difference [c.f. SM.HN = 79.12% Vs HM.HN = 65.46%; and HM.LN = 56.01% Vs HM.HN = 65.46%; and SM.LN = 52.23% Vs SM.HN = 79.12%].Thus the higher the boiling range of the naphtha the higher the yield of the maltenes. This is in fact expected in the light of increased solubility of higher homologues at higher temperatures and higher molecular weight of the solvent [9a and b,10].

In the case of maltenes extraction with n-heptane, where the solvent is possessing an intermediate molecular size and boiling point as compared to LN and HN, the results indicated inverse relationship with API [c.f. HM.HEPT = 70.68% Vs SM.HEPT = 75.56%].We believe that the most likely reason for this is factor 4, related to incomplete homogeneity of the analyzed samples. It was mentioned in Part 1 [6] that it was very difficult to homogenize the sample because of its extreme high viscosity and the separation of pools of viscous oil and some floating water on cooling to room temperature.

### Maltenes Analysis:

The results of elemental analysis are given in Table 3. Main observations from these results on aspects related to the chemical nature of maltenes separated by the three solvents, are the following:

1- Except the slightly different case of SM.HN, the H/C ratio is about identical in all maltenes. Also the value of this ratio of all maltenes samples being approximately 2, reflects the predominance of the saturation nature of carbon to carbon bond in these maltenes.

2- About 13 folds increase is observed in the sulfur content of HM compared to the parent Hamada crude oil (refer to Table 1).

3- In a similar comparison as in 2 above, with respect to nitrogen content, the values of 15 and 5.3 fold increase are found in HM and SM respectively compared to the parent crude oils.

These observations on the increased magnitudes of S,N and most probably O(calculated by difference) in the sludge maltenes, further supplement the previously suggested mechanism [6a] for the sludge separation and deposition. It was suggested then, that the most polar species containing S,N,O, etc, are attracted to salt saturated, water droplets suspended in the parent crude oil. The coalescence of these droplets and the effects of gravitational pull on them results

in sludge accumulation at the bottom, comprising the most polar and the most heavy constituents of petroleum.

The analysis of ash and heavy metal contents in the maltenes separated by the three naphtha solvents are given in Table 4 and plotted in figures 1 and 2. It is clear that maltenes separated with light naphtha from the two sludges (HM.LN and SM.LN) contain about 100 ppm of total ash with relatively low concentrations of V, Ni, Mn and Fe as compared to the case of separation by heavy naphtha (HM.HN and SM.HN).

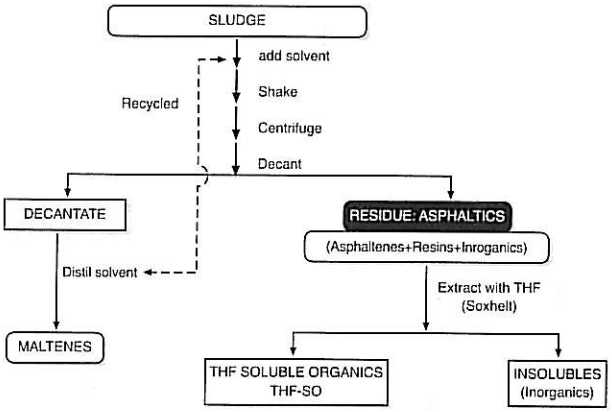



Fig. 1. Solvent fractionation of sludge deposits using petroleum naphtha.

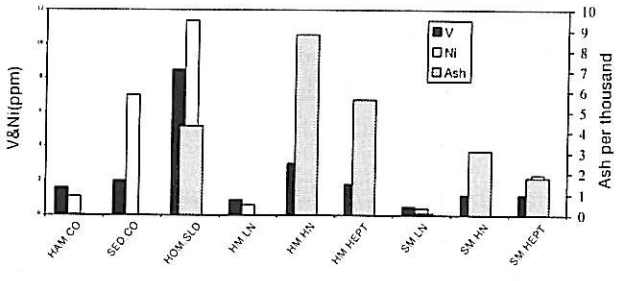



Fig. 2. Ash, vanadium and nickel distribution in crude oil, homogenized sludge and maltenes.

The analysis of heavy metals content showed a noticeable increase of Pb in HM and of in both HM and SM. Similar trend was also observed for Mn and Zn in both HM and SM. Tentative explanation of these increments may partly be due to contamination of sludge by ions released to it as a resulf of corrosion of the storage tanks internal metallic surface. The building materials of crud oil storage tanks are usually alloys of iron with some of the above mentioned heavy metals. Corrosion usually occurs when protection against it is inadequate.

A comparison is given in Table 6 between ash and some of the heavy metal contents in HM and SM separated by petroleum naphtha and their contents in a homogenized 50% Hamada + 50% Sedra sludge [6a and b] and in parent crude oils [8].

**Table 6: Ash vanadium and nickel contents in homogenized sludge and parent crude oils.**

| Type of sample | Percent ash | V (ppm) | Ni (ppm) |
|---|---|---|---|
| Homogenized sludge | 4.31 | 8.50 | 11.40 |
| Hamada crude oil* | < 0.01 | 1.60 | 1.10 |
| Sedra crude oil* | < 0.01 | 2.00 | 7.00 |

(*) Analyzed by SGS.

It is obvious from Tables 3, 4 and 6 and Figure 2 that a noticeable reduction in ash and heavy metals contents occurred in the maltenes separated by heavy naphtha from the two sludges under investigation. With respect to V and Ni contents, the corresponding sludge maltenes contains twice as much as the parent crude oils. On the other hand separation of maltenes by light naphtha yields heavy metals and ash contents comparable with their contents in the parent crude oils.

One last observation, on the heavy metals analysis of maltenes separated by n-heptane (both HM.HEPT and SM.HEPT) that, ash and heavy metal concentration values are intermediate between the values obtained by LN and HN. This in fact is expected to be dependant on the molecular size of the three solvents used in separating the maltenes. In other words, higher molecular weight solvents are expected to dissolve higher molecular weight resinous type materials with their higher metallic contents [10].

For efficient stripping of asphaltenic compounds from the inorganic constituents in the asphalt portion obtained after the separation of maltenes, tetrahydrofuran (THF) was used to accomplish this purpose. The results are given in Table 5. Mixed Hamada (H) and Sedra (S)

asphaltics were used and the yield of organics (asphaltenes and some resinous compounds) increased several folds on what was expected. The reaction with the solvent; by a mechanism which is until now not understood; is the only possible cause for the weight increase.

No such increase in weight occurred when the extraction was carried out using toluene ($C_7H_8$) instead of THF. The following points need further investigation on this unexpected phenomenon:

- The nature of the yield and whether polymerization of the solvent is a part of the reaction taking place.
- Is the reaction catalyzed by the indigenous inorganic constituents in the asphaltics portion?
- Is the new product beneficial for any use in the petroleum and other operations?

## CONCLUSIONS

Higher boiling petroleum naphtha produced a noticeable increase in the amount of separated maltenes compared to the case of separation by light naphtha. The average percentage increase was 9.5% and 16.9% for Hamada and Sedra sludges respectively.

The several fold increase in the heteroatom contents (S,N and O) in sludge maltenes compared to the original parent crude oil suggests a peculiar mechanism; in line with that proposed in Part 1; for the separation and deposition of sludge at the bottom of storage tank.

The H/C ratio being approximately 2 reflects the predominance of the saturation nature of the C-C bond in these maltenes. The value of 1.78 for this ratio in SM.HN indicates a relatively higher aromatic carbon content in this maltene.

Maltenes separated by light naphtha showed ash and heavy metals contents comparable to the parent crude oils, while separation by heavy naphtha produced maltenes of higher ash content and about twice as much of V and Ni as in the parent crudes.

Most relevant conclusion from this work is that: about 70% of the organic matter in the studied sludges is of maltenic nature, which can be easily separated by petroleum naphtha. The separated maltenes can be blended with gas oil naphtha to produce a good quality fuel oil. Alternatively, blending a petroleum naphtha sludge maltenes, in a predetermined ratio, with a compatible exported crude oil may represent another way of reclaiming this polluting material.

## AKNOWLEDGEMENT

The authors wish to express thanks to the management of PRC for supporting the project and giving permission for publishing it.

## REFERENCES

[1] Fujtsu, H ; Sakanshi, K and Mochida, I, 1986. *J. Japan Petrol. Inst*, **29**:482.

[2] Gifes, H.N.; Woodward, P.W. and Neihof, R.A., 1988. Intern. Conf. On Stability and Handling of Liquid Fuels, London, Sept, paper No. **22**.

[3] Mochida,I.; Sakanshi, K. and Fujitsu, H., 1986. *Oil and Gas* J. Nov 17, 5.

[4] Thomson, J.S.; Grisby, R.D.; Doughty, D.A.; Woodward, P.W. and Giles, H.N., 1989. AGS preprints Div. *Petrol.* **34**:275.

[5] Abul Fazal, S.; Zarapkar, S.S. and Joshi, G.C., 1995. *Fuel Sci. and Technol.* **13,** No. 10, 1239.

[6] (a)- Ali, L.H. and Shebli, A.B., 1997. Organic matter in petroleum sludges: A scource of useful materials. Part I : Separation of organics and Fractionation by alkane solvents. Petrolem Resconch Centre internal report.

[6] (b)- Ali, L.H. and Shebli, A.B.,1999. Ibid. *Petrol. Sci and Technol.* **17,** No. 3&4, 333.

[7] Ali, L.H and Oun, M.N., 1977. Organic matter in petroleum sludges: A source of useful materials. Part 2: Separation and analysis of petroleum naphtha soluble fraction. A poster presented at the Second Intern. Sci. Conf. Faculty. of Sci., Al-Azhar Univ., 17-20 March, Cairo, Egypt.

[8] Society General Surveillance SGS, London. Branch, 217 / 221 London Rd, Camberly., 1994. EPL 3/2946, 13/93, 23 March.

[9] (a)- Hobson, G.D. and Pohl, E., 1975. *Modern Petroleum Technology.* 4th Edition. Applied Science Ltd., London, England.

[9] (b)- Speight, J.G., 1981. *The Chemistry and Technology of Petroleum.* Marcel Dekker Inc. New York. p: 417.

[10] Ali, L.H. and Al- Ghannam, K. A.., 1981. Investigation into asphaltenes in heavy crude oils : I : Effect of temperature on precipitation by alkane solvents. *Fuel*, **50** : 1043. UK.

Petroleum Res. J. Vol. 11 (1999); P. 35-44, 11 Figs.

# Solar Detoxification of A Petroleum Wastewater in Aqueous Suspensions of Titanium Dioxide Photocatalyst

Muftah Al-Ghazali and Gamil Alhakimi

# معالجة المياه الملوثة باستخدام الطاقة الشمسية وعامل مساعد

مفتاح الغزالي و جميل الحكيمي

تم دراسة إمكانية استخدام مادة ثاني أكسيد التيتانيوم كمحفز ضوئي في تنقية المياه الملوثة بمواد عضوية والناتجة من مجمع رأس لانوف البتروكيماوي وذلك في وجود ضوء الشمس كمصدر للأشعة فوق البنفسجية. ظروف التفاعل تم تغييرها للحصول على أفضل النتائج حيث استخدمت مادة فثالات هيدروجين البوتاسيوم لهذا الغرض وذلك كمادة نموذجية. إختفاء مادة فثالات هيدروجين البوتاسيوم تم متابعتها بواسطة فحص كمية الاستهلاك الكيميائي للأكسجين (COD) للمحلول المعرّض للشمس.

وجد أن معدل تفاعل المحفز الضوئي ثاني أكسيد التيتانيوم يكون في ذروته عند التركيز 3 جم/لتر للمحفز الضوئي ديجوسا و10جم/لتر للمحفز الضوئي هومبيكات (UV100) أما بالنسبة لوسط التفاعل فقد وجد أن أفضل وسط يكون عند الرقم الهيدروجيني 5 لكل من المحفزين الضوئيين. الاختفاء المباشر لمادة فثالات هيدروجين البوتاسيوم عند خلطها بالمحفز الضوئي هومبيكات UV100 ناتج عن عملية إمتزاز الملوث عند سطح الحفاز.

التحطيم الكلي للمواد العضوية الموجودة بمياه الصرف بمجمع رأس لانوف (Wastewater) لوحظ أنه يستغرق مدة من التفاعل قدرها 6 ساعات بنفس الظروف المختارة لمدة فثالات هيدروجين البوتاسيوم. كفاءة الفوتونات الناتجة من ضوء الشمس تم حسابها ووجد أنها تنخفض عند كثافة الضوء المنخفض ($0.311-2.29$ µmol photon.s$^{-1}$.l$^{-1}$) بقيمة $I^{-0.243}$ وعند كثافة الضوء العالية ($2.29-2.919$ µmol photon.s$^{-1}$.l$^{-1}$) تنخفض بقيمة قدرها $I^{-0.94}$.

---

**Abstract:** *The applicability of the photocatalytic detoxification, using titanium dioxide, for the treatment of wastewater from Ras Lanuf Petrochemical Complex was studied. The conditions of the photocatalytic degradation were optimised using the model compound potassium hydrogen phthalate (KHP). The disappearance of KHP was followed by chemical oxygen demand (COD) determination of irradiated solutions by sunlight. The optimal catalyst concentration was found at 3g/l of Degussa P25 and 10g/l of Sachtleben Hombikat UV 100. The best degradation rate was obtained at pH 5.0 for the two catalysts types. The disappearance of KHP in the dark, using Sachtleben Hombikat UV100 was due to the adsorption of the pollutant on the catalyst surface. The complete degradation of organic pollutant in Ras Lanuf Oil and Gas Processing Co. (RASCO) wastewater was reached after 6 hours irradiation using the optimal reaction conditions. The photonic efficiency decreased at low light intensities (0.311–2.29 µmol photon $s^{-1}$ $l^{-1}$) with I-0.243 and at higher light intensities (2.29–2.919 µmol photon $s^{-1}$ $l^{-1}$) with $I^{-0.94}$.*

* Ras Lanuf Oil and Gas Processing Co. Technical Department, Laboratory Division, P.O. Box 1971, Benghazi, Libya

## INTRODUCTION

It is well known that wastewater from refinery and petrochemical plants contain many types of toxic organic substances such as phenol compounds, aldehydes, polyaromatic compounds, etc. These compounds are produced from different types of processes and must therefore be purified or treated before being discharged into the sea. The most applicable method for the waste treatment of such industry complexes is the biological treatment. There are also several treatment processes used for the cleaning up of pollutant wastewater. One of them is the adsorption of organic pollutants on the activated carbon[1]. In this process the pollutants are transferred from the aqueous to the solid phase and must be again desorbed by heat treatment that may cause the formation of new toxic products.

Another method for the clean up of wastewater is the application of hydrogen peroxide/UV. This method is used efficiently to purify drinking water[2]. The hydroxyl radical produced from peroxide and UV-light is non-selective and can oxidize all pollutants in the mixture[3]. The main disadvantage of this method is the high cost of hydrogen peroxide and the adsorption of the UV-light by contaminants that lead to the complete termination of the reaction.

The combination of ozone/UV and hydrogen peroxide is also a method for the detoxification of water which used two oxidizing agents ozone and produced hydroxyl radicals[4,5].

The treatment of sewage with ozone and ozone/UV is also a well established technical process[6]. It was found that the treatment of water with ozone in the most cases does not lead to the complete mineralization. Therefore ozone/UV system was developed[7]. In this system the destruction of organic compounds becomes effective, that is due to the reaction of ozone with water and formation of hydroxyl radicals. The use of g-radiolysis in wastewater treatment is a modern technique that does not need the addition of chemicals[8]. The high energetic light ionized water molecules and produces hydroxyl radicals for the destruction of organic pollutants.

A new promising method for the wastewater treatment is the photocatalytic detoxification. With this technique the pollutants are degraded by irradiating suspensions of metal oxide semiconductors, acting as photocatalyst in the presence of light and oxygen or air[9]. The most applied metal oxide in this process is titanium dioxide. Many works are carried out in this field for distraction of hydrocarbon, chlorinated compounds and organic compounds with heteroatoms[10,11,12]. To reach the complete mineralization an additional method is required, for example biological treatment. An unsolved problem in this technique is the separation of titanium dioxide suspension after clean up the wastewater. On the other hand the fixation of photocatalyst on surfaces lead to the decreasing of the degradation rate[13].

This work is dealing with determination of the applicability of photocatalytic detoxification for the treatment of wastewater of Ras Lanuf Petrochemical Complex in Libya under the field conditions. This was carried out using the model compound potassium hydrogen phthalate (KHP). The concentration of the catalyst, the pH, the type of the catalyst and light intensity were varied and optimized. The obtained optimal conditions were used for the detoxification of the RASCO actual wastewater.

## EXPERIMENTAL

### *Equipment and Chemicals:*

*Equipment*

- Seta-IEC oil test centrifuge from Stan-hop-seta
- pH meter Beckman "select Ion 2000" ion analyzer.
- GC, Carlo Erba 4100, equipped with FID and column SS, 3m × $^3/_4$ mm, porapak R, mesh 80/100. Including methanizer at 400 °C. Detector temp. =
- 200 °C. Carrier gas was $N_2$.
- Balance from Mettler PM 34 Delta range.
- UVA-meter from Dr Hoenle GmbH.

*Chemicals:*

Potassium dichromat, mercuric sulphate, potassium hydrogen phthalate, nitric acid, sulfiric acid, sodium hydroxide (convol), chloroform,

methylene chloride and 1,10-phenanthroline and hydrogen peroxide are of BDH product and purified before use. Silver sulphate and ferrous sulphate are from Merk and used without any purification. Ferrous ammonium sulphate hepta hydrate are obtained from Riedel de Hain and directly used. Degussa P25 (primary particle size 20–30 nm, BET surface area 50 ± 15 $m^2/g$, 70% anatase and 30% rutile) is obtained from Degussa GmbH and Sachtleben Hombikate UV 100 (primary particle size <10 nm BET surface area >250 $m^2/g$, > 99% anatase) is from Sachtleben Chemie GmbH. The high purity oxygen 99.99% is obtained form B.O.C, Ltd. and the nitrogen gas from nitrogen plant in RASCO Company.

***Preparation of Potassium Hydrogen Phthalate (KHP) Stock Solution***

10.0 g of potassium hydrogen phthalate were dissolved in 1 litre water (distilled and demineralized) to prepare a stock solution, which is equal to 11670 mg $O_2$/l. To prepare KHP solution with 200 mg $O_2$/l for the degradation experiments, 34 mls were taken from the stock solution and diluted with water to a final volume of 2 litres.

***Degradation Experiments with the Model Compound KHP***

*Variation of the photocatalyst concentration:*

The photoreactor was a 3 litres beaker made of Pyrex-glass, equipped with a magnetic stirring and an oxygen purging devices, consisting of two gas washing bottles and two sintered glasses. One bottle was filled with pure water to humidify the oxygen and to minimise evaporation of water in the beaker. For the experiments with the model compound potassium hydrogen phthalate (KHP), a 2 litre KHP solution of a concentration of 200 ppm and the required amount of the photocatalyst were introduced into the reactor, (1 g/l, 2 g/l, 3 g/l, 4 g/l, and 5 g/l of Degussa P25 and 1 g/l, 5 g/l, 7 g/l, 10 g/l and 15 g/l of Sachtleben Hombikat UV100 respectively). The pH of the suspension was adjusted to 5.0. The suspensions were stirred, under continuous bubbling of oxygen, for at least one hour inside the laboratory to reach a state of system equilibrium. Then the reactor was exposed to sun light and the suspensions were irradiated for 5 hours. 75 mls sample was taken before the addition of photocatalyst and directly before exposing the system to the sun and in regular intervals (every 60 minutes) during irradiation. The pH was measured by a pH meter. The COD was determined after centrifuging the suspension for 15 minutes at 1500 rpm according to a standard method ASTM D 1252 (ASTM, 1993). The UV-intensity was determined in regular intervals at the top of the reactor by a UV-meter (Dr Hoenle UV-A meter)

***Variation of the initial pH:***

The degradation experiments were carried out following the procedure described above. The photocatalyst concentration were chosen as 3 g/l of Degussa P25 and 10 g/l of Sachtleben Hombikat UV 100, respectively, which were found to be the optimum concentration for the degradation of the model compound KHP. The degradation of KHP was carried out at different pH (3.0, 5.0, 7.0 and 11.0). The COD determination of the irradiated solution was performed every 60 minutes for every pH value.

***Variation of the light intensity:***

Degradation experiments were performed by the same procedure as described. Degussa P25 was chosen as the photocatalyst with concentration of 3 g/l and initial pH 5.0. The photodegradation reactions were carried out at different sun light intensities. The COD's of the solutions were carried out as mentioned above.

***Running the experiments for the photodegradation of RASCO wastewater:***

The wastewater sample was collected in 25 litres plastic drum from the inlet of the effluent treatment plant (ETP). The collection place of the sample was the overflow of the oil separator to the equalization basin. The sample was then shaked well and 2 litres of the solution were added to 3 g/l Degussa P25 or 10 g/l Sachtleben Hombikat UV 100, respectively. During stirring and continuously bubbling of oxygen. The pH of the solution was adjusted to 5.0. The treatment, collection of the samples and the COD determination were performed similar as described before.

### *Determination of Chemical Oxygen Demand (COD)*

50 ml sample were placed in a 500 ml refluxing flask with 1 g of mercuric sulphate. Slowly, 5 mls of silver sulphate reagent (prepared from 5.5 g silver sulphate per kilogram concentrated sulphuric acid) were added to the solution. In order to avoid possible loss of volatile materials cooling of the mixture was necessary. While stirring, 10 ml of 0.25 N potassium dichromate, solution was added to the mixture. The flask was attached to the condenser and 70 ml silver sulphate reagent was added. After refluxing for 2 hours the solution was cooled down to room temperature. The condenser was washed with distilled water to about twice of the volume of the sample. Five drops of ferroin indicator were added and then titrated against a standard solution of ferrous ammonium sulphate (prepared from 98 g ferrous ammonium sulphate hexahydrate dissolved in 20 ml concentrated sulphuric acid and diluted to one litre with distilled water) until the appearance of the first sharp colour change from bluish-green to reddish brown. The concentration of the titrant was determined daily by adding 10 ml standard potassium dichromate to 100 ml distilled water, and 30 ml concentrated sulphuric acid. The distilled water, as a blank solution, was also daily titrated against the standard solution following the same procedure. The COD values can be calculated in terms of mg $O_2$/l by the following equation (ASTM 1252, ASTM 1993)

$$\text{COD (mg}O_2\text{/l)} = \frac{(B - A) \times N \times 8000}{S}$$

where,

B = mls of ferrous ammonium sulphate hexahydrate consumed by blank
A = mls of ferrous ammonium sulphate hexahydrate consumed by sample
N = Normality of ferrous ammonium sulphate hexahydrate
S = Sample volume

### *Experimental Determination of $CO_2$ Released from the Photodegradation Process*

Six g of catalyst Degussa P25 was taken into 5 litres Erlenmeyer flask containing 1966 mls of distilled water as a first step towards the preparation of final catalyst concentration (3 g/l). The flask was connected to a dropper funnel for KHP injection into the suspension. The flask was also equipped with oxygen purging system, which consists of two wash flasks and stoppers. The system was purged with oxygen under vigorous stirring for about 3 hours. During this period the $CO_2$ concentration was registered. After that, 34 mls KHP was added and after one hour stirring in the laboratory a sample of gas from the outlet was collected with gas bag. The content of the bag was determined of $CO_2$ concentration by GC-FID. The experimental set-up was transferred outside laboratory and exposed to direct sun light. At intervals of 15 min for 160 minutes, the $CO_2$ concentration at the outlet stream of gases was measured using Gas Chromatography.

## RESULTS AND DISCUSSION

### *Calculation Methods and Evaluation of Poor Man's Model:*

This model allows the prediction of non-linear dependence of the reaction rate on the light intensity or catalyst load without the consideration of any adsorption parameters[14,15]

The reaction rate in the Poor Man's Model can be derived from equation:

$$h \quad \text{Substrate} \quad \text{Product} \qquad (1)$$

It can therefore be written as follows:

$$\text{Rate} = \frac{d[\text{product}]}{dt} = K_1[\text{substance}][h] \qquad (2)$$

The photonic efficiency can be written as follow:

$$\text{Photonic efficiency} = \frac{d[\text{product}]/dt}{d[hn]/dt} = \frac{\text{rate}}{\text{light intensity}} \qquad (3)$$

### *Degradation of the KHP and RASCO Wastewater:*

To ensure that no degradation occurred in the dark or due to oxidation by oxygen, three blank

experiments were carried out. Firstly KHP was dissolved in water and exposed to direct sunlight in the absence of catalyst and excess oxygen (Fig. 1). The COD remained constant for the duration of the experiment (300 min.). This indicates that no degradation of KHP is occurred due to direct photolysis. In the second blank a mixture of 226.3 mg $O_2$/l (COD) of KHP and 3 g/l Degussa P25 was stirred and bubbled with oxygen for 20 hours inside the laboratory. The COD was measured every 60 minutes. In the first hour the COD decreased by 17%. This change in COD was due to the adsorption of KHP on the catalyst surface. In the remaining time of the experiment the COD's remained constant (Fig. 2). In the third experiment, 10 g/l Sachtleben Hombikat UV 100 was used, under the same conditions as the 2nd experiment,

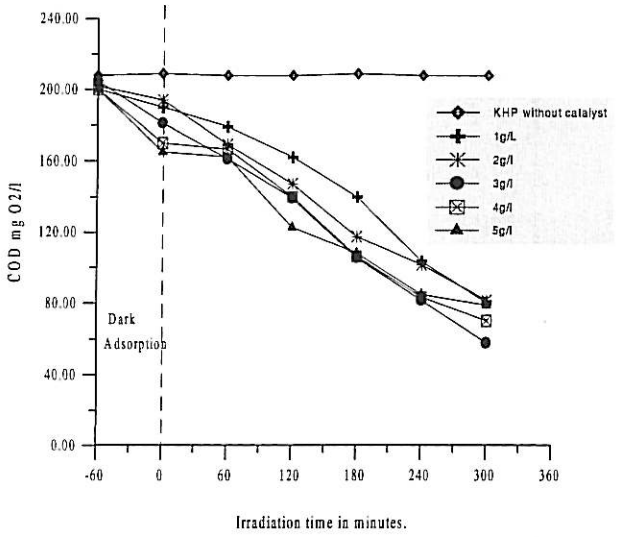



Fig. 1. COD reduction of KHP versus time at different catalyst concentration of Degussa P25, pH 5.0.

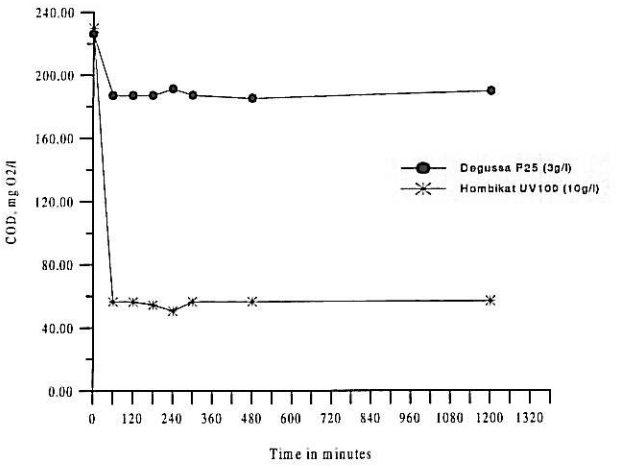



Fig. 2. Influence of catalyst on the COD reduction of KHP without irradiation, at pH 5.0.

and a strong adsorption (ca 75%) was observed in the first 60 minutes (Fig. 2). Therefore no significant change was observed over a period of 20 hours. From these experiments it was concluded that no degradation occurred in the dark or by direct photolysis regarding the COD. It can not be excluded that KHP was converted to other pollutants by direct sunlight which would not lead to a change in the COD of the sample.

To carry out the experiments with best conditions of the photocatalytic degradation reaction of KHP, the catalyst concentration was first optimised. The disappearance of the model compound (KHP) was monitored every 60 minutes by measuring the COD. From the obtained COD-values, the kinetics of the degradation were fitted. The results showed that the degradation rate of KHP followed first order kinetics. The degradation rates were calculated by multiplication of the first order rate constant by the initial COD concentration. The measured COD values (every 60 minutes) at five different catalyst concentrations, are shown in (Fig. 1). The COD showed a non significant adsorption of KHP at low catalyst load 1 and 2 g/l, the adsorption was 5 and 10 mg $O_2$/l, respectively after 60 minutes of stirring in the dark. In contrary, a relative high adsorption of 30 and 43 mg $O_2$/l was detected at 4 and 5 g/l catalyst concentration, respectively. This effect is due to a high concentration of the active sites which able to adsorb KHP molecules. The degradation rate of the model compound KHP was determined at different catalyst loads. The kinetics was calculated by a semi-logarithmic plot, thus, the reaction can be interpreted as pseudo first order kinetics.

The degradation rate increased linearly by increasing the photocatalyst load up to a certain limit. At 3 g/l Degussa P25 a maximum degradation rate was obtained. The degradation rate at this concentration reached more than double of its value in comparison to the 1 g/l concentration. Further increase the $TiO_2$ concentration produced no significant improvement in the degradation rate (Fig. 3). This can be explained by the fact that at 3 g/l catalyst concentration the maximum amount of incident light, which could be absorbed, was reached in the reactor used in this study[15].

For each of the five catalyst loads the photonic efficiencies were calculated from the ratio of the

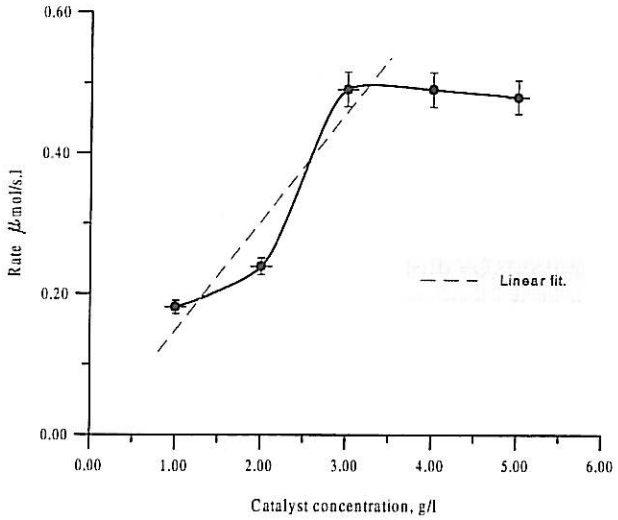



Fig. 3. Degradation rate of KHP at different catalyst concentrations. Degussa P25, pH 5.0).

photocatalytic degradation rates and the corresponding photon fluxes. The results are shown in (Fig. 4). The relatively low values of the photonic efficiency (6%) at low catalyst concentration could be explained by the limited amount of $TiO_2$ particles which absorbe the solar photons. The optimum catalyst dose was reached at 3 g/l Degussa P25. At higher photocatalyst load no further change of the photonic efficiency was achieved.

It is known from the literature that the particle size and the type of the photocatalyst play a significant role in the degradation rate of organic pollutants. Therefore, the photodegradation of KHP by direct sunlight was investigated using different concentrations of Sachtleben Hombikat UV 100 as an alternative photocatalyst. Figure 5 illustrates the behaviour of the COD reduction for different catalyst concentrations. At a catalyst concentration of 1 g/l the adsorption of KHP in the dark was low (21%). Adsorption of KHP was stronger at higher catalyst loadings. The maximum KHP adsorption is reached by 10 g and levelled off for higher concentrations which suggest saturation coverage of the surface active sites with KHP.

The reason for the rapid disappearance of the organic pollutant in the dark is due to strong adsorption of KHP and not to oxidation which was proven by the time controlling of the $CO_2$ development during the experiment.

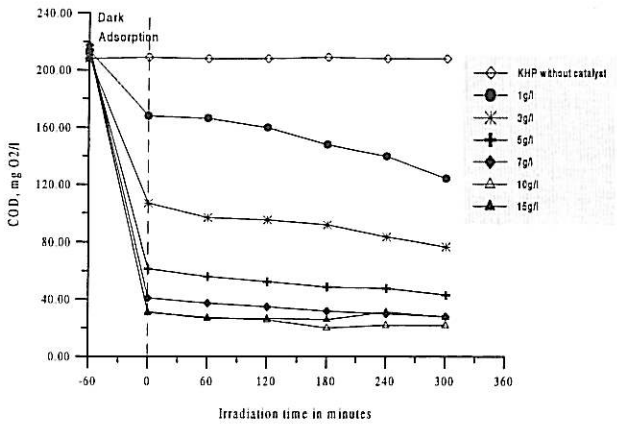



Fig. 5. COD reduction of KHP at different concentrations of Sachtleben Humbikat UV 100, at pH 5.0.

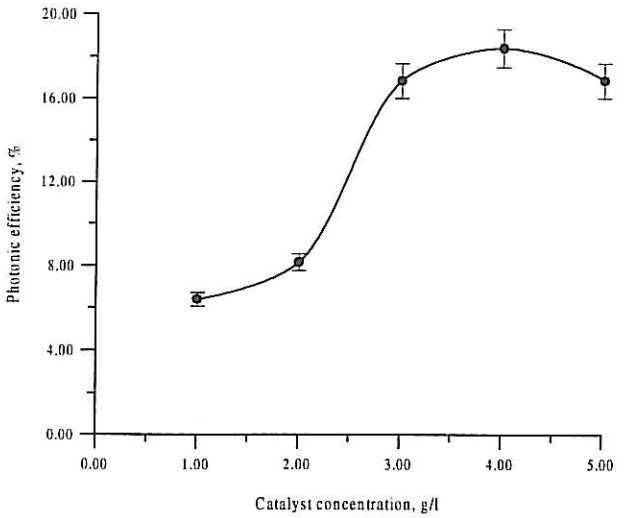



Fig. 4. Photonic efficiency versus catalyst concentration for Degussa P25, at pH 5.0. for KHP model.

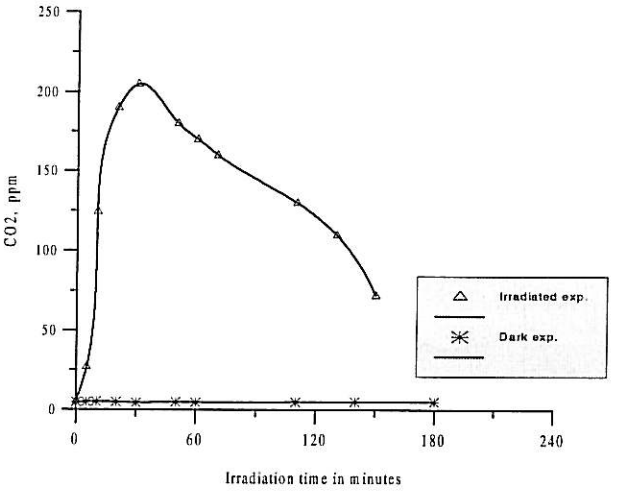
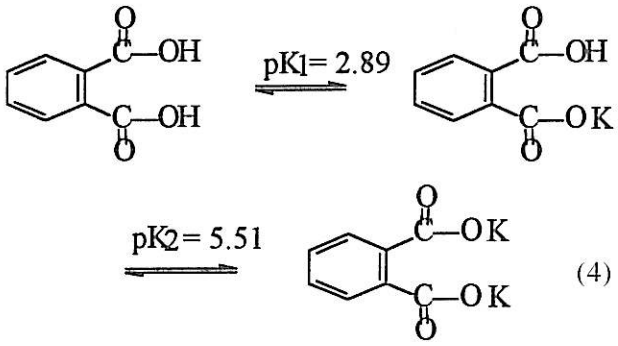



Fig. 6. $CO_2$ production as a function of time using Degussa P25, at pH 5.0 for KHP.

It was found that no $CO_2$ occurs in the dark (for Degussa and Humbikat) despite the disappearance of the KHP in solution (Fig. 6).

Further experiment showed that the adsorption of KHP on the catalyst surface is pH dependence. The dissociation of the organic pollutant and the surface properties of the photocatalyst in aqueous suspensions are highly influenced by the pH. For these reasons the effect of initial pH on the degradation rate of the model compound KHP by direct sunlight was studied. In all pH adjustment experiments the optimum catalyst concentration (3 g/l for Degussa P25) was used. The degradation rates at the different pH values were calculated from the measured COD. A plot of the degradation rate versus pH is illustrated in (Fig. 7). The results showed degradation rate 3.5 times higher in acidic medium (pH 3.0 and 5.0) compared to the basic (pH 7–11) media. The lowering of the degradation rate at high pH can be explained by adsorption desorption effect.




(4)

Ti – OH $OH^-$ Ti – $O^-$ $H_2O$ (5)

At low pH values < 6 the $TiO_2$ surface is positively charged and the KHP is present at this pH as hydrogen phthalate, which is capable to adsorb on the catalyst surface.

At higher pH > 6 the TiO2 surface is negatively charged (eq. 5) and the KHP lies in di-ionic negative form (eq. 4), which would be repelled by the catalyst surface, resulting in negligible adsorption of KHP.

The photonic efficiencies for the pH variation experiments were calculated from the obtained rates and corresponding photon flux. It was obvious that the photonic efficiency reached its maximum at pH 3.0, and then decreased in neutral and basic medium (Fig. 8). Thus, high photonic

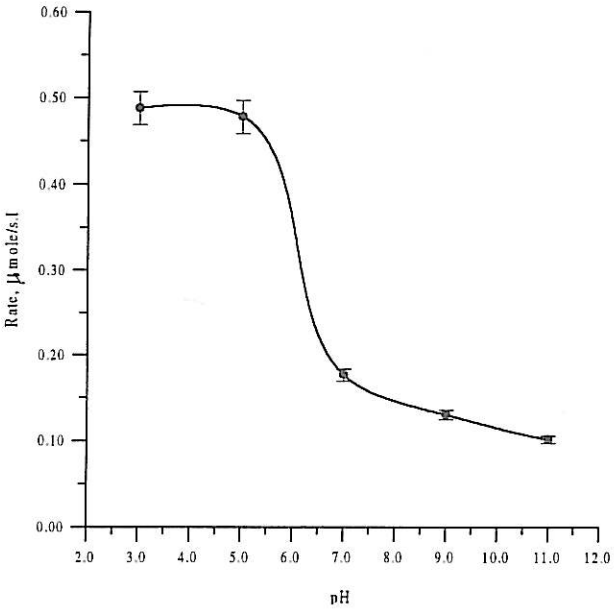



Fig. 7. Degradation rate of KHP at different pH values using 3 g/l of Degussa P25.

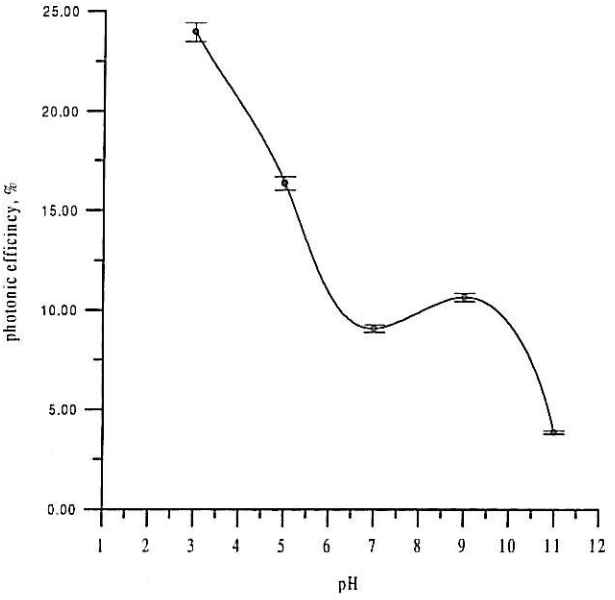



Fig. 8. The effect of pH variation on the photonic efficiency for Degussa P25 using KHP as a model compound.

efficiency was observed for pH values where a strong adsorption of the pollutant at the catalyst surface occurred, i.e., for pH values below 5.0.

The influence of light intensity on the degradation rate for many pollutants classes is reported in the literature[13]. In the present work the effect of the sun light intensity during the day on KHP degradation using Degussa P25 as photocatalyst was examined. All experiments were

carried out at pH 5.0 and the catalyst concentration was 3 g/l under vigorous stirring and continuous supply of oxygen into the suspension. The COD data were collected at different days with different sun light intensities. From the obtained results the degradation rates were calculated. Figure 9 shows the variation in KHP degradation rate as a function of light intensity for the Degussa P25 catalyst. It was obvious that the degradation rate increased linearly at low light intensities (0.311–2.29 μmol photon/s.l). At higher light intensities (2.756 – 2.919 μmol photon/s.l) a non-linear increase was observed. This effect occurred for high photon fluxes due to a predominance of recombination of photogenerated charges[16]. The effect of light intensity on the photonic efficiency of the photocatalytic degradation of KHP using Degussa P25 is illustrated in (Fig. 10). It was noticed that the efficiency considerably decreased as the light intensity increased. This is due to the high recombination rate at high light intensities which makes the photocatalytic oxidation reaction less effective. The maximum reached photonic efficiency value was 33.9 % which was a remarkably high in comparison to data found in literature for other model pollutants[17].

The results showed that when illuminations were carried out with light intensities between 0.311–0.986 μmol photon $s^{-1}$ $l^{-1}$ the photonic efficiency of KHP degradation hardly depended upon the irradiation intensity ($I^{-0.243}$). In the higher ranges, between 2.29 and 2.919 μmol photon $s^{-1}$ $l^{-1}$ the influence of light intensity was more pronounced ($I^{-0.94}$).

The optimal conditions (catalyst type, catalyst concentration, initial pH and sunlight intensity)

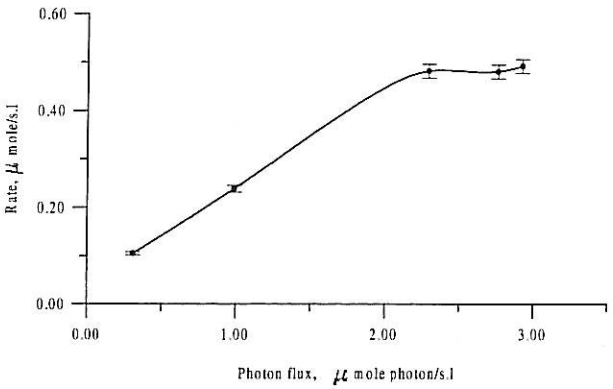



Fig. 9. Degradation rate of KHP against different photon flux for 3 g/l Degussa P25, at pH 5.0.

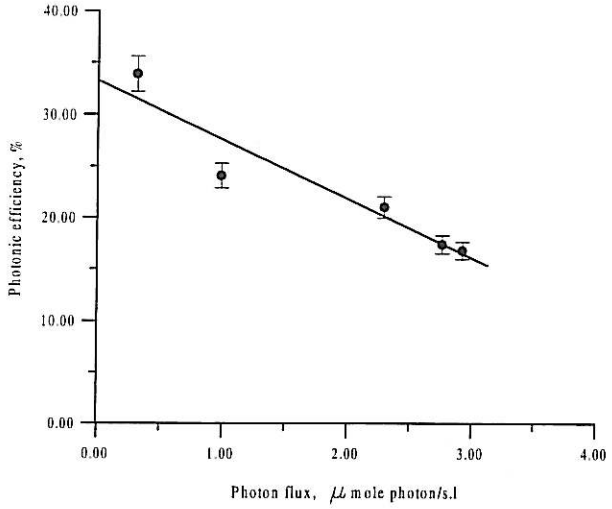



Fig.10. Influence of the photon flux on the photonic efficiency, using 3 g/l Degussa P25 and KHP as a pollutant.

found for KHP degradation were used for RASCO wastewater. The organic and inorganic pollutants present in RASCO wastewater are summarised in Table 1. Figure 11 illustrate the COD values of the degraded pollutants in the RASCO wastewater over a along period of irradiation time (900 minutes). This experiment was carried out with Degussa P25 and Sachtleben Hombikat UV 100. It is obvious that the degradation rate reached a minimum after 300 minutes of irradiation for both photocatalysts. Irradiation of the sample for further 600 minutes produced no detectable degradation. The COD values remain in the range

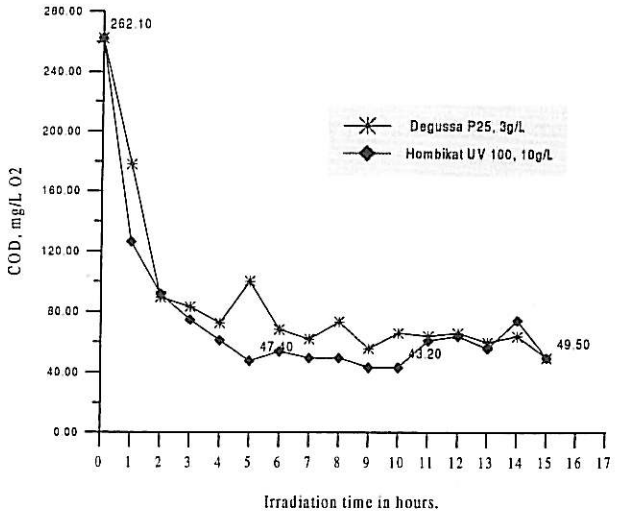



Fig.11. The degradation of organic pollutants in RASCO wastewater using 2 types of photocatalysts at pH 5.0.

of 47–49 mg $O_2$/l. These results indicate a possible existence of inorganic salts (chloride, ammonia etc.), which give a corresponding COD value. The experiments showed that the pollutants in the RASCO wastewater are completely degraded at the mentioned conditions within 300 minutes. Mechanistical study of individual compounds in RASCO wastewater like naphthalene and anthracene was already done[19].

## CONCLUSION

A complete degradation of the model compound KHP using titanium dioxide as photocatalyst and sun light was reached within 6h. The optimal catalyst concentration was found to be by 3 g/l for Degussa and 10 g/l for Humbikat. The best media for the photodegradation rate of the pollutant was found at pH 5.0 in both photocatalyst Degussa and Humbikat. The high values of light intensity affects the degradation rate negatively due to the high recombination rate. The photonic efficiency decreased by increasing the light intensity. The complete destruction of the organic pollutants in the RASCO wastewater was reached in 6 h at the same conditions used for the KHP.

**Table 1: Organic and inorganic pollutants in RASCO wastewater.**

| Pollutant | Quantity in mg/l |
|---|---|
| Total hardness | 290 |
| Silica | 3.15 |
| Chloride | 1420 |
| Nitrate | 1.4 |
| Sulfate | 550 |
| Phosphate | 2.46 |
| Sodium | 724 |
| Potassium | 22.2 |
| Calcium | 99.75 |
| Magnesium | 59.25 |
| Iron | 0.24 |
| Copper | 0.011 |
| Zinc | 0.075 |
| Chromium | 0.00649 |
| Nickel | 0.090 |
| Organic pollutants | Mixture of n-and iso-C8 to C30, cyclopentadiene, benzene, toluene, ethylbenzene, o,m,p xylene, styrene, trimethylbenzene, ethylmethylbenzene, dimethylethylbenzene, indane, indene, 1,2,3,4-tetrahydronaphthalene, naphthalene, benzenecycloheptatriene, cyclopentanon, methyl-cyclpentanon, 2-hexanone, benzeneacetaldehyde, acetophenone, 1-indanone, 3,4-dihydronaphthalenone, phenol, o-, p-methylphenol. |

## REFERENCES


[1] Ollis D. F. 1988. *Process Economics for Water Purification: A Comparative Assessment.* NATO ASI Series, series C, **237**, 663–680, ed. M. Schiavello, Kluwer Academic Publishers, Dordrecht,.

[2] Peyton G. R. 1990. Oxidative treatment methods for removal of organic compounds from drinking water supplies. In Ram N. M., Christman R. F., Cantor K. P., Eds.; *Significance and Treatment of Volatile Organic Compounds in Water Supplies*; Lewis Publ.: Chelsea, MI, (1990); 313–362.

[3] Legrini O. Oliveros E. and Braun A. 1993. Photochemical processes for water treatment. *Chem. Rev.*, **93**, 671–698.

[4] Brunet R.; Bourbigot M.; DorÈ M. 1984. *Ozone Sci. Eng.*, **6**, 163–183.

[5] Duguet J.; Bruchet A.; Mallevialle J., J. 1989. Water Supply, **7**, 115–123.

[6] Prat C.; Vincente M.; Esplugas S. 1990. *Ind. Eng. Chem.* Res. 29, 349–355.

[7] Peyton G. And Glaze W., 1988. Destruction of pollutants in water with ozone in combination with ultraviolet radiation. 3. Photolysis of aqueous ozone. *Environ. Sci. Technol.* **22**, 761–767.

[8] Tolgyessy P., J.Radioanal. 1988. *Nucl. Chem.*, 128.

[9] Carey J. H., Lawrence J., Tosine 1976. Photo-dechlorination of PCB's in the presence of titanium dioxide in aqueous suspensions. *Bull. Environ. Contam. Toxicol.*, **16**, 697–701.

[10] Mathews R.1990. Purification of water near U.V. illuminated suspensions of titanium dioxide. *Wat. Res.*, **24**, 5, 653–660.

[11] Mills G., and Hoffmann M. R. 1993. Photocatalytic degradation of PCP on TiO2 particles: Identification of intermediates and mechanism of reaction. *Environ. Sci. Technol.*, **27**, 1681–1689.

[12] Ahmed S., Ollis D., 1984. Solar photo-assisted catalytic decomposition of the chlorinated hydro-carbons, Trichloroethylene and Trichloromethane. *Solar Energy*, **32**, 5, 597– 601.

[13] Kalli Pacheco, Andrew S. Watt and Craig S. Turchi, 1993. Solar detoxification of water. Outdoor testing of prototype photoreactors joint solar engineering. ASME conference.

[14] Dillert R. and Bahnemann D., 1992. Photocatalytic degradation of organic pollutants: Mechanisms and solar applications. *Newsletter*, **52**, November.

[15] Al-Sayyed G., D'Oliveira J. and Pichat P., 1991. Semiconductor-sensitized photodegradation of 4-chlorophenol in water. *J. Photochem. photobiol. A:Chem.*, **58**, 99–114.

[16] Bahnemann D., Cunningham J., Fox M., Pelizzetti E., Pichat P. and Serpone N., 1994. Photocatalytic treatment of wastewaters In: *Aquatic and Surface Photochemistry*, Lewis publisher.

[17] Egerton T. A., and King C. J., 1979. The influence of light intensity on photoactivity in $TiO_2$ pigmented systems. *J. Oil Colloid. Chem. Assoc.* 386–389.

[18] Theurich J., Linder M. and Bahnemann D., 1997. Photocatalytic degradation of 4-chlorophenol in aerated aqueous titanium dioxide suspensions: A kinetics and mechanistic study Langmuir, in press.

[19] Theurich J., Bahnemann D.W., Vogel R., Ehamed F.E., Alhakimi G., Rajab I., 1997. *Res.Chem. Intermed.* **23**, 3, 247–274.

Petroleum Res. J. Vol. 11 (1999); P. 45-49, 4 Figs.

# Determination of Chromium (III) and Chromium (VI) Using Flow Injection Coupled with Flame Atomic Absorption Spectrometry and Direct Current Plasma Technique

I. S. Bushina*, H. M.Kut*, Seham. S. Elmahmudi*

# تحديد $Cr^{+3}$ و$Cr^{+6}$ بواسطة جهاز لهب طيف الامتصاص الذري وجهاز التيار المباشر باستخدام طريقة الحقن على العمود المصغر

إسماعيل بشينة و حسن كت، و سهام المحمودي

لقد استخدم عمود مصغر للألومينا المنشطة والمتصل بوحدة الحقن المستمر لجهاز لهب طيف الامتصاص الذري وجهاز بلازما التيار المباشر لطيافية الإصدار الذري DCPAES وذلك من أجل تحديد عنصر الكروم $Cr^{+3}$ و$Cr^{+6}$ لعينات مختارة من المياه الجوفية وأخرى من غبار المدارس الابتدائية التي تم تجميعها من منطقة غرب طرابلس. تم تسجيل إشارات الامتصاص الذري بطريقة FIFAAS لكل من $Cr^{+3}$ و $Cr^{+6}$ منفصلة تماماً مع حدود الكشف الأدنى (D.L) تقدر ب 0.03 ميكروجرام/مل بينما عند استخدام DCPAES كانت حدود الكشف الأدنى 0.003 ميكروجرام/مل و 0.002 ميكروجرام/مل لكل من $Cr^{+3}$ و$Cr^{+6}$ على التوالي. تشير النتائج أن عينات المياه قد تحتوي على تركيز أقل من حدود الكشف الأدنى لكلا الجهازين لكل من $Cr^{+3}$ و$Cr^{+6}$. أما عينات غبار المدارس فإنها تحتوي على تركيز يتراوح ما بين 0.9-1.5 ميكروجرام/مل بالنسبة $Cr^{+3}$ بينما كان تركيز $Cr^{+6}$ أقل من 0.05 ميكروجرام/مل عند استخدام DCPAES كما توضح هذه الدراسة أن عينات المياه التي تم تجميعها من المصدر خالية من عنصر الكروم أي أقل من الحد المسموح به لغرض الشرب.

---

**Abstract:** *Micro column of activated alumina was used in Flow Injection coupled with Flame Atomic Absorption and Direct Current Plasma Atomic Emission Spectrometry (DCPAES), for the determination of $Cr^{+3}$ and $Cr^{+6}$ in samples of groundwater used for drinking purposes, from different localities, and dust samples from elementary schools of west of Tripoli area. Atomic signals for both species $Cr^{+3}$ and $Cr^{+6}$ were analyzed by (FIFAAS) with limited detection of 0.03 µg/ml, while in DCPAES it was 0.003 µg/ml and 0.002 µg/ml for $Cr^{+3}$ and $Cr^{+6}$ respectively. Concentration data obtained for potable water for $Cr^{+3}$ and $Cr^{+6}$ were found less than the detection limit of both instruments, and concentration data of dust samples for $Cr^{+3}$ was in the range of 0.9 to 1.5 µg/ml whereas $Cr^{+6}$ was less than 0.05 µg/ml when analyses by DCPAES were used. The results obtained provided evidence that water samples collected from the above mentioned sources were free from any presence of chromium metal.*

## INTRODUCTION

The presence of some toxic elements in natural water has been studied by many workers (Hallam, *et al*, 1985) due to their toxicity properties. Particulate matter, such as dust produced by

*Petroleum Research Centre, P.O. Box. 6431 Tripoli, Libya,

human activity, leads to the distribution of those elements and pollutes the environment. These particulate matters are toxic and cause serious damage to the breathing system. Pollution of the environment by chromium metal is usually generated from different sources such as electro-plating, heat exchanger system and metallurgical foundries. Metal speculation became a major interest of researchers and, therefore, it has expanded to the areas of clinical (Cornelis, *et al*, 1993) and environmental (Byrdy and Carusa, 1994) fields. Metal speculation of these fields plays a role for toxicity and some degree of mobility. The toxicity of metals actually depends upon the oxidation state of these metals being present.

In a solution, chromium primarily exists in either the $Cr^{+3}$ or $Cr^{+6}$ oxidation state and the toxicity of chromium metal actually depends upon the oxidation state of this element. $Cr^{+3}$ is acidic and non toxic if it does not exceed the limit, and is even considered to be an essential nutrient for most mammals, whereas $Cr^{+6}$ is a basic and powerful oxidizing agent and quite toxic. Thus for this reason, the determination of the element speciation is necessary. There are many methods that are sensitive and selective for the determination of $Cr^{+3}$ and $Cr^{+6}$ such as liquid chromatography (Schwedt, 1979), ion exchange (Pankow and Janauer, 1974 & Battistoni, *et al, 1983*) and chelating resins (Leyden, *et al 1972,* Miyazaki and Barnes, 1981). These procedures are time consuming and prolong sample manipulation, and may disturb the natural chromium speciation state. However, atomic spectroscopic methods have some limitation of which only total metal content could be determined, thus, when metal speciation is an interest then other method must be incorporated (Cox, *et al, 1985*). The flow injection method demonstrated an advantage over conventional direct nebulization, (Bushina, *et al, 1997*) in that it allows the identification and analyzation of a micro sample and prevents the nebulizer from blockage.

In this study, an on-line pre concentration of a micro column of activated alumina was incorporated with Flame Atomic Absorption and Direct Current Plasma Atomic Emission Spectrometer used for a sequential determination of $Cr^{+3}$ and $Cr^{+6}$ in eight groundwater samples (Bushina, *et al, 1997*) and dust. The latter samples were collected from 9 schools in the Abu Isa and Surman towns. The selected areas of the sample source have not been studied before.

## EXPERIMENTAL

### *Methods of Sample Collection*

Water samples collected at the source were immediately acidified with (0.5 ml/l) a concentrated nitric acid (sp.gr. about 1.42) and kept in polyethylene containers before the analysis was performed.

Dust samples (mixed with soil) A & B were collected from inside classrooms and elementary school play ground areas during the period of 28–12–1996 to 26–3–1997. Plastic brushes were used for sample collections. All samples were collected in plastic containers and dried in an oven for 24h at 105 °C, and then sieved through 150 μm stainless steel sieve. Table 1, summarizes a typical example of %wt of dust in the samples.

### *Materials and Reagents*

Unless stated otherwise, all chemicals used were of high purity analytical grade. Nitric acid and ammonia solutions were obtained from BDH chemicals, Pool, England. Working standard solutions were prepared daily by serial dilution in nitric acid to give a final acid concentration 0.01M from stock standard solution supplied by VHG lab. Activated acidic, aluminum oxide, (Aldrich Chemicals Co. Ltd.), and further activation

**Table 1. Typical examples of %wt of dust in the samples**

| Sample no. | Total wt (g) | Dust wt (g) | Dust wt (%) |
|---|---|---|---|
| $2A_2$ | 200 | 151.8 | 75.90 |
| $3A_2$ | 200 | 154.2 | 77.10 |
| $3A_3$ | 370 | 216.8 | 58.59 |
| $4A_3$ | 200 | 182.2 | 91.10 |
| $5A_3$ | 200 | 185.8 | 84.45 |
| $6A_3$ | 110 | 87.0 | 79.09 |
| $9A_3$ | 200 | 138.5 | 69.25 |
| $10A_3$ | 200 | 144.7 | 72.35 |
| 10B | 290 | 224.05 | 77.73 |

(Perrin, *et al. 1980*) was performed before it was used for packing the column. The PTFE (2.5 cm long, 3 mm i.d.) mini column was packed with the activated alumina (140 mesh). Water of high purity was used throughout the experimental work. A buffer solution of pH = 4 (ingold, Besell. Nr. 9863) was used for calibration of pH meter. All the glassware used was immersed in a dilute nitric acid (2M) for 24h, followed by washing in high purity distilled water

### *Instrumentation and Apparatus*

The determination of $Cr^{+3}$ and $Cr^{+6}$ was carried out with the SOLAR 959 automatic atomic absorption spectrometer with direct control via external PC data station and software. The instrument has facilities of graphite furnace GF90 coupled with auto sampler, automatic flame auto sampler and Epson parallel Dot Matrix printer. The experimental conditions are summarized in Table 2. Direct Current Plasma (DCP) Spectrospan (V) Beckman, model V-DUAL, Cat No. 487105 was used. The instrument is coupled with printer Epson and chart recorder, and also has the facilities of Inductive Coupled Plasma (ICP). The operating conditions are depicted in Table 3.

The solutions were adjusted at pH = 2 by Knick Digital pH Meter 646. This was conducted by adding a suitable volume of nitric acid and ammonia solutions. PTFE syringes were used to inject the solutions.

### *Methods of Digestion of Dust Samples*

10 g of each sample were placed in a round bottom flask, then 20 ml of concentrated nitric acid (65%) was added. The samples were then refluxed for 2h. The contents were cooled and filtered, and the residue was washed with 0.1M $HNO_3$ and diluted with distilled water to a volume of 100 ml in a volumetric flask

**Table 2. Experimental conditions for flame atomic absorption**

| | $Cr^{+3}$ | $Cr^{+6}$ |
|---|---|---|
| Conc. range (µg/ml) | 0.05 – 0.8 | 0.05 – 0.8 |
| Absorbance | 0.005 – 0.076 | 0.038 – 0.459 |
| Wavelength (nm) | 357.9 | 357.9 |
| Background | Off | Off |
| Sample loop (ml) | 1.0 | 1.0 |
| Flow rate (ml/min.) | 3.0 | 3.0 |
| Detec.limit (µg/ml) | 0.03 | 0.03 |
| Sensitivity (µg/ml) | < 0.04 | < 0.007 |

**Table. 3. Operating condition for DCPAES**

| | $Cr^{+3}$ | $Cr^{+6}$ |
|---|---|---|
| Conc. range (µg/ml) | 0.01– 0.1 | 0.01– 0.1 |
| PMT voltage | 4.0 | 4.0 |
| Wavelength (nm) | 357.9 | 357.9 |
| Sample uptake rate (ml/min.) | 3.0 | 3.0 |
| Nebulizer pressure (psi) | 23.0 | 23.0 |
| Sleeve pressure (psi) | 50.0 | 50.0 |
| Detc. limit (µg/ml) | 0.003 | 0.002 |
| Sample loop (ml) | 1.0 | 1.0 |
| Sample injected (ml) | 1.0 | 1.0 |

### *Analytical Procedure*

The flow injection manifold consists of a pristatic pump, rotary injections valve and a micro column of activated alumina, which were connected to the nebulizer of the used instrument as shown in Figure 1. An acid carrier stream (0.01M $HNO_3$) passes through the column to maintain its acidity. For the mixture to be eluted, the standard solutions were loaded into the injection valve manifold by syringe and then injected to the carrier stream. This was done since $Cr^{+3}$ is acidic and does not deposit on the column. Ammonia solution (2M) was injected to elute $Cr^{+6}$.

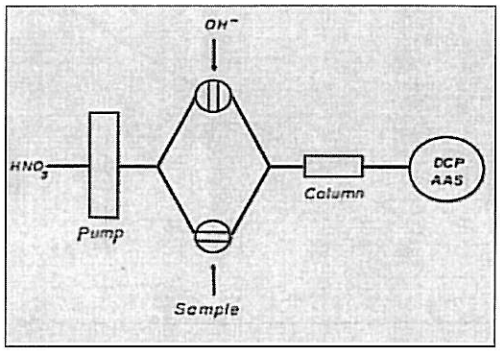



Fig. 1. Flow injection system for determination of $Cr^{+3}$ and $Cr^{+6}$.

## RESULTS AND DISCUSSION

Allumina displays amphoteric properties. The activated allumina, under acidic conditions, has an affinity for ionic species. In contrast, under basic solution, it will have an affinity to cationic species. Thus when using 2M $HNO_3$ as an eluent for the determination of chromium speciation, $Cr^{+3}$ is eluted, whereas Cr+6 is retained, and upon injection of $OH^-$ the $Cr^{+6}$ is also eluted. Results for the determination of $Cr^{+3}$ and $Cr^{+6}$ using Flow Injection Flame Atomic Absorption Spectrometry (FIFAAS) in water samples were found to be less than the detection limit of this procedure which equaled 0.03 $\mu gml^{-1}$ for $Cr^{+3}$ and $Cr^{+6}$. But the atomic signal for standard solutions shows a good separation of both chromium species when a mixture of both chromium species was used in the range of 0.05, 0.1, 0.2, 0.4, 0.8 $\mu gml^{-1}$. It shows good linear calibration graphs for both species as shown in Figures 2a. and 2b. Characteristic mass of $Cr^{+3}$ = 0.045 µg/ml and $Cr^{+6}$ = 0.007µg/ml.

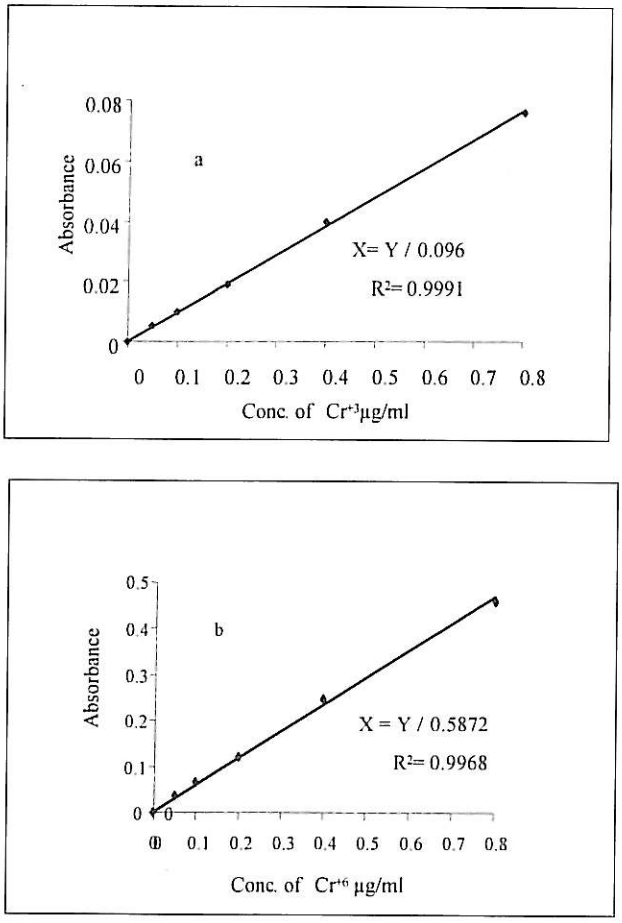



Fig. 2. Calibration curve for (a) $Cr^{+3}$ and (b) $Cr^{+6}$ obtained by FIFAAS.

Analytical line 357.9 nm for chromium AES was used for its maximum sensitivity and lower detection limit. This was used for determination of $Cr^{+3}$ and $Cr^{+6}$ by DCPAES. Figure 3 clearly shows a good dynamic range of 0.01,0.05, 0.1, 0.5 $\mu gml^{-1}$ -for good separation of the two chromium species when optimum conditions were used, such as acid concentration flow rate, separation column capacity, injection loop capacity and ammonia concentration. 1000 µl of the mentioned standard containing both species was loaded into the injection port to the sample loop via injection valve with a stream of 0.01M $HNO_3$ solution was passed through the nebulizer immediately after the sample and standard. The atomic emission signal of $Cr^{+3}$ was recorded as shown in Figure. 3. As soon as the emission signal got to the baseline, 1 ml of ammonia solution (2M) was injected. An atomic emission signal of $Cr^{+6}$ was clearly recorded. As in Figure 3, by this technique, good broadening emission peak of $Cr^{+3}$ and a sharp one of $Cr^{+6}$ were obtained.

The calibration graphs of $Cr^{+3}$ and $Cr^{+6}$ using aqueous standard solution were straight lines with good linearity. All the plots passed through the origin. Results are depicted in Figures 4a and 4b. The limit of detection for both chromium species using DCPAES when water samples were analyzed for $Cr^{+3}$ = 0.003 µg/ml and $Cr^{+6}$ = 0.002 µg/ml. However, analysis of water samples collected at

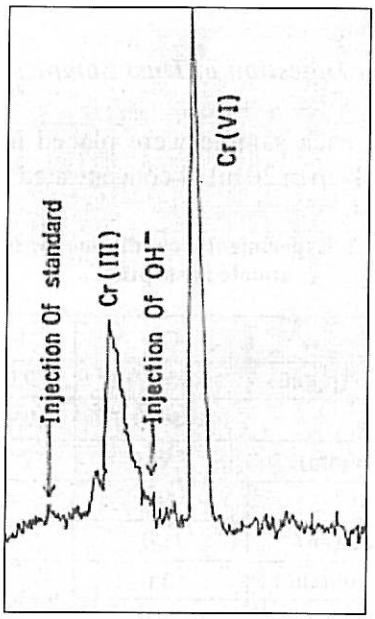



Fig. 3. Recorded signals for standard solution of $Cr^{+3}$ and $Cr^{+6}$ using DCPAES. Concentrations are in µg/ml.

the source in Tripoli city of $Cr^{+3}$ and $Cr^{+6}$ were found to be below the detection limit of this technique. This detection limit was calculated as three times the standard deviation of blank reading. It is clear that no contamination of chromium species was present in the sample that might cause toxicity to humans, but it may need further pre-concentration for the larger samples collected.

Table 4, shows the results of $Cr^{+3}$ and $Cr^{+6}$ concentrations (average of four determinations) and associated relative standard deviation for a selected group of dust sample. As seen, it is quite clear that maximum (1.57 $\mu gml^{-1}$) characteristic mass of $Cr^{+3}$ was found in sample $6A_2$, whereas minimum (0.97 $\mu gml^{-1}$) content was found in samples $3A_3$, $10A_3$. $Cr^{+6}$ content of the all samples was found to be less than 0.05 $\mu gml^{-1}$. This value was calculated from the atomic signals obtained for 10 times the value of detection limit for each sample.

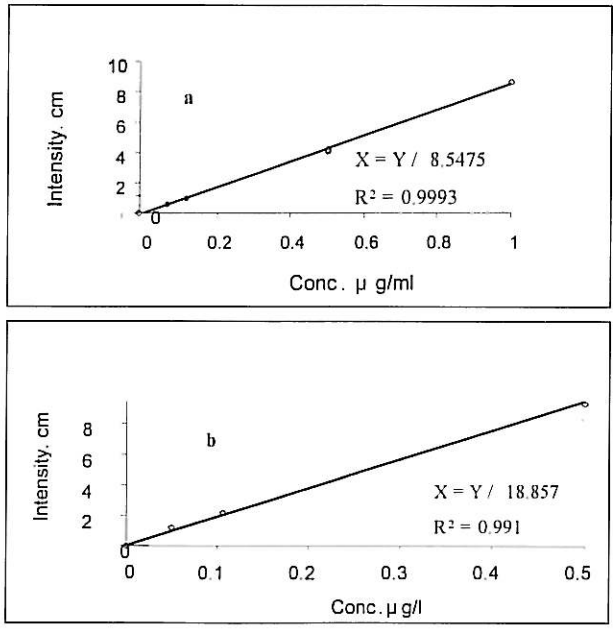



Fig. 4. Calibration curve for (a) $Cr^{+3}$ and (b) $Cr^{+6}$ obtained by DCPAES.

**Table 4. Repetitive chromium species in dust sample**

| Sample | $Cr^{+3}$ (conc.μg/ml) | $Cr^{+6}$ (conc.μg/ml) |
|---|---|---|
| $2A_2$ | 1.09 ± 3.0% | < 0.05 |
| $3A_2$ | 0.97 ± 7.9% | < 0.05 |
| $4A_3$ | 1.45 ± 0.8% | < 0.05 |
| $5A_3$ | 1.35 ± 9.2% | < 0.05 |
| $6A_2$ | 1.57 ± 0.8% | < 0.05 |
| $9A_3$ | 0.99 ± 6.7% | < 0.05 |
| $10A_3$ | 0.97 ± 2.2% | < 0.05 |
| 10B | 1.15 ± 5.5% | < 0.05 |

No. of replicate n = 4

## ACKNOWLEDGMENT

We are indebted to our colleagues from the spectrochemical laboratory of Petroleum Research Centre for their assistance in many ways. Thanks are extended to the management of the PRC for their support of this research project.

## REFERENCES

Battistoni, P., Bompadre, S., Fava, G., and Cobbi, G., 1983. Talanta, **30**, 15

Bushina.I.S., Kut, H.M., Elmahmudi.S.Seham. 1997. *Petroleum Res.* J., **9**. 67.

Byrdy, F. A., and Caruso, J. A., 1994. *Environ. Sci. Technol.*, **28**, 528A.

Cox Alan G., Cook, Ian G., and Mcleod, Cameron W., 1985. *Analyst*, **110**. 331

Cornelis, R., Borguet, F., and de Kimpe, 1993. *J., Anal. Chim. Acta*, **283**, 183

Hallam, C., and Thompson., C., 1985. *Analyst*, **110**, 497

Leyden, D. E., Channell, R. E., and Blount, C. W., 1972. *Anal, Chem.*, **44**, 607

Miyazaki, A., and Barnes, R. M., 1981. *Anal, Chem.*, **53**,364

Schwedt, G., 1979. Fresenius, Z. *Anal. Chem.*, **295**, 382

Pankow, J. F., and Janauer, G. E., 1974. *Anal. Chim. Acta*, **69**,97

Perrin. D. D., Armarego. L. F., and Perrin. D. R., 1980. *Purification of Laboratory Chemicals*. Pergamon Press Oxford. p. 26

Petroleum Res. J. Vol. 11 (1999): P. 51-59, 9 Figs.

# 35S-Radiotracer Studies of Sulphur Poisoning of Platinum Supported Catalysts: 2. Hydrogenation of Ethyne

Ezziddin A. Arafa*

# دراسة سمومية الكبريت – $35_S$ لحفازات البلاتين المدعم على السيليكا والألومنيا وتتبعها بالتقفي بالأثر الأشعاعي: 2 – هدرجة الإيثين

عز الدين أحمد عرفة

تم دراسة سمومية الكبريت لحفازات البلاتين المدعم على السيليكا (Europt-1) 6% Pt/SiO2 والألومينا (Europt-3) 0.3% Pt/$Al_2O_3$، لامتزاز أول أكسيد الكربون (CO) والمواد الهيدروكربونية، الإيثاين ($C_2H_2$) والإيثين ($C_2H_4$) وتفاعل الإيثين مع الهيدروجين ($C_2H_2/H_2$) باستخدام ظاهرة التقفي بالأثر الأشعاعي وباستعمال كبريتيد الهيدروجين المرقم بعنصر الكبريت المشع ($35_S$-$H_2S$) والكربون -14 بنظام مغلق عند درجة 293±2K.

سلوك إمتزاز $35_S$-$H_2S$ تم على مرحلتين، بالمرحلة الأولى كان الامتزاز كبيراً وسريعاً وبالمرحلة الثانية بيّن خط للتشبع كدليل لتكوّن طبقة أولية من كبريتيد الهيدروجين الممتز. نسبة 5% فقط من كبريتيد الهيدروجين الممتز يمكن أزالتها بالتفريغ. من خلال النتائج فقط اقترح بأنه عند ضغوط عالية من كبريتيد الهيدروجين$H_2S$>2.5 ، هذه الحفازات تمر بعملية إعادة بناء لسطحها وأن امتزاز الكبريت يرغم أول أكسيد الكربون والإيثين للامتزاز على المواقع الحامضية الموجودة على $Al_2O_3$.

من خلال النتائج لوحظ أنه، كلما زادت درجة التسمم بعنصر الكبريت فإن انتقائية النواتج تزداد على الحفازات المدعمة على الألومينا بينما وجد العكس على الحفازات المدعمة على السيليكا وأن آلية تسميم الكبريت لهذه الحفازات هي غلق للمواقع التي يتم عليها إمتزاز المواد الهيدروكربونية وهدرجتها.

مجمل النتائج بيّنت أن إنتقائية المنتوجات بتفاعل الإيثاين على هذه الحفازات، تحت الظروف الاعتيادية وظروف التسمم بالكبريت، محكومة بعامل حركي حراري مما يعزز مقترحاتنا السابقة بأنه تحت ظروف امتزاز وهدرجة المواد الهيدروكربونية فإن هذه الحفازات تمر بعملية إعادة بناء لسطحها.

---

**Abstract:** *The sulphur deactivation of 6 % $Pt/SiO_2$ (Europt–1) and 0.3% $Pt/Al_2O_3$ (Europt–3) catalysts for carbon monoxide, ethene and ethyne adsorption and ethyne hydrogenation has been investigated, using sulphur labelled hydrogen sulphide, $^{35}S$-$H_2S$ and 14C-radiotracer of the corresponding adsorbate at 293±2K. Adsorption of $^{35}S$-$H_2S$ occurs in two stages. On Europt-1, it showed a non-linear primary region followed by a linear secondary region, while on Europt-3, it showed a linear primary region followed by a plateau region. A small fraction ca. 5% of the adsorbed sulphur species can be removed by evacuation. It is suggested that at high sulphur coverages, $H_2S$ < 0.5, these catalysts surfaces undergo some reconstruction.*

*It was observed that the effect of sulphur poisoning on the selectivity for ethene formation was beneficial for the alumina-supported catalysts*

* Tajoura Nuclear Research Centre, P. O. Box 30878, Tajoura – Libya.

*whilst detrimental to the silica-supported catalysts. Furthermore, sulphur promotes carbon monoxide and ethene adsorption on the $Al_2O_3$ acidic sites. In addition, it appears that the poisoning behavior of sulphur on the hydrocarbons adsorption and ethyne hydrogenation on these catalysts is simply due to a hydrocarbon site-blocking effect.*

*Evidence has been obtained to support our previous proposals that, on steady state catalysts and under the influence of hydrocarbon adsorption and ethyne hydrogenation reactions a surface reconstruction process occurs and ethyne hydrogenation takes place in the secondary adsorption region. Collectively, the results indicate that Europt-1 and Europt-3 catalysts under clean and sulphur poisoning conditions exhibited a high thermodynamic selectivity but low mechanistic selectivity towards ethyne hydrogenation reaction.*

## INTRODUCTION

The phenomenon of catalyst poisoning is one of the most serious problems associated with the industrial applications of supported metal catalysts in numerous catalytic reactions, especially those involving hydrogen, such as, methanation of coal and its conversion to fuels and chemicals, reforming of naphtha or hydrocarbon hydrogenations. The extremely harsh poisoning encountered in these catalytic systems is that induced by sulphur, mainly because of the fact that the feed stock of these reactions usually contains significant amounts of sulphur containing compounds, such as, $H_2S$, COS, $SO_2$, $CS_2$, or organic sulphides. Sulphur apparently bonds so strongly to metal surfaces and a marked reduction in the catalyst activity may occur even at extremely low concentrations (PPb quantities). Hence, the life of the catalyst may be reduced and its regeneration process is impossible or impractical[1]. On the other hand, the chemisorption of sulphur on metal catalysts may cause beneficial effects on the selectivity by partial and well controlled poisoning. The topic of sulphur poisoning of metallic catalysts has been reviewed comprehensively by many investigators[1–3].

From our previous results[4,5] on ethyne hydrogenation on the same stock of these catalysts, it was apparent that these catalysts possessed poor selectivities (~0.30–0.6) for the production of mono-olefins from di-unsaturated hydrocarbons. The objectives of the present studies were a detailed investigation of the effects of the presence of sulphur upon the adsorption characteristics of carbon monoxide (CO), ethyne ($C_2H_2$) and ethene ($C_2H_4$) and on the selectivities of ethyne hydrogenation ($C_2H_2/H_2$) processes on the same platinum catalysts.

## EXPERIMENTAL

### *Apparatus*

The apparatus which was used in this work consisted of a conventional vacuum system which was maintained at a pressure of ~0.01 Pascal (Pa) by using a mercury diffusion pump backed by an oil rotary pump. The system contained a series of bulbs for the storage of non-radioactive and radioactive gases and a reaction vessel where the adsorption of $^{14}C$-labelled hydrocarbons, the reaction of ethyne with hydrogen and the $^{35}S$-sulphur poisoning experiments were carried out (Fig. 1).

### *Catalysts*

The catalysts employed in this study are standard reference catalysts designed by the Council of Europe Catalysis Group (EUROCAT). Europt–1, is a 6% (w/w) $Pt/SiO_2$ catalyst with a total surface area of 185 $m^2\ g^{-1}$ and a pore volume of 0.72 $cm^3\ g^{-1}$, prepared by Johnson Matthey Chemicals plc [6]. Europt$^{-3}$, is a 0.3% (w/w) $Pt/Al_2O_3$–0.82 % Cl catalyst and is being used

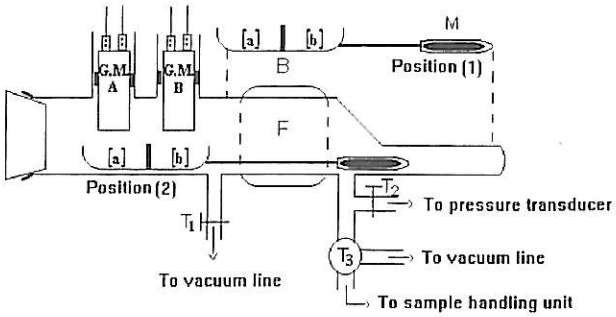



Fig. 1. Reaction vessel used for direct monitoring of surface adsorbed-species. (G.M, Geiger-Muller counters; F, furnace region; B, catalyst boat, position (1) for catalyst reduction and position (2) for surface monitoring; M, glass magnet; $T_{1,2,3}$, glass stopcocks.

commercially under the code KETJEN-CK 303 with a surface area of 184 $m^2 g^{-1}$ and a pore volume of 0.49 $cm^3 g^{-1}$ [7].

Another two platinum catalysts supported on silica (Cab-O-Sil) and γ-alumina (Degusa Ltd.) were prepared at Glasgow University[8] by the impregnation method and characterised as, (w/w), 0.8% $Pt/SiO_2$ and 0.8% $Pt/Al_2O_3$. They were used in this study for comparison of the results of variation of selectivity with extent of sulphur poisoning with those obtained on the EUROPT-catalysts.

### *Materials*

Hydrogen gas (B.O.C., Commercial grade) was used in the catalysts reduction and hydrogenation reactions without further purification. The non radioactive hydrocarbons, $C_2H_2$, $C_2H_4$ and $C_2H_6$ (Air Products Ltd.) were degassed at liquid nitrogen temperature (77 K) for ~ 15 minutes followed by bulb-to-bulb distillation using liquid nitrogen and methylene chloride + solid $CO_2$ mixture. Helium, methane and carbon monoxide (Air Products Ltd.) were used as supplied. The $^{14}C$-radioactive hydrocarbons, $^{14}C_2H_2$ and $^{14}C_2H_4$ were purchased from the Radiochemical Centre, Amersham, U.K. and diluted with the corresponding non-radioactive gas to give a count rate of about 25 counts $min^{-1}$ $Pa^{-1}$. $^{14}CO$ was prepared by the reduction of $^{14}CO_2$ using metallic zinc as described elsewhere[9]. $^{35}S$-hydrogen sulphide was supplied by Sigma Radiochemicals and diluted with the non-radioactive $H_2S$ to produce a count rate in the range of 20–25 counts $min^{-1}$ $Pa^{-1}$.

### *Procedure*

The procedures employed in the reduction of catalysts, adsorption of $^{14}C$-hydrocarbons and ethyne hydrogenation reactions have been described previously[5]. In the $^{35}S$-hydrogen sulphide poisoning experiments, catalysts in a finely grinded form (typically 0.30 0.05g, 100 B.S.S. mesh) were reduced in flowing H2 (30 $cm^3$ $min^{-1}$) at 523K for 2 h and then cooled *in vacuo* to room temperature (*ca.*293±2K). When $^{14}C$-hydrocarbons, $^{14}CO$ adsorptions or $C_2H_2/H_2$ hydrogenation experiments were required, an aliquot of 0–0.5 Kpa (1Kpa = 1000 pa) of $^{35}S$-$H_2S$ was admitted into the reaction vessel, and kept in contact with the catalyst for 15 minutes. The radioactivity content was counted, the reaction vessel was then evacuated for 15 minutes to remove any gas phase $^{35}S$-$H_2S$ and three successive count rates, which represent the sulphur-uptake by the catalyst were recorded. The adsorptions of $^{14}C$-hydrocarbons and ethyne hydrogenation were then performed as described[5].

## RESULTS AND DISCUSSION

### *Adsorption of $^{35}S$-$H_2S$*

Samples of Europt-1 and Europt-3 were reduced with hydrogen and activated as described above. Controlled aliquots of $^{35}S$-$H_2S$ were admitted to the reaction vessel and the surface and gas phase count rates were determined after each addition. Figure 2 presents the adsorption isotherms produced. The isotherms showed a pattern similar to that reported for $^{14}C$-hydrocarbons on these catalysts[4,5]. These showed two distinct regions, a steep primary region followed by a linear secondary region. The secondary region of the isotherms (in particular on Europt-1)) rose linearly with increasing gas pressure. This behavior is in accordance with the results of kinetic studies[10] of the rate of sulphur adsorption on Pt-catalysts which revealed that $H_2S$ adsorption was very rapid at low sulphur coverages ($H_2S$ = 0.25–0.3) while at $H_2S$ > 0.3, sulphur adsorbed slowly. It has been suggested this may be due to the decrease in the sticking coefficient.

On Europt-1, *ca.* 5% of the total amount of the $^{35}S$-adsorbed species was removed by evacuation for 30 minutes. Hydrogen sulphide has been reported[11,12] to adsorb dissociatively as one sulphur atom strongly bonded to two Pt atoms or one sulphur atom weakly bonded to one Pt atom at similar experimental conditions. This observation proposes that sulphur is adsorbed on the metal surface and an indication that the adsorption process is partially reversible with the removable proportion likely to belong to the weakly bonded sulphur species.

Admission of further aliquots of $^{35}S$-$H_2S$ to the catalyst (Europt-1) resulted in a continuous build-up of the sulphur species on the catalysts until a

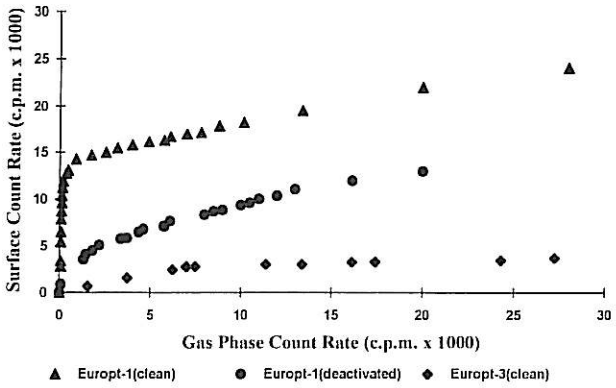



Fig. 2. Adsorption of $^{35}S$-$H_2S$ on Europt-1 and Europt-3 at 293±2K.

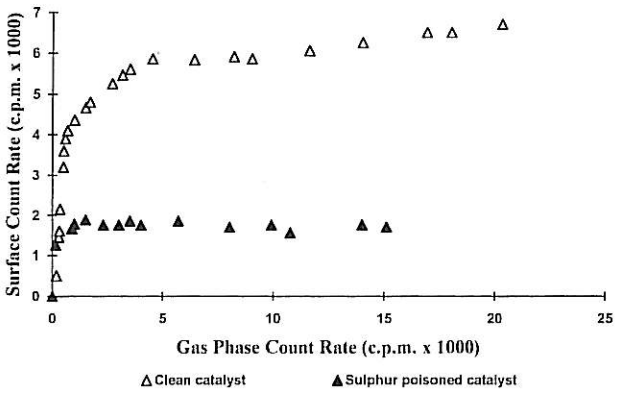



Fig. 3. Adsorption of $^{14}C$-ethyne on clean- and sulphur-poisoned Europt-1 at 293±2K.

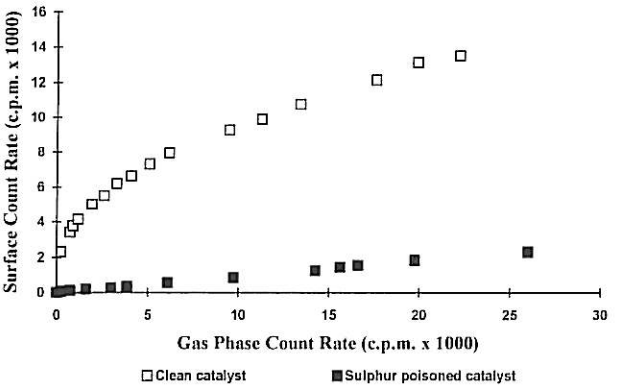



Fig. 4. Adsorption of $^{14}C$-ethyne on clean- and sulphur-poisoned Europt-3 at 293±2K.

plateau region was reached (at *ca.* 30 Kpa per gram catalyst). The saturation value was then taken as to correspond to the completion of monolayer coverage and used to calculate sulphur coverage ($H_2S$) in the subsequent poisoning experiments.

When $^{35}S$-$H_2S$ adsorption on steady state catalysts (catalysts deactivated with $C_2H_2/H_2$ reactions) was investigated, the extent of sulphur adsorption on the primary region was substantially reduced. Although the amount adsorbed in the secondary region was less than that adsorbed on clean catalysts, the isotherms had similar gradients. This suggests that some of the sites in the primary adsorption region, possibly for geometric reasons, can not accommodate hydrocarbon species and were available for sulphur adsorption and that these sites are responsible for the adsorption-activation of hydrogen in ethyne hydrogenation.

### *Adsorption of $^{14}C$-ethyne on poisoned catalysts*

A number of $^{14}C$-ethyne adsorption isotherms have been determined as described above on clean catalysts and catalysts being poisoned with an amount of $^{35}S$-$H_2S$ corresponds to $H_2S$ = 0.25, under identical conditions. The results obtained on Europt-1 and Europt-3 are shown in figures 3 and 4 respectively. As it can be seen, pre-adsorption of sulphur on the catalysts surfaces considerably suppressed the amounts of $^{14}C$-ethyne that could be adsorbed compared with those adsorbed on sulphur-free surfaces. This effect was remarkably pronounced in the secondary adsorption region which showed a plateau behavior as the pressure of adsorbates was increased. Since the hydrocarbon species undergoing hydrogenation as reported[14,5,9] are located in this region, the latter behaviour tempts to conclude that the poisoning effects of sulphur is due simply to hydrocarbon site-blocking effect.

On Europt-1, evacuation of the catalysts for 30 minutes, resulted in the removal of ca. 20% of the hydrocarbon species adsorbed in this region. Admission of $^{14}C$-ethyne on to catalysts with high sulphur coverages, $H_2S > 0.25$, resulted in continuous drop in the surface radioactivity, presumably as a consequence of an interaction between the adsorbed sulphur species and ethyne molecules, leading to the formation of unidentified sulphur containing carbonaceous species. These results also provide evidence to suggest that a surface reconstruction process takes place as a result of sulphur adsorption, thus limiting the extent of $C_2H_2$ adsorption to the exposed metal sites left vacant, probably as electron deficient

sites. They also provide evidence to support the suggestion made previously[4,5] that the turning point of the hydrocarbon adsorption isotherms corresponds to a surface reconstruction process involving the migration of the metal atoms, left vacant at the surface after completion of the primary adsorption process. These form an array with the hydrocarbonaceous residues, thus enhancing the hydrocarbon adsorption as a secondary adsorption process which takes place on these modified sites.

On Europt-3, it is likely that sulphur has completely poisoned the metallic sites of this catalyst, whilst, at the same time promoting some adsorption of hydrocarbons on the support material ($Al_2O_3$).

### *Adsorption of $^{14}$C-ethene on Poisoned Catalysts*

In a series of adsorption experiments on $H_2S$ poisoned catalysts, samples of the catalysts under investigation were reduced and poisoned with $^{35}S$-$H_2S$ in the described manner. This was followed by measuring the $^{14}$C-ethene adsorption isotherms. Figures 5 and 6 show the isotherms obtained on Europt-1 and Europt-3 respectively. On Europt-1, striking features emerged at varied sulphur coverages. At $H_2S = 0.25$, the adsorptive capacity of $^{14}C_2H_4$ in the primary and secondary regions were enhanced. At $H_2S = 0.35$–$0.5$, the adsorption of $^{14}C_2H_4$ in the secondary region was remarkably reduced showing a plateau behavior, while the position of the turning point remained unchanged. At $H_2S$ 0.5, and as noticed in the $^{14}C_2H_2$ adsorptions, a continuous drop in the surface count rate was observed, suggesting the occurrence of

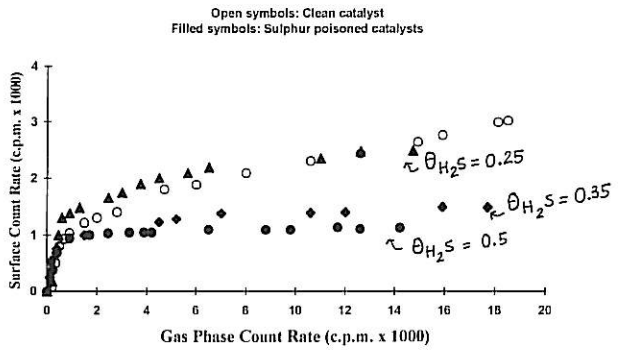



Fig. 5. Adsorption of $^{14}$C-ethene on clean- and sulphur-poisoned Europt-1 at 293±2K.

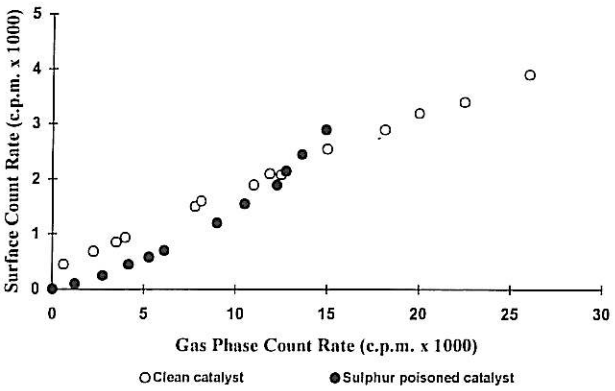



Fig. 6. Adsorption of $^{14}$C-ethene on clean- and sulphur-poisoned Europt-3 at 293±2K.

an interaction between the pre-adsorbed sulphur and the $^{14}C_2H_4$ molecules, forming some sulphided carbonaceous species. Evacuation of the reaction vessel for 30 minutes after the build-up of the $^{14}C$-$C_2H_4$ isotherms resulted in a decrease in the surface count rate to a value corresponding to the turning point of the adsorption isotherms.

On Europt-3, at $H_2S = 0.25$, sulphur completely suppressed the adsorption of $^{14}C_2H_4$ in the primary region, whereas an enhanced uptake of ethene was observed to occur as the pressure of $^{14}C_2H_4$ was increased, showing an up-ward concave curve which is a characteristic of a physical adsorption process[13].

It is important to note that, on the catalysts under study, the extent of sulphur-induced suppression of the hydrocarbon adsorption capacity was less with ethene than with ethyne.

### *Adsorption of 14C-Carbon Monoxide on Poisoned Catalysts*

Carbon monoxide adsorption has been widely used as a probe for catalyst surface area determination and to distinguish the active centres in the catalytic reactions[9,13,18,19]. In order to gain an insight to the fate of such centres as a result of sulphur poisoning in the ethyne hydrogenation reaction on platinum catalysts the adsorption of $^{14}$CO on these catalysts has been examined. Controlled pulses of $^{35}S$-$H_2S$ were admitted to the freshly reduced catalysts as described above to give a sulphur coverage of $H_2S = 0.25$. $^{14}$C-carbon monoxide adsorption isotherms were obtained by admitting successive aliquots of $^{14}$CO to the S-

poisoned catalysts. These isotherms are shown in figure 7 (for Europt-1) and figure 8 (for Europt-3). The isotherms show interesting and important differences between the adsorption of $^{14}CO$ on freshly reduced and S-poisoned catalysts. On (Europt-1), at low sulphur coverages, $H_2S$ 0.5, the isotherms showed similar shapes to that observed on the clean catalyst, in the sense that the adsorption continued to increase as further $^{14}CO$ was admitted to the reaction vessel. At $H_2S$ 0.5, the $^{14}CO$ showed different behavior. The surface count rate rose rapidly with increased gas pressure to a saturation value, then remained constant as the $^{14}CO$ pressure was increased (Langmuir type isotherm). These results are consistent with the suggestion made above, that in the presence of sulphur, a surface reconstruction process takes place on the catalyst. Such a phenomenon has also been proposed on surfaces of single crystals[14].

Evacuation of the reaction vessel for 30 minutes resulted in the removal of *ca.*10% of the

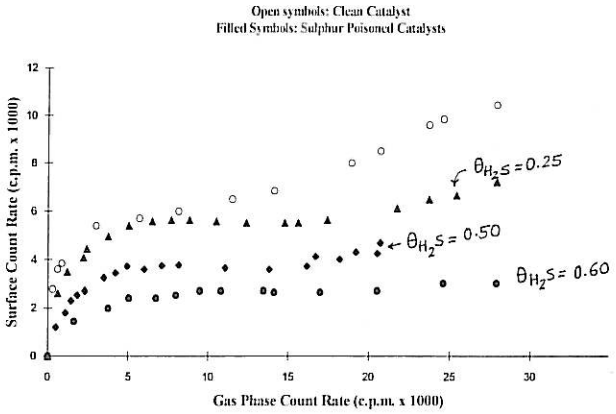



Fig. 7. Adsorption of $^{14}C$-carbon monoxide on clean- and sulphur-poisoned Europt-1 at 293±2K.

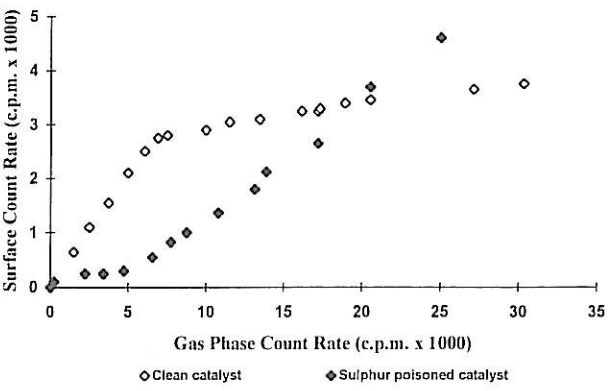



Fig. 8. Adsorption of $^{14}C$-carbon monoxide on clean- and sulphur-poisoned Europt-3 at 293±2K.

adsorbed $^{14}CO$ species. According to an IR study[15] such removable species may be assigned to weakly adsorbed CO on sulphur-poisoned sites.

On (Europt-3), and at $H_2S$ = 0.25, the sulphur poisoned catalyst showed an isotherm indicating an initial small $^{14}CO$ uptake with a short plateau region followed by a linear increase of $^{14}CO$ adsorption, as further gas pressure was admitted on the catalyst. The latter behavior was also observed in ethene adsorption isotherm and attributed to physical adsorption process.

### *Effects of $^{35}S$-$H_2S$ Poisoning on the Selectivity of ethyne Hydrogenation*

In a series of ethyne hydrogenation reactions using different Pt-catalysts, the selectivities on these catalysts was studied as a function of $H_2S$-uptake. Controlled pulses of $^{35}S$-$H_2S$ were admitted to the catalyst surface and left to equilibrate for 15 minutes, followed by 15 minutes evacuation of the reaction vessel. A 6.66 Kpa, 3:1, $H_2$:$C_2H_2$ mixture was then introduced on to the catalyst in the reaction vessel and the extent of the reaction was monitored by the pressure transducer. At pressure fall of 1.33 Kpa, the products were analysed by the gas chromatography. This procedure was repeated with various amounts of pre-adsorbed $H_2S$.

Figure 9, shows the variation of selectivity with $H_2S$-coverage ($H_2S$). From these results it can be seen that, over (Europt–1) (6% $Pt/SiO_2$) and (0.8% $Pt/SiO_2$) catalysts, the selectivity decreased considerably as the pressure of $H_2S$ was increased. The effect was greater with the former catalyst as compared with the latter. On (Europt-3) (0.3% $Pt/Al_2O_3$) and (0.8% $Pt/Al_2O_3$) catalysts, the presence of sulphur was beneficial in that a steady increase in the selectivity occurred as the $H_2S$-coverage was increased. This may be attributed to the influence of the acidic sites present on the alumina. This is indeed a possible explanation when the adsorption isotherms of ethyne and ethene on the sulphur-poisoned catalysts are compared with those obtained on the clean catalysts (Figs. 4, 6). The shapes of the secondary adsorption regions of these isotherms continued to increase sharply as further hydrocarbon gas was admitted to the catalyst. This latter behavior, which has been observed in the adsorption of n-pentane on various

supports, such as carbon and $BaSO_4$, is characteristic of a physical adsorption process[13,15]. Thus, the possibility exists that, in the presence of sulphur, the gas phase ethene formed from ethyne hydrogenation being adsorbed at the chlorinated alumina sites, while the double bond character of the molecule was retained[16]. This, in the presence of hydrogen, would lead to the desorption of ethene to the gas phase, hence, increasing the selectivity.

When $^{35}S$-$H_2S$ was pre-mixed with the reaction mixture (3:1, $H_2$:$C_2H_2$) before the hydrogenation reactions on clean catalysts, the effect of sulphur on the selectivity with each catalyst was identical to that observed above. It is important to note that the presence of sulphur did not completely poison the catalysts for ethyne hydrogenation, and hydrogen effectively competes with sulphur for the sites suggestd above as active for both hydrogen dissociation and sulphur adsorption in the presence of ethyne and ethene. However, there is a strong evidence in the literature[17] to suggest that sulphur has a minor effect on the reactivity of the sites which were active for hydrogen adsorption.

The hydrogenation of ethyne in the presence of $^{14}C$-ethene as a tracer was also examined on sulphur-poisoned catalysts, to gain further knowledge of the effect of sulphur on the different reaction pathways in ethyne hydrogenation on (Europt-1) which has been studied previously[4]. Samples of (Europt-1) were reduced and poisoned with known amounts of $^{35}S$-$H_2S$ and then a pre-mixed mixture of 1.66 Kpa $C_2H_2$, 5.0 Kpa $H_2$ and 0.27 Kpa $14C_2H_4$ was admitted to the reaction vessel. In another set of reactions the amount of added $^{14}C_2H4$ was increased to 0.5 Kpa and 0.67 Kpa. The content of radioactivity in the individual reaction products was determined using radio-gas chromatography. As observed on the sulphur-free catalysts, the amount of $^{14}C$-ethane ($C_2H_6$) produced constituted only a small fraction (~ 1%) of the total ethane yield, relative to the amount expected from the amounts of added $^{14}C$-$C_2H_4$ present in the reaction vessel.

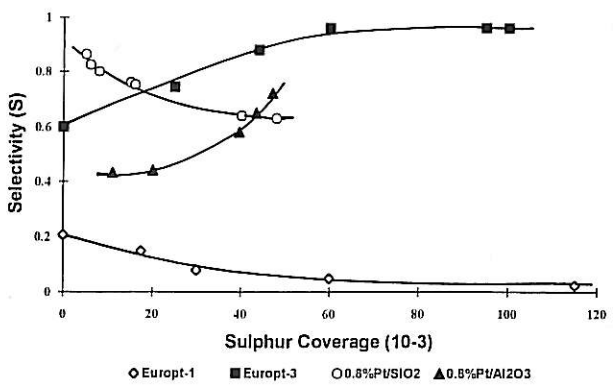
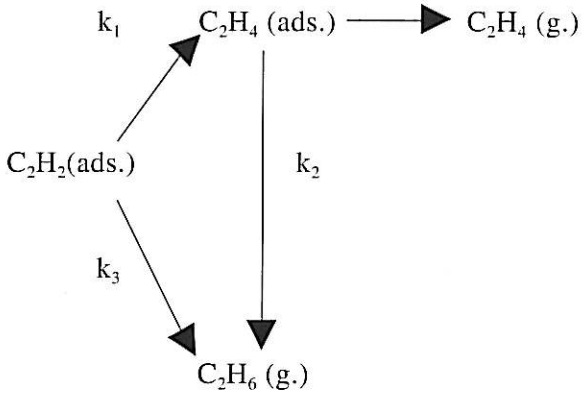



Fig. 9. Variation of selectivity with $H_2S$ coverage ($\theta H_2S$) for ethyne hydrogenation on Pt-supported catalysts for ethyne hydrogenation at 293±2K.

The proposed pathways for ethyne hydrogenation on the supported-Pt catalysts used in this work[4,5,9] are:




It is possible to calculate relative values for the rate constants $k_1$, $k_2$ and $k_3$, using a developed steady state procedure[18] and values of $k_1$ = 0.020 3.5%; $k_2$ = 0.006 0.13% and $k_3$ = 0.066 0.08% were obtained for ethyne hydrogenation on sulphur-poisoned (Europt-1). When these rate constants are compared with the values of k1= 0.014 3%; $k_2$ = 0.002 4% and $k_3$ = 0.091 1%, obtained for ethyne hydrogenation on clean (Europt-1)[4], an interesting feature emerges. While the effect of sulphur was to decrease the hydrogenation rate occurring via the route $k_3$, it showed a beneficial effect in that an increase in the rate of the reactions proceeding via the routes k1and $k_2$ ($k_1$ $k_2$ $k_3$) leading to $C_2H_6$ formation. These findings suggest that the presence of one sulphur atom on a given site neither affected the catalytic activity or the selectivity of the neighboring sites (pure site effect) nor the mechanism of ethyne hydrogenation on these catalysts proposed previously[4,5]. For this reason (Europt-1) displayed a substantial decrease in the selectivity as the catalyst was poisoned with sulphur (Fig. 9). Similar behavior has been also

observed in the hydrogenation of buta–1,3-diene on sulphur poisoned (Europt-1) and (Europt-3) catalysts[20].

## CONCLUSIONS

In conclusion, the results obtained in this study of sulphur poisoning on $Pt/SiO_2$ and $Pt/Al_2O_3$ catalysts at 293 2K showed:

(i) During sulphur adsorption and at $H_2S$ 0.5, a rearrangement of the surface occurs resulting in the freeing of metal sites on the surface. The precise origins of this rearrangement cannot be established from the present studies, however, it could arise from the movement of metal atoms through the sulphur species adsorbed in the primary layer.

(ii) The poisoning effects of sulphur are simply due to hydrocarbon site-blocking effect and not to ligand or electronic effects usually observed in sulphur poisoning[17].

(iii) The $^{35}S$-$H_2S$ tracer studies of sulphur poisoning presented in this work support our previous proposal[4,5,20] that the turning point observed in the hydrocarbon adsorption isotherms corresponds to a surface reconstruction process and ethyne hydrogenation takes place in the ad-layer (the secondary adsorption region) on the hydrocarbonaceous layer.

(iv) Sulphur promotes the adsorption of ethene and carbon monoxide on the acidic sites of the support material such as, $Al_2O_3$.

## ACKNOWLEDGEMENTS

The author wishes to thank Professors G. Shraiha and M. Omar of the Chemistry Department, Al-Fateh University for their continuous encouragement and support and Dr Y. Khribish for reading the manuscript.

## REFERENCES

[1] Oudar, J. 1980. Sulphur adsorption and poisoning of metallic catalysts. *Catal. Rev. Sci. Eng.*, **22**, 171–195

[2] Bartholomew, C. H., Agrawal, P. K. and Katzer, J. R., 1982. Sulphur poisoning of metals. *Adv. Catal.*, **31**, 136–235.

[3] Barbier, J., 1985. Effect of poisons on the activity and selectivity of metallic catalysts. In J. Oudar and H. Wise (eds.). *Deactivation and Poisoning of Catalysts*, **3**, 109–150. Marcel Dekker Inc.

[4] Arafa, E. A. and Webb, G., 1993. A $^{14}C$-Radiotracer study of the hydrogenation of ethyne over EUROPT–1. *Catal. Today*, **17**, 411–418.

[5] Arafa, E. A., 1998. A $^{14}C$-Radiotracer study of the hydrogenation of ethyne on 0.3% Pt/Al2O3 (Europt-3). *Petroleum Res. J.*, **10**, 31–37.

[6] Bond, G.C. and Wells, P.B., 1985. Characterization of the standard platinum/silica catalyst Europt-1. *Appl. Catal.*, **18**, 225–230.

[7] Musso, J. C. and Parera, J. M., 1987. Adsorption and spillover of hydrogen on $Al_2O_3$ and Pt/Al2O3. *Appl. Catal.*, **30**, 81–90.

[8] Arafa, E. A., 1988. *Ph.D. thesis*, Glasgow University.

[9] Al-Ammar, A. S. and Webb, G., 1978. Hydrogenation of acetylene over supported metal catalysts. *J. Chem. Soc., Faraday Trans. I*, **74**, 195–205; 657–664.

[10] Bonzel, H. P. and Ku, R., 1973. Kinetics of sulphur adsorption on supported catalysts. *J. Chem. Phys.*, **58**, 4617; **59**, 1641.

[11] Protopopopoff, E. and Marcus, P., 1986. Coadsorption of sulphur and hydrogen on platinum. *Surface Sci.*, **169**, 237–244.

[12] Barbouth, N. and Salame, M.,1987. Influence of adsorbed sulphur on catalytical activity of platinum in ethylene hydrogenation reaction. *J. Catal.*, **104**, 240–245.

[13] Arafa, E. A., 1985. *M. Sc. thesis*, Glasgow University.

[14] Somorjai, G. A., 1990. Modern concepts in surface science and heterogeneous catalysis. *J. Phys. Chem.*, **94**, 1013–1023.

[15] Satterfield, C. N., 1980. *Hetrogenous Catalysis in Practice*. McGraw-Hill. 320 P.

[16] Peri, J. B., 1964. *Proceedings 3rd International Congress in Catalysis*. **2**, 1100.

[17] Oudar, J., 1986. Sulphur poisoning of metal catalyst. *Proceedings International Symposium in Heterogeneous Catalysis*. 245–250, ACS, New York.

[18] Berndt, G. F., Thomson, S. J. and Webb, G., 1983. Radiotracer studies of the hydrogenation of acethylene over nickel catalysts. *J. Chem. Soc. Faraday Trans.*, **79**, 195–207.

[19] Bond, G. C. and Burch, R., 1983. Metal-Support Interactions. In: G. C. Bond and G. Webb (eds.), *"Catalysis", Specialist Periodical Reports*, **6**, 27–60. The Chemical Society, London.

[20] Arafa, E. A., 1998. $^{35}$S-Radiotracer studies of sulphur poisoning of platinum supported catalysts: 1. Hydrogenation of Buta–1,3-diene, *Proceedings 4th Arab Conference on Peaceful Uses of Atomic Energy*, Tunisia.

Petroleum Res. J. Vol. 11 (1999); P. 61-64, 2 Figs.

# The Role of Lanthanum Chloride as a Releasing Agent for Iron in its Determination by Flame Atomic Absorption Spectrophotometer in Nitrate and Sulphate Media

H.M.Kut*

# دور كلوريد اللانثانيوم كمحرر لتحديد الحديد باستخدام لهب طيف الامتصاص الذري في وسطى النترات والكبريتات

حسن محمد كت

لقد تم دراسة تأثير إضافة كلوريد اللانثانيوم لتحديد عنصر الحديد في عينات من النفط الخام تم تحضيرها في حمض النيتريك (15% بالحجم) وحمض الكبريتيك (5% بالحجم)، وتُشير النتائج أن كلوريد اللانثانيوم (0.5–1.0% كتلة/حجم) يعمل كمحرر لإمتصاص عنصر الحديد في وسط النترات بينما هبط تأثيره كخافض للإمتصاص في وسط حمض الكبريتيك في مدى تركيز للحديد يتراوح بين 0.5–3.0 جزء في المليون.

**Abstract:** *The effect of lanthanum chloride addition for iron content determination in crude oil samples prepared in 15% v/v $HNO_3$ and 5% v/v $H_2SO_4$, respectively, was studied. The results indicated that the addition of lanthanum chloride (0.5–1.0% m/v) serves as releasing agent for iron determination in nitrate medium, whereas the absorption is depressed in sulphate medium and this depression is proportionally increased by increasing iron concentration in the range of 0.5–3.0 ppm.*

## INTRODUCTION

Flame Atomic Absorption is commonly used for trace metals determination (Sychra *et al,* 1981). Because of the fact that the absorption of radiation by individual atoms is a characteristic of the element, atoms of any other element do not normally absorb this radiation, which results in almost complete freedom from spectral interference in the method. However, other types of interference, for example, vaporization, ionization, or background, may be present (Willard *et al,* 1988). Different approaches are normally employed to overcome such interference. These include the addition of specific chemicals to minimize interference (Price, 1974). In this respect, some metal chlorides are commonly added to overcome various kind of interference, such as the addition of calcium and lanthanum chlorides to eliminate the phosphate and silicon interferences on strontium (Amos and Willis 1966). Similarly, excess sulphuric and hydrochloric acids were found to enhance the absorption of iron. On the other hand, Silicon was reported to suppress the absorption by iron, calcium and magnesium and the addition of lanthanum salt overcomes silicon interference of the aforementioned elements (Roos and Price, 1969, and Thompson and Reynolds, 1978). Although lanthanum chloride is widely used as a

*Petroleum Research Centre P. O. Box 6431, Tripoli, Libya.

releasing agent during iron determination, in order to enhance the absorption signal produced by iron (Platte, and Marcy 1965), the effect of lanthanum chloride was found to depend on the digestion media. This paper describes the effects of adding variable concentrations of Lanthanum (as $LaCl_3$) for iron determination, in different acidic media.

## EXPERIMENTAL

### *Analytical Procedure*

A known amount (10 grams) of two crude oil samples A and B were dry ashed, and digested with 15% v/v $HNO_3$ and 5% v/v $H_2SO_4$, respectively. They were then subjected to Atomic Absorption Spectrometry using Pye Unicam, model SP9, equipped with a PU 9090 data graphic system and Pu 998 video graphic programmer. The instrument also has facilities of graphite furnace automatic sampling. Measurements were made with air acetylene flame in the absorbance mode; hollow cathode lamp and gases of high purity were used. The experimental parameters including spectral wavelength, hollow cathode lamp current, burner height, flame gases and spectral slit are listed in Table 1. The data were obtained by using calibration graph least mean square method with regression coefficient (r = 0.99969. Calibration graph of iron in aqueous media is represented (Fig.1).

### *Reagents*

Chemicals of analytical reagents grade were used without further purification. The standard solutions of the element of interest were prepared by appropriate dilution from stock standard solution supplied by BDH chemicals Ltd, Poole, England. High purity doubly distilled water was used throughout this study.

**Table 1. FAAS experimental conditions for iron determination**

| Wave length (nm) | Lamp current (mA) | Burner height (cm) | Fuel/oxida -nt (ratio) | Slit (nm) |
|---|---|---|---|---|
| 248.3 | 14 | 7 | 20/35 | 0.2 |

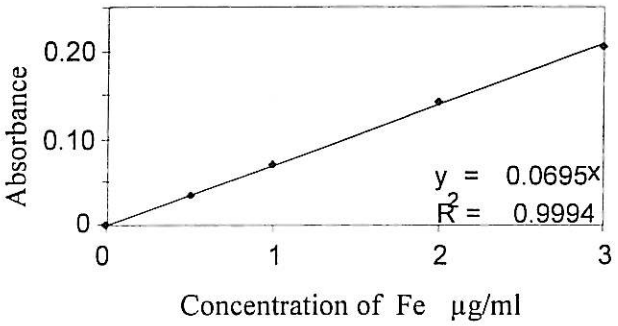



Fig. 1. Calibration curve of iron.

## RESULTS AND DISCUSSION

The effect of interference which is generally accompanied by the addition of lanthanum chloride, on the iron determination, was studied. In the present study two sets of experiments were performed to assess the efficiency of the addition of $LaCl_3$ in nitric acid and sulfuric acid media. Also, four standard solutions of iron were used to assess the effect of lanthanum addition on iron absorption in sulphate medium. Table 2 summarizes the addition of $LaCl_3$ in nitric acid medium.

The results from Table 2 suggest that the addition of $LaCl_3$ liberate some iron from an interfering matrix so that sample A increased by 0.22 $\mu gg^{-1}$ and sample B, by 1.00 $\mu gg^{-1}$. The addition of 1.0% m/v $La^{3+}$ showed no significant increase which probably indicates that 0.5% m/v $La^{3+}$ (as $LaCl_3$) is enough to overcome the problem of interference with iron. However results from Table 3 indicate that there is an obvious decrease in the results for the two samples through the addition of $LaCl_3$ in $H_2SO_4$ medium (A, –0.32; B, –1.03 for 0.5 m/v% $La^{3+}$ addition and: A, –0.79; B, –1.64 for 1.0 m/v% $La^{3+}$ addition respectively; all values are in $\mu gg^{-1}$. The reduction in the results

**Table 2. Effects of $LaCl_3$ addition in nitric acid medium**

| Addition of $La^{3+}$ (m/v%) | Concentration of iron in ($\mu gg^{-1}$)* | |
|---|---|---|
| | Sample A | Sample B |
| 0.0 | 20.87 | 25.07 |
| 0.5 | 25.07 | 26.07 |
| 1.0 | 21.10 | 26.09 |

*Average of triplicate results

**Table 3. Effects of $LaCl_3$ addition in $H_2SO_4$ medium**

| Addition of $La^{3+}$ (m/v%) | Concentration of iron in ($\mu gg^{-1}$)* | |
|---|---|---|
| | Sample A | Sample B |
| 0.0 | 21.19 | 25.64 |
| 0.5 | 20.87 | 24.61 |
| 1.0 | 20.40 | 24.00 |

*Average of triplicate results

remains roughly proportional to the increasing $LaCl_3$ concentration. This indicates that the addition of $LaCl_3$ in $H_2SO_4$ medium depresses the iron absorbance.

Table 4 gives the iron absorbances in different media, and these results are illustrated (Fig. 2).

The percentage depression and the percentage enhancement were compared to the aqueous medium. From Table 4 it is clear that a general enhancement is caused by the addition of 5% v/v $H_2SO_4$ and this enhancement decreased with increasing iron concentration. The results indicate that the percentage enhancement, made by 5% v/v $H_2SO_4$ addition, is found to assume optimum value (62.8%) at low concentration. On other hand, the addition of 0.5% m/v $La^{3+}$ to these acidified solutions caused a noticeable depression in iron absorption values. The percentage depression, contrary to the acidified only solutions was found to increase with iron concentration. It might be conjectured that the addition of $LaCl_3$ may react with H2SO4 to form a stable compound according to the following reaction.

$$2LaCl_3 + 3H_2SO_4 \rightarrow La_2(SO_4)_3 + 6HCl \quad (1)$$

Somehow, the formation of $La_2(SO_4)_3$ retards the nebulization process, resulting in a depressive effect on the iron absorption value. Another tentative explanation that sulfuric acid causes the precipitation of a relatively insoluble lanthanum sulphate (as given in equation 1 above) containing some of the iron occluded within the precipitate. Otherwise, iron absorption in nitric acid media has no noticeable effect compared to aqueous media. A final, concluding remark is supporting evidence from literature, where Curtis (1969), reported that for iron determination using air acetylene flame, interference is more pronounced in sulphate medium than in nitrate or chloride media. Therefore, for satisfactory iron determination in $H_2SO_4$ medium, the standard should contain the

**Table 4. Iron absorbance values (by FAAS) in different media**

| Fe(Conc.) $\mu gml^{-1}$ | $H_2O$ | 5%v/v $H_2SO_4$ | Enhancement (%) | 0.5%m/v $La^{3+}$ 5% $H_2SO_4$ | Depression (%) |
|---|---|---|---|---|---|
| 0.5 | 0.035 | 0.057 | 62.8 | 0.030 | 14.2 |
| 1.0 | 0.071 | 0.093 | 31.0 | 0.045 | 36.6 |
| 2.0 | 0.142 | 0.166 | 16.9 | 0.057 | 59.8 |
| 3.0 | 0.206 | 0.229 | 11.1 | 0.077 | 62.6 |

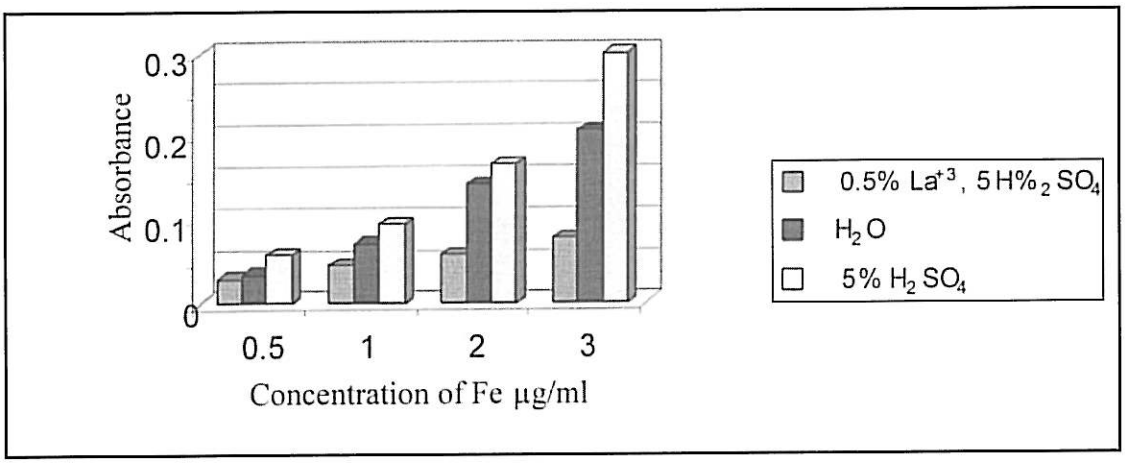



Fig. 2. Iron absorbance values (By FAAS) in different media.

same concentration of acid as that present in the analyte sample.

## CONCLUSIONS

1. The addition of $LaCl_3$ serves as a releasing agent for iron in its determination by FAAS in nitric acid medium.
2. The addition of 1.0 – %m/v $La^{+3}$ as ($LaCl_3$) showed no significant increase than that of 0.5% m/v $La^{+3}$.
3. In sulfuric acid medium $LaCl_3$ is considered as a severe depressant.

## ACKNOWLEDGMENTS

The author wishes to thank Dr G. Nickles from the Chemistry Department of Bristol University, England, for supervising this work and also Dr A. Elaseer from the Nuclear Research Centre (Tripoli, Libya), for his useful discussion.

## REFERENCES

Amos, M. D. and Willis, J.B.,1966. *Spectrochim. Acta*, **22**, 1325.

Curtis, K. E., 1969. *Analyst*, **94**, 1068.

Platte, J. A. and Marcy, V. M.,1965. *At. Absorption Atom. Spect.*, 4,341–426.

Price, J. W.,1974. *Analytical Atomic Absorption* Spectrometry, Heyden & Son. Ltd.

Roos, J. T. H, and Price, W.J.,1969. *Analyst*, **94**,89.

Sychra, V., Lang, I. and Sebor, G., 1981. *Progr. Anal. Newsletter*, **4**, 289,

Thompson, K. C. and Reynolds, R.J.,1978. *Atomic Absorption, Fluorescence and Flame Emission Spectroscopy: Practical Approach*, 2nd ed., Charles

Griffin & Co, Ltd.

Willard, H, H., Merritt, L, L, Jr., Dean, J. A., and Settle, F, A., Jr., 1988. *Instrumental Method of Analysis*, Seventh, Edition, Wadsworth, Inc.P.250.

Petroleum Res. J. Vol. 11 (1999); P. 65-68.

# Lead Contamination in Soil and Vegetation Around Al Fossool Al arbaa Lead Plant in Tripoli District

S. A. Jawashi* & M. A. Abuhameda

# تركيز الرصاص في التربة وأوراق النباتات حول مصنع الفصول الأربعة لاستعادة الرصاص بمنطقة طرابلس

سالم عبد الله الجواشي ومحمد علي أبو حميدة

تم قياس تركيز الرصاص في عينات من التربة والغطاء النباتي بالمنطقة المحيطة بمصنع الفصول الأربعة لاستعادة الرصاص حيث تم تحديد متوسط تركيز الرصاص في عينات تم تجميعها من أبعاد واتجاهات مختلفة من مكان المصنع. تبيّن من هذه الدراسة أن متوسط تركيز الرصاص في الكساء الخضري لعينات مغسولة بالماء يتراوح ما بين 541.3 و5.8 جزء لكل مليون، تم جمعها على بعد 100 و50 متر من المصنع على التوالي و1173.1 و8.7 جزء لكل مليون للعينات غير المغسولة والتي تم تجميعها على نفس الأبعاد السابقة وعلى التوالي أيضاً.

وبالمثل فإن متوسط تركيز الرصاص المقاس لعينات التربة المجمعة من نفس الأبعاد السابقة ذكرها تقع بين 5439.8 و12.0 جزأ لكل مليون على التوالي.

كما قورن تركيز الرصاص للمنطقة المحيطة بالمصنع مع تركيز الرصاص في مناطق القربولي والعزيزيّة وقصر بن غَشير حيث وجد أن تركيز الرصاص حول المصنع موضوع هذه الدراسة أعلى بكثير من تركيزه في المناطق الثلاثة المذكورة.

---

**Abstract:** *Lead contamination in soil and vegetation samples have been determined at different locations in Al Fossool Al arbaa lead plant (FALP) area. Average lead content was determined at different locations and directions from the plant in washed and unwashed vegetation samples, which ranged from 5.8 to 541.3 ppm and 8.7 to 1173.1 ppm respectively. Similarly, lead content in soil samples has also been determined at different locations and directions from the plant, which ranged from 12.0 to 5439.8 ppm. The observed lead content data were compared with newly obtained data from Al Aziziyah , Al Qarabulli and Ben Ghashir towns. The lead content in soil and vegetation of Al Fossool Al arbaa plant area was found to be much higher than that in the above mentioned locations.*

## INTRODUCTION

Lead pollution and its effects on health are matters of general concern[1-3] . The potential danger to children is now receiving particular attention. Lead in various inorganic forms may be inhaled or ingested, and various sources of ingested lead are recognized and tolerable limits

*Petroleum Research Centre, P. O. Box 6431, Tripoli, Libya

have been established[4–6]. One of the most important sources of lead contamination is the combustion of leaded gasoline by automobiles and the subsequent release of lead particles through exhaust. Lead contamination of soil appears to be virtually irreversible and lead finds access into plant and animals, and thus enters into the food web.

The small Al Fossool Al Arbaa Lead Plant (FALP), which recycled lead from used batteries, was in operation until early 1994. It was located at Bir Al-Usta Milad Area, about 15 kilometres east of Tripoli. The operation used to involve direct burning of lead-containing cores and the collection of molten lead manually. Combustion gases and particulate were directly released to the environment by means of an inadequate 15-metres-high chimney made of metal barrel.

The aim of this study is to determine the lead contents, in both, vegetation and soil, at various distances and directions from the plant

## EXPERIMENTAL METHODS AND RESULTS

All glassware was leached in 50% nitric acid for 24 hrs. and washed in distilled water prior to use. Atomic absorption analyses were performed on a Varian Model 1475 instrument at 217 nm using an air-acetylene flame. Dilute standard solutions were prepared in the same acid matrix as the samples.

## PREPARATION OF SAMPLES

a) ***Vegetation Samples:*** samples of plant leaves were collected in plastic bags from different locations and directions in Al Fossool Al arbaa lead plant area. These samples were prepared for analysis of lead content by atomic absorption spectrophotometer according to a standard procedure[7,8]. The samples were divided into two portions (i.e. washed and unwashed). Washing was carried out with about 20 litres of running water to remove the surface dust. Both samples (5–10 grams each) were oven dried at 105 °C for 2 hrs. and ashed by using a muffle furnace at 450 °C for 4 hrs. The samples were then cooled in a dessicator in the presence of anhydrous calcium chloride and were kept overnight. The dry weights of the samples were noted and the ash was dissolved in 2M HCl and filtered through Whatman No.50 filter paper and the volume was made up to 50 ml. These solutions were analyzed and the results are reported in Table 1.

b) ***Soil Samples:*** Ten soil samples were collected from different locations and directions in FALP area. The distance between one sample and another is about 10 metres. The soil samples collected were obtained from the surface to a depth of about 5 cm. These samples were prepared for analysis of lead content by atomic absorption according to the same standard procedure[7,8]. All samples were oven dried at 105 °C for 24 hrs. An accurately weighed (1–5 g) sample was taken into 250 ml beaker then 10 ml of 65% nitric acid was added and the mixture was evaporated to dryness by heating on a hot plate. After cooling this operation was repeated using a second aliquot of nitric acid. 10 ml of conc. HCl was added and the mixture was again evaporated to dryness. The residue was warmed to 40–50 °C with 75 ml of 1M HCl

**Table 1. Lead levels in vegetation samples in ppm around Al Fossool Al arbaa lead plant. (Averages ± S.D.)**

| Location | Conc. of lead [wt. of dry ash] | |
|---|---|---|
| | washed sample | unwashed sample |
| **South of plant** | | |
| 100 – 150 m | 290.2 ± 20.0 | 765.7 ± 51.3 |
| 400 m | 94.1 ± 24. | 103.2 ± 23.76 |
| 1000 m | 11.86 ± 2.7 | 13.0 ± 2.5 |
| **North of plant** | | |
| 20 m | 489.4 ± 95.2 | 1158.0 ± 55.7 |
| 100 m | 108.5 ± 21.4 | 113.5 ± 22.1 |
| 400 m | 17.3 ± 2.3 | 21.1 ± 4.1 |
| 800 m | 11.0 ± 1.3 | 13.4 ± 2.4 |
| 1000 m | 5.8 ± 1.1 | 8.7 ± 2.1 |
| **West of plant** | | |
| 20 m | 413.2 ± 80.0 | 877.2 ± 46.2 |
| 100 m | 105.0 ± 10.5 | 194.9 ± 12.1 |
| 1000 m | 13.7 ± 2.0 | 20.6 ± 5.5 |
| **East of plant** | | |
| 50 m | 541.3 ± 32.4 | 1173.1 ± 111.9 |
| 150 m | 480.0 ± 36.2 | 933.6 ± 28.9 |
| 500 m | 15.7 ± 2.0 | 22.8 ± 4.0 |
| 1000 m | 6.5 ± 2.2 | 16.0 ± 3.3 |

and the mixture was filtered through Whatman No.50 filter paper into 100 ml volumetric flask. The residue was washed with 1M HCl and the volume was made up to 100 ml by adding 1M HCl. This solution was analyzed by flame atomic absorption spectrophotometric method. The results are presented statistically in Table 2.

The wide deviation observed in the results of the measured soil samples (Tables 1 and 2), reflect the uneven spread of the lead deposit on the area surrounding the plant.

**Table 2. Lead levels in soil samples in ppm around Al Fosool Al arbaa lead plant. (Averages ± S.D.)**

| Location | Average concentration of lead (Averages ± S.D.) |
|---|---|
| 50 m away in all directions from FALP | 5439.8 ± 181.6 |
| **West of plant** | |
| 100 m | 813.1 ± 6.3 |
| 200 m | 124.8 ± 7.7 |
| 500 m | 21.9 ± 0.63 |
| 1000 m | 21.6 ± 1.9 |
| **East of plant** | |
| 100 m | 109.5 ± 25.5 |
| 1000 m | 34.7 ± 8.5 |
| **South of plant** | |
| 150 m | 172.3 ± 23.9 |
| 300m | 34.6 ± 6.3 |
| 1000 m | 19.4 ± 1.3 |
| **North of plant** | |
| 150 m | 70.4 ± 3.6 |
| 300 m | 30.9 ± 12.5 |
| 500 m | 25.5 ± 1.7 |

**Table 3. Comparative study between mean lead content in vegetation of Al Fossool Al arbaa lead plant area and other agricultural regions**

| Location | Overall average conc. of lead (in ppm of dry ash wt/wt) | |
|---|---|---|
| | washed sample | unwashed sample |
| (FALP) area | 245.9* | 501.9* |
| Al Aziziyah town | 2.0 | 3.4 |
| Al Qarabulli town | 2.5 | 4.1 |
| Ben Ghashir town | 2.3 | 3.8 |

* Average of the averages at 100–150 meter distance from FALP in the four geographical directions.

**Table 4. Comparative study between means of lead content in soil samples of Al Fossool Al arbaa lead plant area and other agricultural regions.**

| Location | Mean of lead concentration in ppm (wt/wt) |
|---|---|
| FALP area | 291.3* |
| Al Aziziyah town | 18.7 |
| Al Qarabulli town | 21.2 |
| Qasar Ben Ghashir town | 18.7 |

* Average of the average in the 100–150 metres distance from FALP in the four geographical directions.

## DISCUSSION

The results reported in Table 1 show that the average level of lead in washed and unwashed vegetation samples increases as the distance from the FALP lessens, and that the east side of the plant (at 50 m) is more polluted with lead than in the other three directions. This may be due to the consistency of the west to east wind blow direction.

It is also observed from Table 1, that the average lead concentration in unwashed vegetation samples ranges (8.7 to 1173.1 ppm at distance of 1000 and 50 metres from FALP respectively) are higher than those of washed samples (5.8 to 541.3 ppm at the same above-mentioned distance). These differences, especially at 50 metres, reflect the amount of contaminating lead, which can be removed by washing. The results of the soil sample reported in Table 2 show a great similarity in the vegetation samples. However, the concentration of the lead at a 50 metres distance from FALP is about five times greater than that of the vegetation one. The results also show that the west side of the plant (at 100 m) has the highest concentration in comparison with the other directions.

This may be due to the fact that the waste disposal is situated on the west side of the plant. The comparative study of mean lead content in vegetation and soil of the FALP area and of other towns, namely, Al Aziziyah, Al Qarabulli and Ben Gashir[9] which are given in Tables 3 and 4 respectively, clearly indicates that the FALP area has much higher levels than those of the above-

mentioned towns. This reflects the extent of the lead pollution,(which exceeds the international permissible limit[5,6]), caused by the past operations of FALP in the studied area.

## ACKNOWLEDGEMENT

The authors would like to express their gratitude to the Technical Centre for Protecting the Environment in Tripoli for suggesting this project, and to PRC management for support during this work.

## REFERENCES

[1] Chow, T.J, 1973. *Chemy, Br.*, **9**. 258–263.

[2] Public Safety 1973. Lead (Consumers Association, London), pp 104–111 April 1973.

[3] Grandjean, P, 1975. Lead in Danes Historical and Toxicological Studies in Environmental Quality and Safety, Suppl. Vol. II, Lead (ed. f. Coulston and F Korte), Academic Press, New York, San Francisco; London, 6–75.

[4] Ali, L. H., 1987. *Industrial Pollution, Sources, Chemistry and Control*. No. 1241. The National Library, Baghdad (in arabic).

[5] Ueno,Y. Rosner, D.E., de Pena, R.G. and Heicklen, J.P., 1982. Studies In Environmental Science 20. Atmospheric Pollution. Proceedings of the15th International Collequium, Paris, May 4–7, 1982. Edited by Michel M. Benarie Elsevier.

[6] Sell, N. j, 1992.(ed.) *Industrial Pollution Control: Issues and Techniques* 2nd Edition. Van Nostrand Reinhold. New York.

[7] Harrison, R. M. Duncan, P.H. and Laxen, P.H., 1977. A comparative study of methods for the analysis of total lead in soil, *Water, Air and Soil Pollution*, **8**, 387–397.

[8] Jawashi, S. A. Busaiffi, M. and Ahmad, I, 1993. A case study of monitoring of lead levels from petroleum emission and reduction of lead concentration in motor gasoline. Proceeding of OAPEC Conference on Safety and Environmental Protection in the Oil Industries in the Arab Countries held at Cairo on 11–13 October, 1993.

[9] unpublished result.